Impact of millennial-scale Atlantic meridional overturning circulation (AMOC) changes on tropical South American precipitation during the last glacial period

Dissertation

zur Erlangung des
Doktorgrades in den Naturwissenschaften (Dr. rer. nat.)

im Fachbereich Geowissenschaften
der Universität Bremen

vorgelegt von

Yancheng Zhang

Bremen, Juni 2016

Universität Bremen

PRÜFUNGSAUSSCHUSS

---------- **Gutachter** ----------

Herr Prof. Dr. Dr. Gerold Wefer

Herr Prof. Dr. Dierk Hebbeln

----- **Tag des öffentlichen Kolloquiums** -----

20 Sep. 2016

----- **Mitglieder der Kommission** -----

Herr Prof. Dr. Dr. Gerold Wefer

Herr Prof. Dr. Dierk Hebbeln

Herr Prof. Dr. Michal Kucera

Herr Dr. Matthias Zabel

Frau Dr. Ines Voigt

Frau Johanna Marquardt

Name: Yancheng Zhang Datum: 15-06-2016

Anschrift: MARUM Raum 1340 Leobenerstr., D-28359 Bremen

E r k l ä r u n g

Hiermit versichere ich, dass ich

1. die Arbeit ohne unerlaubte fremde Hilfe angefertigt habe,

2. keine anderen als die von mir angegebenen Quellen und Hilfsmittel benutzt habe und

3. die den benutzten Werken wörtlich oder inhaltlich entnommenen Stellen als solche kenntlich gemacht habe.

----------, den ----------

(Unterschrift)

Acknowledgements

More steps towards my PhD, more memories cross my mind.

First of all I would like to express my deepest gratitude to Prof. Dr. Gerold Wefer, Dr. Stefan Mulitza and Dr. Cristiano M. Chiessi for their support and supervision during the past years. Prof. Dr. Gerold Wefer offered me the great opportunity to pursue my PhD at MARUM and also provided constructive suggestions to develop scientific topics. Stefan not only designed research objectives but also gave lots of encouragement throughout my PhD. Cristiano guided me step by step for both the analytical techniques and revisions of manuscripts.

I particularly thank Cristiano for hosting me within his group at University of São Paulo in Brazil and also supporting me to attend graduate course and academic conference there. Special thanks go to Prof. Dr. André O. Sawakuchi and Prof. Dr. Paulo C. Giannini who scheduled the fieldtrip in Piauí state, NE Brazil during my stay. I would also like to thank many great Brazilian colleagues, Prof. Dr. Francisco W. Cruz Jr., Prof. Dr. Maria H. B. M. Holanda, Dr. Adriana Perretti, Vinícius Mendes, André Zular, Maria C. Catunda, Marília C. Campos and others, who made external stay a fascinating and informative experience for me.

I am grateful to Dr. Matthias Zabel, Dr. Ursula Röhl, Dr. Monika Segl and Dr. Henning Kuhnert and their teams for technical support in the labs, Dr. Xiao Zhang, Dr. Matthias Prange, Dr. Xu Zhang and Prof. Dr. Gerrit Lohmann for operating the climate models, Dr. Aline Govin and Dr. Janna Just for fruitful discussions. I appreciate the assistance from Dr. Vera B. Bender for accessing sediment materials in MARUM core repository.

I thank all colleagues from Bremen International Graduate School for Marine Sciences (GLOMAR), Dr. Christina Klose, Carmen Murken and Jutta Bülten for their kind help in administrative affairs. Furthermore, I would like to thank Dr. Ulrike Holzwarth, Dr. Janna Just, Dr. Henry Wu and Dr. Daniela Pittauer for organizing interesting monthly seminars.

I shared an office and had lots of fun with Rony, Francesca and William for years. Time with great friends in Bremen (in alphabetical order), Amanda, Anna, Catarina, Christoph, Claudia, Enqing, Francesca, Hendrik, Igor, Ines, James, Jia, Mariem, Rodrigo, Shuwen, William, Xiao, Xu, Yanlong, Yann, Yufang and many others, made my PhD life colorful and enjoyable.

Finally, I thank my parents for their long-term unconditional love and understanding that gives me endless motivation.

路漫漫其修远兮，吾将上下而求索。——屈原（约公元前 340-278 年）

The way to truth has no ending, yet high and low I will search with my will unbending.

Yuán Qū (ca. 340-278 B.C.)

Abstract

Modern precipitation over tropical South America, the host to the largest terrestrial biome on Earth, is mainly dominated by the South American summer monsoon (SASM) and the Intertropical Convergence Zone (ITCZ). Analyses of instrumental data demonstrated that tropical South American precipitation is substantially affected by sea surface temperature (SST) conditions over the Pacific and the Atlantic Oceans, such as the El Niño-Southern Oscillation (ENSO) and the North Atlantic Oscillation (NAO) on seasonal to multiannual timescales respectively. An increasing number of studies, based on both observation data and model simulations, showed that decadal-to-centennial scale variations in the Atlantic Meridional Overturning Circulation (AMOC) are also able to modulate precipitation over tropical South America. The future evolution of tropical rainforest and biodiversity across such region, which strongly interacts with global climate, is of great concern to scientific community, policy maker and general public. Understanding this issue depends greatly on our knowledge about the response of tropical South American precipitation to the AMOC slowdown under global warming scenario, which however never occurred throughout the era of instrumental data. This thesis thus refers to similar states of the AMOC reduction in the past, e.g., the Heinrich Stadials (HS) and the Dansgaard-Oeschger (DO) Stadials during the last glacial period, to explore the ocean-atmosphere interaction over tropical South America.

To the east of South America, the North Brazil Current (NBC) in the continental margin was simulated to be reversed along with the AMOC slowdown during HS1 (ca. 18-15 ka before present, BP). If it was indeed the case, then the fluvial terrigenous materials would be redistributed southeastward along the northeastern (NE) South American continental margin. To clarify the role of the NBC during HS1, we here in **Chapter 2** i) compile the stratigraphic data of 108 sediment cores over western tropical Atlantic for sedimentation rates and ii) analyze two cores GeoB16206-1 and GeoB16224-1 (raised to the southeast

and the northwest of the Amazon River mouth during cruise MSM20/3, respectively) for neodymium (Nd) isotopic compositions. The compilation highlights an extreme rise in sedimentation rate off the Parnaíba River mouth during HS1. Sediment core GeoB16206-1 (ca. 2°S) offshore the Parnaíba River mouth documents relatively constant $^{143}Nd/^{144}Nd$ ratios (expressed as $\varepsilon_{Nd(0)}$) for the last 30 ka, which were evidently different from the $\varepsilon_{Nd(0)}$ data of sediment core GeoB16224-1 off French Guiana (ca. 7°N). Combined with $\varepsilon_{Nd(0)}$ values from a set of geological units in the Parnaíba River basin and terrestrial sediment samples in the Amazon River basin, we suggest that terrigenous materials from these two basins dominate fluvial sediments input at the core sites GeoB16206-1 and GeoB16224-1 throughout the last 30 ka, respectively. The NBC hence was unlikely reversed during HS1, and we further attribute the extremely high volume of terrigenous sediment deposited off the Parnaíba River mouth during HS1 to (i) an increased precipitation in NE Brazil and (ii) a reduced NBC, both associated with a weakened AMOC.

During the HS, millennial-scale slowdown of the AMOC had substantially influenced the tropical South American precipitation. The wet conditions prevailing over the Andes, NE Brazil and southeastern (SE) Brazil, although always attributed to a strengthening of the SASM by previous studies, are still poorly investigated into the physical mechanism. To address this issue, we integrate paleodata compilation and model simulations to determine the impacts of climate changes over the Atlantic and other ocean basins (e.g., the eastern equatorial Pacific) on South American precipitation during HS1 (**Chapter 3**). We realize that the Atlantic interhemispheric SST gradient alone is unable to produce an enhanced rainfall over the Andes and western Amazonia. Instead, the superimposition of the eastern equatorial Pacific SST changes upon the Atlantic SST gradient can well capture the main characteristics of South American precipitation as observed by the paleodata compilation. The eastern equatorial Pacific SST variations (ca. 0.5-1.5°C), in response to the weakened AMOC during HS1, yield anomalous low sea level pressures over such region that are of vital importance to promote moisture recycling from central Amazon towards the western Amazon. We propose that the thermal anomalies over the eastern equatorial Pacific are very relevant to the wet condition over the Andes. Thus, consideration of both the eastern

equatorial Pacific and the Atlantic SST changes allows more reliable projection of South American precipitation in the future.

Unlike the HS when the AMOC was significantly slowdown, the DO Stadials underwent moderate magnitudes of the AMOC reduction as supported by both proxy data and model simulations. Comparison between the responses of tropical South American precipitation to these two types of climate oscillations would improve estimation of biodiversity over South America. In **Chapter 4**, we differentiate the regional structures of tropical South American precipitation in response to the HS and the DO Stadials. Element compositions of sediment core GeoB16224-1, together with the $\varepsilon_{Nd(0)}$ values, show enhanced input of Andean-sourced terrigenous materials during both the HS and the DO Stadials. Five highly-resolved sediment cores across Central-to-South America between ca. 17°N and 4°S suggest that the HS and the DO Stadials both resulted in decreased precipitation over northernmost South America and increased precipitation in western Amazonia. Notably, NE Brazilian precipitation, which experienced significant increases during the HS, was characterized by no evident changes during the DO Stadials. We speculate that southward migration of the ITCZ mean position during the DO Stadials was unlikely to reach NE Brazil, probably related to moderate reductions of the AMOC. Future AMOC slowdown, e.g., 20%-50% by the end of this century derived from climate simulations, is therefore likely to influence precipitation over northernmost South America and western Amazonia rather than NE Brazil.

Kurzfassung

Die gegenwärtigen Niederschläge über dem tropischen Teil Südamerikas, eines der weltweit größten terrestrischen Biome, werden vor allem durch den südamerikanischen Sommermonsun (SASM) und die Innertropische Konvergenzzone (ITCZ) dominiert. Analysen instrumenteller Daten haben gezeigt, dass die Niederschläge über dem tropischen Teil Südamerikas substantiell von den Meeresoberflächentemperaturen (SST) des Pazifiks und des Atlantischen Ozeans beeinflußt werden. Gute Beispiele für solche Telekonnektionen sind die El Niño-Southern Oscillation (ENSO) und die Nordatlantische Oszillation (NAO), die auf saisonalen bzw. mehrjährigen Zeitskalen schwanken. Eine wachsende Zahl von Studien zeigt, dass Schwankungen der Atlantischen Meridionalen Umwälzbewegung (AMOC) auf dekadischen bis hundertjährigen Zeitskalen in der Lage sind, Niederschläge über Südamerika zu beeinflussen. Die zukünftige Entwicklung des tropischen Regenwalds ist von zentraler Bedeutung für das das globale Klimasystem und die globale Biodiversität. Paläoklimadaten bieten die Möglichkeit, die Auswirkungen von Veränderungen der AMOC in der jüngeren geologischen Vergangenheit zu dokumentieren. Diese Dissertation untersucht die sogenannten Heinrich Stadiale (HS) und Dansgaard-Oeschger (DO) Stadiale der letzten Eiszeit, Zeiträume in der Vergangenheit, für die deutliche AMOC Reduktionen nachgewiesen wurden, um die Auswirkungen und Mechanismen von Veränderungen der AMOC auf den Niederschlag über dem tropischen Teil Südamerikas besser zu verstehen.

Experimente mit Klimamodellen zeigen, dass der Nordbrasilstrom (NBC) am Kontinentalrand des östlichen Südamerikas seine Fließrichtung in Reaktion auf eine Verlangsamung der AMOC während des HS1 (ca. 18-15 ka vor heute, BP) umkehren kann. Wenn dies tatsächlich der Fall war, dann wäre das fluviatil angelieferte terrigene Material entlang des nordöstlichen (NE) südamerikanischen Kontinentalrands in südöstlicher statt in nordwestlicher Richtung verdriftet worden. Um die Rolle des NBC

während des HS1 zu klären, werden deshalb im **Kapitel 2**: i) die stratigraphischen Daten und Sedimentationsraten von 108 Sedimentkernen aus dem westlichen tropischen Atlantik kompiliert und ii) die Sedimente der Kerne GeoB16206-1 und GeoB16224-1 (südöstlich und nordwestlich der Amazonasmündung; erbohrt während der Forschungsausfahrt MSM20/3), auf ihre Neodym (Nd) Isotopenzusammensetzungen analysiert. Die Zusammenstellung ergab einen extremen Anstieg der Sedimentationsrate vor der Parnaíba Flussmündung während des HS1. Bohrkern GeoB16206-1 (ca. 2°S), entnommen vor der Parnaíba Flussmündung, zeigt während der letzten 30 ka relativ konstante $^{143}Nd/^{144}Nd$-Verhältnisse (ausgedrückt als $\varepsilon_{Nd(0)}$), die sich aber signifikant von den $\varepsilon_{Nd(0)}$ Daten des Sedimentkerns GeoB16224-1 von vor der Küste Französisch-Guayanas (ca. 7°N) unterscheiden. In Kombination mit $\varepsilon_{Nd(0)}$ Werten aus einer Reihe von geologischen Einheiten im Parnaíba Einzugsgebiet und terrestrischen Sedimentproben des Amazonas-Beckens zeigen wir, dass während der letzten 30 ka die Hauptquelle für die terrigenen Sedimente des Kerns GeoB16206-1 der Parnaíba und von GeoB16224-1 der Amazonas war. Es ist daher unwahrscheinlich, dass der NBC während des HS1 in umgekehrter Richtung floss und wir führen die extrem hohen Ablagerungsraten terrigenen Materials vor der Parnaíba Flussmündung während des HS1 auf (i) verstärkte Niederschläge in NE Brasilien und (ii) einen abgeschwächten NBC zurück, jeweils assoziiert mit einer abgeschwächten AMOC.

Während des HS, hatte die auf tausendjährigen Skalen angelegte Verlangsamung der AMOC den tropisch-südamerikanischen Niederschlag wesentlich beeinflusst. Obwohl feuchtere Bedingungen in den Anden, NE Brasilien und Südost (SE) Brasilien in früheren Studien immer einer Verstärkung des SASM zugeschrieben wurden, ist der physikalische Mechanismus noch unzureichend erforscht. Um diese Wissenslücke zu schließen, vergleichen wir eine Kompilation von Paläodaten und Modellsimulationen, um die Auswirkungen von Klimaveränderungen im Gebiet des Atlantiks und anderer Meeresbecken (wie zum Beispiel des östlichen äquatorialen Pazifiks) auf den südamerikanischen Niederschlag während des HS1 zu belegen (**Kapitel 3**). Unsere Befunde zeigen, dass der interhemisphärische SST Gradient des Atlantiks allein nicht in der Lage ist, verstärkte Niederschläge über den Anden und im westlichen

Amazonasgebiet zu erzeugen. Stattdessen kann die Überlagerung des atlantischen SST Gradienten durch SST Änderungen des östlichen äquatorialen Pazifiks die wichtigsten Muster des südamerikanischen Niederschlags erklären, die in der Zusammenstellung der Paläodaten zu beobachten war. Die SST Variationen des östlichen äquatorialen Pazifiks (ca. 0,5 bis 1,5°C) verursachten in Folge der abgeschwächten AMOC während des HS1, einen anomal niedrigen barometrischen Luftdruck in dieser Region, was wiederum den Feuchtigkeitstransport vom zentralen in den westlichen Amazonas beeinflußte. Wir zeigen, dass die thermischen Anomalien über dem östlichen äquatorialen Pazifik die feuchteren Bedingungen in den Anden erklären können.

Im Gegensatz zu den HS war die AMOC in DO Stadialen wohl nur mäßig reduziert, wie sowohl in Proxy-Daten als auch in Modellsimulationen zu erkennen ist. In **Kapitel 4**, unterscheiden wir die regionalen Auswirkungen von Veränderungen des tropisch-südamerikanischen Niederschlags in Reaktion auf die HS und DO Stadiale. Elementzusammensetzungen des Sedimentkerns GeoB16224-1 und $\varepsilon_{Nd(0)}$ Werte zeigen den verstärkten Eintrag von terrigenem Material aus den Anden sowohl während der HS als auch während der DO Stadiale. Fünf hochaufgelöste Sedimentkerne von Zentral- bis Südamerika (zwischen 17°N und 4°S) legen nahe, dass HS und DO Stadiale zu verminderten Niederschlägen über dem nördlichsten Südamerika und zu verstärkten Niederschlägen im westlichen Amazonasgebiet führten. Bemerkenswert ist, dass die NE brasilianischen Niederschläge zwar signifikante Anstiege während des HS aber keine offensichtlichen Veränderungen während der DO Stadiale zeigten. Wir vermuten, dass eine südliche Migration der ITCZ Position während der DO Stadiale, wahrscheinlich verursacht durch die nur moderate Abschwächung der AMOC, NE Brasilien wohl nicht erreicht hat. Die von Klimamodellen projizierte zukünftige Abschwächung der AMOC von 20-50% sollte daher eher die Niederschläge über dem nördlichsten Südamerika und westlichen Amazonasgebiet beeinflussen als die NE Brasiliens.

Abbreviations

(Listed in alphabetical order)

AGCM	Atmospheric General Circulation Model
AMOC	Atlantic Meridional Overturning Circulation
BA	Bølling-Allerød (14.5-13 ka)
BC	Brazil Current
CRI	Chronological Reliability Index
DJF	December-January-February
DO	Dansgaard-Oeschger
ENSO	El Niño-Southern Oscillation
GC	Guiana Current
HS	Heinrich Stadials
HS1	Heinrich Stadials 1 (18-15 ka)
IRD	Ice-Rafted Debris
ITCZ	Intertropical Convergence Zone
JJA	June-July-August
LGM	Last Glacial Maximum (23-19 ka)
MSM20/3	RV Maria S. Merian cruise MSM20/3
NBC	North Brazil Current
NEC	North Equatorial Current
NECC	North Equatorial Counter Current
PCR	Representative Concentration Pathways
RNBC	Retroflection of the North Brazil Current
SACZ	South Atlantic Convergence Zone
SALLJ	South America Low Level Jet
SASM	South American Summer Monsoon
SEC	South Equatorial Current
SLP	Sea Level Pressure
SSS	Sea Surface Salinity
SST	Sea Surface Temperature
YD	Younger Dryas (13-11.5 ka)

Contents

Chapter I

Introduction

1.1. Atlantic Meridional Overturning Circulation

Seawater is characterized by a wide range of temperature, salinity, density and other variables. The gradient in density (dependent on its temperature and salinity) drives large-scale movement of water masses around the global ocean, which, known as thermohaline circulation, redistributes the fluxes of heat and freshwater across the sea surface and leads to interior mixing of heat and salt (e.g., Rahmstorf, 2003). Because it is difficult to separate the density-driven circulation and wind (or/and tidal force)-driven circulation (Wunsch, 2002), the term Meridional Overturning Circulation is most often used to refer to zonally-integrated volume transport in the ocean (Cunningham and Marsh, 2010). The Atlantic Meridional Overturning Circulation (AMOC), variations of which have greatly affected climate changes on the regional scale (e.g., Europe and North Atlantic, Sutton and Hodson 2005; Curry and Mauritzen 2005) and global scale (e.g., Jackson et al., 2015), is of great concern to the scientific community across different disciplines.

The AMOC is comprised of an upper and a lower branch (Fig.1-1). In the upper branch, warm-saline surface (and also some intermediate) waters from the Pacific and the Indian Oceans are transported into the South Atlantic through the Drake Passage off South America and ocean currents around South Africa (e.g., the Agulhas system, Beal et al., 2011), respectively. These waters subsequently flow towards to the North Atlantic, as illustrated by a northwestward direction in the South Atlantic and a northeastward direction in the North Atlantic due to the Ekman transport (Fig.1-1). Along the pathway, the surface waters generally experience an increase in salinity (mainly through net

evaporation in the northern subtropical gyre) and decrease in temperature (mainly due to air-ocean exchange in the mid-to-high latitude). These characteristics then enhance density of the waters, which, as a result, enable them to sink in the high latitudes of the North Atlantic (e.g., the Norwegian-Greenland Sea and the Labrador Sea) forming the North Atlantic Deep Water (NADW) (at depth between about 1500-4000 m, e.g., Marshall and Speer, 2012). The NADW, as the lower branch of the AMOC, is transported towards the South Atlantic along the deep western boundary in opposite direction with the upper branch. At the southern end, the NADW mixes with Circumpolar Deep Water (CDW) that in turn enters into the deep Indian Ocean and part of the South Pacific. Below, the abyssal Atlantic is filled by Antarctic bottom water (AABW) produced in the Ross Sea and the Weddell Sea, off the Adélie Coast and Cape Darnley polynya (e.g., Ohshima et al., 2013) through ocean/ice-shelf interactions (e.g., intensive evaporation) and brine rejection from sea-ice growth.

Fig.1-1. The AMOC and its role over the global ocean (from Marshall and Speer 2012). Cooler colors indicate denser water masses, ranging from warmer mode and thermocline waters in red to bottom waters in blue. In the southern ocean, the rising blue-green-yellow and yellow-red arrows denote the upwelling systems across surfaces of equal density.

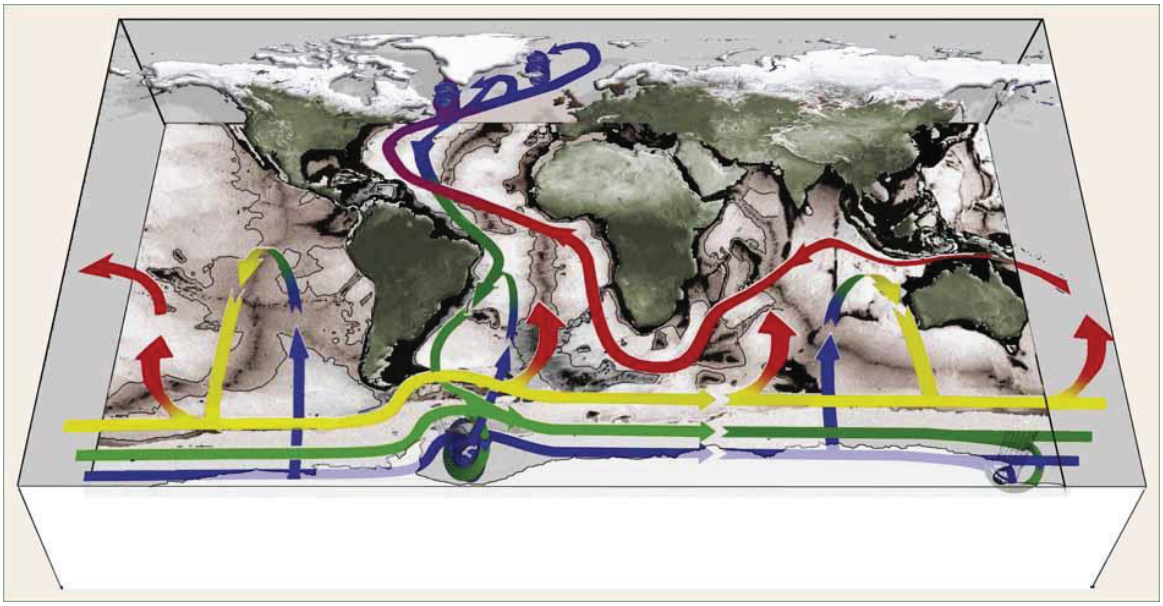

Today, the AMOC contributes a large fraction (ca. 88%) of total oceanic northward heat transport in the Atlantic (ca. 1.33 ± 0.40 PW, 1 PW = 10^{15} Watt, Johns et al., 2011). A weakening of the AMOC thus leads to i) decreased air temperature in the North Atlantic

region (e.g., Manabe and Stouffer, 1995; Vellinga and Wood, 2002) and ii) variations in sea level along the coasts of North America and Europe (e.g., Levermann et al., 2005; Vellinga and Wood 2008). Because of large scale ocean-atmosphere interaction, impacts of the AMOC changes can also be transmitted around the world (e.g., Ganopolski and Rahmstorf, 2001; Knutti et al., 2004), such as the meridional shift of the Intertropical Convergence Zone (ITCZ). Numerical simulations suggested that, by the end of this century, the AMOC is very likely to undergo a considerable slowdown against the global warming scenarios (Kirtman et al., 2013; Rahmstorf et al., 2015). The possible influences of such AMOC reductions, which never occurred across the era of instrumental data (e.g., Cheng et al., 2013a), on global climate and ecosystem are therefore of great interest. To address this issue, we refer to analogous intervals of the AMOC reduction over the past due probably to freshwater perturbations into the high latitudes of the North Atlantic, e.g., the Heinrich Stadials (HS) (Bond et al., 1993) and the stadial phases of the Dansgaard-Oeschger (DO) cycles (Dansgaard et al., 1993), which were widely documented by an abundance of paleoclimate records.

1.2. Environmental background over Amazon Basin

With an area of about 7 million km², the Amazon Basin (Amazonia) hosts one of the largest and most diverse terrestrial ecosystems on Earth (Fig.1-2) which sequesters a vast amount of carbon (e.g., ca. 150-200 Pg, Pg = 10^{15} grams, Feldpausch et al., 2012). Recent studies found that, during the last decades, Amazonia generally experienced carbon loss by ca. 0.48 ± 0.18 Pg in the dry years (e.g., Gatti et al., 2014; especially ca. 1.4 ± 0.2 Pg in the 2005 extreme drought, Phillips et al., 2009) and carbon neutral (ca. 0.06 ± 0.1 Pg) in the wet year. The large amount of net carbon loss, roughly equivalent to one-tenth of anthropogenic fossil fuel emissions (8.3 ± 0.7 Pg per year over the period of 2002-2011, Ciais et al., 2013), may plays a crucial role in the global climate system through its influences on atmospheric greenhouse-gas concentrations, water cycle and atmospheric circulation. Therefore, some authors (e.g., Gatti et al., 2014) suggested that moisture is essential to store carbon in the living biomass and soils across Amazonia, substantially influencing the Amazonian carbon storage.

Fig.1-2. Modern vegetation types over South America (cited from Eva et al., 2004)

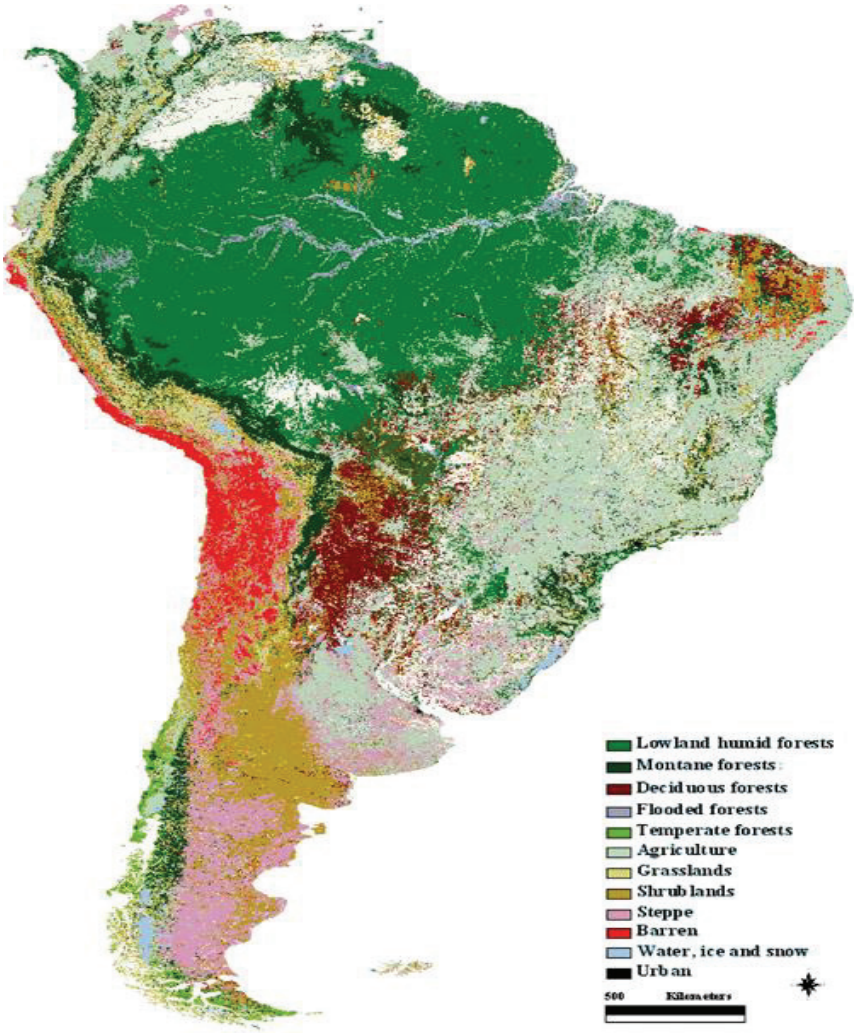

Modern precipitation over Amazonia is mainly supplied by the South American summer monsoon (SASM) and the ITCZ (Fig.1-3). During the austral summer December-January-February (DJF) when the SASM is well developed and the ITCZ migrates to its southern limits, tropical Atlantic moisture is transported across central Amazon towards the Andes, which then deflects the warm-humid air masses southward towards southeastern (SE) South America (Fig.1-3a). Meanwhile, the South Atlantic Convergence Zone (SACZ), an important component of the SASM, is also in its mature phase and transports the moisture from western subtropical Atlantic towards SE Brazil and the western Amazon (Fig.1-3a). When the SASM fails and the ITCZ shifts to its northern limits during the austral winter June-July-August (JJA), most regions of Amazonia exhibit deceased precipitation while northernmost South America exhibits an increased precipitation (Fig.1-3b). In addition, SE South American rainfall is also decreased as the SACZ is weakened.

Fig.1-3. Monthly averaged 1981-2010 terrestrial precipitation from the University of Delaware (http://climate.geog.udel.edu/~climate/) and the 850hPa wind field from the NOAA/OAR/ESRL PSD (http://www.esrl.noaa.gov/psd/) as well as mean sea surface salinity (SSS) from the World Ocean Atlas 2013 (Zweng et al., 2013) for (a) austral summer season (December-January-February (DJF) for precipitation, March for SSS) and (b) austral winter season (June-July-August (JJA) for precipitation, September for SSS). Black lines present the schematic position of the Intertropical Convergence Zone (ITCZ) over the Atlantic during DJF and JJA.

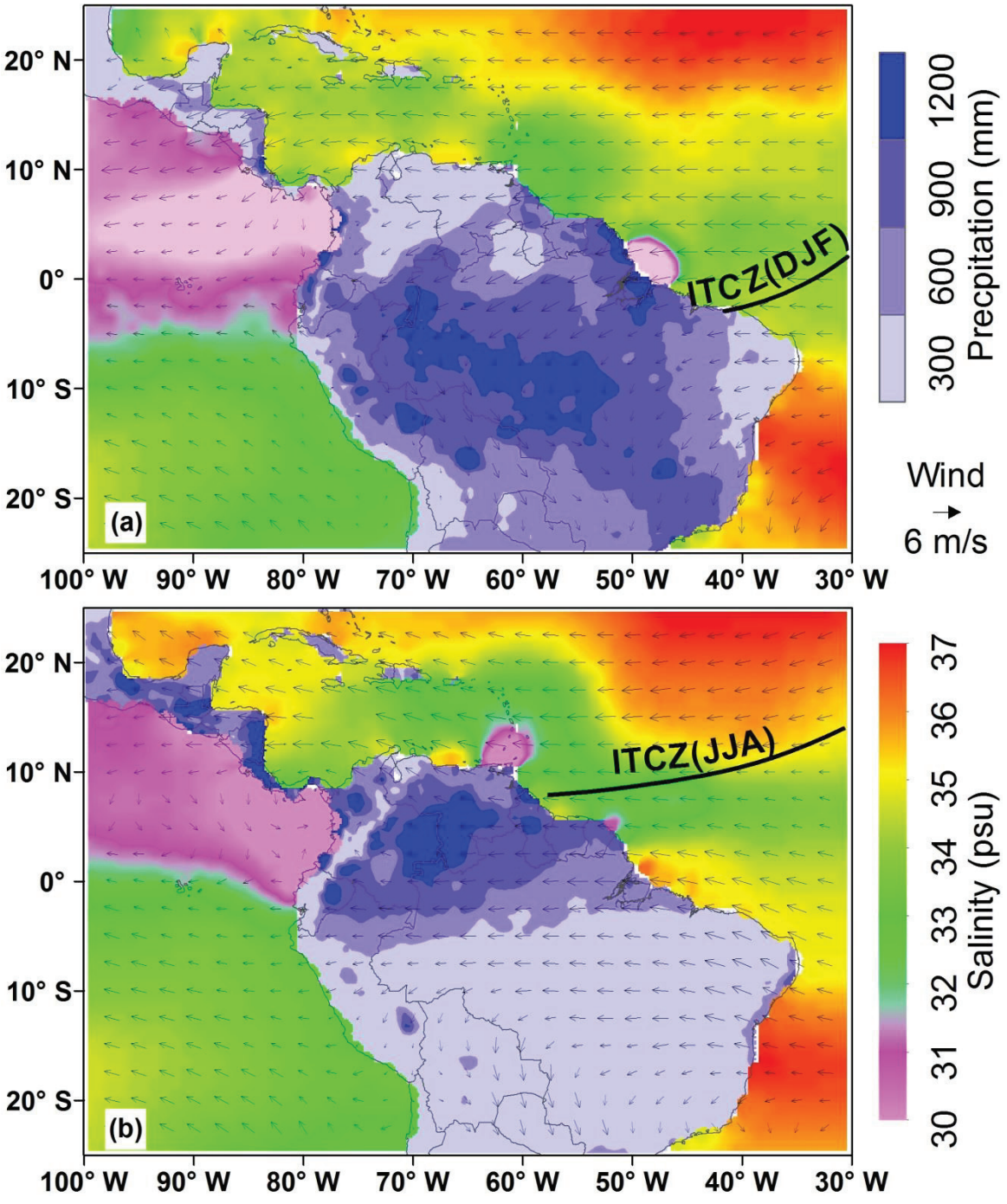

Analyses of instrumental data suggested that precipitation across tropical South America (and thus Amazonia) is substantially affected by climate oscillations over the Atlantic and the Pacific Oceans, for instance, the North Atlantic Oscillation (NAO) and the Atlantic Multidecadal Oscillation (AMO) (e.g., Wu et al., 2007; Yoon and Zeng, 2010), the El Niño-Southern Oscillation (ENSO) and the Pacific Decadal Oscillation (PDO) (Marengo et al., 2004; Andreoli et al., 2012) from seasonal to decadal timescales respectively (e.g., Kayano et al., 2009; Villar et al., 2009). Such climate variations are closely related to changes in AMOC (to some certain degree) based on a number of previous studies using observation data and model simulations. Combined with its impacts on the northeast trade winds (Wu et al., 2007) and the ITCZ meridional displacement, the AMOC is thus also of importance to regulate Amazonian precipitation. Understanding responses of Amazonian precipitation to the future AMOC slowdown, e.g., a decline of ca. 20% (35%-55%) by the end of this century under global warming scenario RCP4.5 (RCP8.5) from climate models (e.g., Coupled Model Intercomparison Project (CMIP5; Cheng et al., 2013a); Max Planck Institute Ocean Model (MPIOM; Rahmstorf et al., 2015)), depends on our understanding about the regional characteristics of tropical South American precipitation along with the AMOC slowdown in the past like the Heinrich and the DO Stadials.

1.3. South American precipitation during the HS and the DO Stadials

Based on the measurements of $^{231}Pa/^{230}Th$ ratios from marine sediment cores in the North Atlantic, previous studies suggested that the AMOC was significantly weakened during the HS, specifically during HS1 (ca. 18-15 ka before present, BP). Millennial-scale AMOC reductions during HS had substantially influenced the SASM and the ITCZ, and therefore the South American precipitation as registered in proxy data over South America. Generally, a southward displacement of the ITCZ during HS resulted in a considerable decrease of precipitation over northernmost South America (Peterson et al., 2000) and a significant increase in northeastern (NE) Brazil (Wang et al., 2004). Based on well-dated stalagmite $\delta^{18}O$ records from the Ecuadorian Andes (Mosblech et al., 2012) and the Peruvian Andes (Kanner et al., 2012; Cheng et al., 2013b) as well as SE Brazil (Wang et al., 2006), some studies also associated the wet conditions over these regions

directly to a strengthening of the SASM during HS. In comparison to the HS, the DO Stadials often involved moderate magnitudes of the AMOC reductions (Böhm et al., 2015; Zhang et al., 2014a, b), which, as a result, also led to millennial-scale variations of South American precipitation. For example, available paleoclimate records showed decreased precipitation in northernmost South America (e.g., sediment core MD03-2621; Deplazes et al., 2013) and increased precipitation in the Andes (e.g., stalagmite $\delta^{18}O$ records from the Peruvian Andes; Kanner et al., 2012; Cheng et al., 2013b) during the DO Stadials.

Apart from proxy data, a number of freshwater-hosing experiments with climate models of different complexity were used to investigate the HS1. Outputs of these numerical simulations successfully captured the southward shift of the Atlantic ITCZ under both modern (e.g., Stouffer et al., 2006) and the LGM boundary conditions (e.g., Kageyama et al., 2013), but still exhibited a large spread of rainfall patterns across central and western Amazon that are today mainly dominated by the SASM. Besides, some model simulations were also conducted to investigate the DO Stadials, e.g., Zhang et al. (2014a, b; 2015), which demonstrated dry conditions over northernmost South America and wet conditions over the Peruvian Andes. Such patterns are in general consistent with the available paleo-climate records over tropical South America as mentioned above.

Both proxy data (e.g., Böhm et al., 2015) and model simulations (e.g., Kageyama et al., 2013; Zhang et al., 2014a, b) have already suggested different magnitudes of the AMOC reductions during the HS and the DO Stadials. However, difference between regional characteristics of South American precipitation in response to these two types of climate oscillations is still poorly investigated. Because the AMOC is projected to experience moderate reduction in the future, e.g., by ca. 20% under global warming scenario RCP4.5 and by ca. 35% -55% under RCP8.5 in numerical simulations (e.g., Cheng et al., 2013a; Rahmstorf et al., 2015), a clear understanding on how South American precipitation responded to the HS and the DO Stadials (including both regional structures and physical mechanism) would allow better insight into possible changes of Amazonian precipitation in the future.

1.4. Research objectives

In this thesis, I aim to document the interactions between South American precipitation and millennial-scale cold climate in the North Atlantic, e.g., the HS and the DO Stadials respectively, by integrating paleoclimate records (published and newly retrieved during cruise MSM20/3 (Mulitza et al., 2013)) and climate model simulations.

Here I mainly focused on the following three scientific hypotheses as research objectives in this study:

Hypothesis 1: If the North Brazil Current (NBC) was reversed during HS1, Amazon sediments delivered to the continental margin offshore NE South America would be redistributed along the NBC pathway.

Today, the NBC transports a large amount of freshwater and sediment discharge from the Amazon River along the NE South American continental margin northwestward towards Caribbean Sea (Fig.1-1). If the NBC was reversed during HS1, as simulated by some climate model experiments (e.g., Chang et al., 2008; Schmidt et al., 2012), the Amazon-sourced suspension then would be transported southeastwards rather than northwestwards. As a result, Amazon sediments would be expected to be deposited offshore NE Brazil, considering a large difference in amounts of the NBC-carried sediments from the Amazon River (ca. 8 t/s) and the small rivers over NE Brazil (ca. 0.2 t/s from the Parnaíba River) (Allison et al., 2000; Nace et al., 2014). The marine paleoclimate records off NE Brazil thus cannot be used to document the past climate change onshore directly over NE Brazil. Since the provenances of sediments from the Amazon basin and small river basin in NE Brazil are apparently different, we test this hypothesis by analyzing the neodymium (Nd) isotopic compositions ($^{143}Nd/^{144}Nd$ values, expressed as $\varepsilon_{Nd(0)}$) of two well-dated marine sediment cores retrieved to the northwest and the southeast of the Amazon River mouth, respectively.

Hypothesis 2: If South American precipitation during HS1 was only influenced by the North Atlantic climate, other oceans would have no contribution to the regional characteristics of South American precipitation.

Modern precipitation over tropical South America is controlled by the SASM and the location of the ITCZ (Fig.1-3). Abundant evidence supported the southward shift of the ITCZ during HS1, but a strengthening of the SASM, that was proposed to explain the wet conditions over the Andes, is still unknown about the physical mechanism. A number of studies demonstrated that the AMOC slowdown (or nearly shutdown), one of the most important features during HS1, resulted in the thermal anomalies over western tropical Atlantic and eastern tropical Pacific (e.g., Rühlemann et al., 1999; Merkel et al., 2010; Schmidt et al., 2012). Because the SST changes over the Atlantic and the Pacific Oceans indeed greatly affect South American precipitation today as substantiated by analyses of instrumental data, it would be interesting to clarify the impact of such thermal anomalies over eastern tropical Pacific on the regional features of South American precipitation during HS1. If other oceans (e.g., the eastern tropical Pacific) also contributed to South American precipitation during HS1, one should scrutinize the trigger (e.g., a strengthened SASM due to Atlantic meridional SST gradient) to explain the wet conditions over the Andes. It thus could improve our knowledge on the mechanism of how South American precipitation responded to the AMOC slowdown, and also reliable estimation of Amazon ecosystem in the future.

Hypothesis 3: If the AMOC strength underwent moderate reduction during the DO Stadials in comparison to the HS, then an intermediate response in tropical South American precipitation (e.g., between weak AMOC during HS1 and strong AMOC during the late Holocene) should be observed during the DO Stadials.

Based on available paleoclimate records over tropical South America, we summarized the regional characteristics of South American precipitation along with the HS, e.g., decrease in northernmost South America (Peterson et al., 2000; Deplazes et al., 2013) and increase over NE Brazil (Wang et al., 2004; Jaeschke et al., 2007) due to the ITCZ southward shift.

In addition, the HS also led to wet conditions over SE Brazil (Wang et al., 2006) and the Andes (Kanner et al., 2012; Mosblech et al., 2012), likely through the mechanism as described in **Chapter 2**. Responses of South American precipitation to the DO Stadials are also of importance to our knowledge, since model simulations suggested that global warming scenarios are likely to drive moderate magnitudes of the AMOC slowdown by the end of this century (e.g., Cheng et al., 2013a; Rahmstorf et al., 2015). However, only few paleoclimate records are available so far to document the DO Stadials across South America. Comparisons amongst previously published and new high resolution sediment cores along a meridional transect across Central and South America underline the impacts of the DO Stadials. We thus differentiate the regional characteristics of South American precipitation in response to the HS and the DO Stadials.

1.5. Outline of the thesis

This thesis includes three manuscripts, which are published (Chapter 2) in and submitted (Chapter 3) or ready for submission (Chapter 4) to international peer-reviewed journals.

Chapter 2 (1st manuscript, published in *Earth and Planetary Science Letters*)
Origin of increased terrigenous supply to the NE South American continental margin during Heinrich Stadial 1 and the Younger Dryas

By Yancheng Zhang, Cristiano M. Chiessi, Stefan Mulitza, Matthias Zabel, Ricardo I. F. Trindade, Maria H. B. M. Hollanda, Elton L. Dantas, Aline Govin, Ralf Tiedemann, Gerold Wefer

We confirm for the first time that fluvial terrigenous materials in the NE South American continental margin were not redistributed along with the AMOC slowdown (even nearly shutdown) during HS1. The compilation of 108 sediment cores over the western tropical Atlantic shows an extreme rise of sedimentation rate off the Parnaíba River mouth (about 2°S, NE Brazil), while a decrease off the Amazon River mouth (about 4°N) during HS1 in comparison to the LGM. The $\varepsilon_{Nd(0)}$) values of sediment core GeoB16224-1(about 7°N)

offshore French Guiana, together with published $\varepsilon_{Nd(0)}$ data of terrestrial materials in the Amazon Basin, indicate dominance of Amazon-sourced terrigenous sediments input over the last 30 ka. In contrast, the $\varepsilon_{Nd(0)}$) data of core GeoB16206-1 off the Parnaíba River mouth are comparable with the $\varepsilon_{Nd(0)}$) values from a set of different geological units in the Parnaíba Basin, which supports the source origin directly onshore. The NBC was thus unlikely to be reversed during HS1, otherwise it could lead to a mixing of Amazon-sourced materials and NE Brazil-sourced sediments offshore the Parnaíba River mouth. Accordingly, we strengthen the relationship between precipitation change over NE Brazil and terrigenous input to the continental margin nearby.

Chapter 3 (2nd manuscript, Submitted to *Scientific Reports*)
Equatorial Pacific forcing of western Amazonian precipitation during Heinrich Stadial 1

By Yancheng Zhang, Xu Zhang, Cristiano M. Chiessi, Stefan Mulitza, Xiao Zhang, Gerrit Lohmann, Matthias Prange, Hermann Behling, Matthias Zabel, Aline Govin, André O. Sawakuchi, Francisco W. Cruz, Gerold Wefer

By combining the paleodata compilation and sensitivity model experiments, we examine the physical mechanism behind regional characteristics of South American precipitation during HS1. The Atlantic interhemispheric SST gradient alone, in relation to freshwater perturbation at the high latitudes of the North Atlantic, successfully captures the ITCZ southward migration as evidenced by dry condition in northernmost South America and wet condition over NE Brazil. However, it is still unable to produce the widespread wet conditions over the Andes which were widely registered by an abundance of paleoclimate records. Interestingly, if the eastern equatorial Pacific SST changes were superimposed upon the Atlantic SST experiment, we find that the overall structures are well reproduced in the climate model. This is because the eastern equatorial Pacific SST variations (ca. 0.5-1.5°C), coupled to the weakened AMOC, can yield anomalous low sea level pressures over such region that are of crucial importance to promote moisture recycling from the central Amazonia towards the western Amazonia. Combined also with a set of sensitivity

experiments, we suggest that SST changes over the eastern equatorial Pacific rather than the Atlantic are responsible for an increased precipitation over the Andes.

Chapter 4 (3rd manuscript, Ready for submission to *Geophysical Research Letters*)
Discriminating the impacts of Heinrich and Dansgaard-Oeschger stadials over tropical South America

By Yancheng Zhang, Cristiano M. Chiessi, Stefan Mulitza, André O. Sawakuchi, Matthias Zabel, Stefano Crivellari, Gerold Wefer

We differentiate the regional structures of South American precipitation in response to the HS and the DO Stadials. In general, the HS led to decreased precipitation in northernmost South America but increased precipitation over NE Brazil, SE Brazil and the Andes. By using geochemical data (e.g., Fe/Ca) of sediment core GeoB16224-1, together with $\varepsilon_{Nd(0)}$) analyses (in **Chapter 2**), we determine an enhanced input of Andean-sourced terrigenous sediments during both the HS and the DO Stadials. Comparison with four highly-resolved paleoprecipitation records across Central and South America allow us to disentangle the impacts of the Hs and DO Stadials, respectively. We recognize that both the HS and the DO Stadials decreased precipitation over northernmost South America and increased precipitation in western Amazonia. Most interestingly, NE Brazilian precipitation, which experienced significant increases during the HS, was characterized by no evident changes during the DO Stadials. Since the DO Stadials involved smaller magnitudes of the AMOC slowdown than the HS, we suppose that the southward migration of ITCZ mean position during the DO Stadials was unlikely to reach NE Brazil, then producing no increase of terrigenous materials input to the continental margin nearby.

Conclusion and outlook are summarized in **Chapter 5**.
All the data presented in this thesis will be archived in the PANGAEA database (http://www.pangaea.de).

1.6. References

Allison, M.A., et al. 2000. Origin of Amazon mudbanks along the northeastern coast of South America. Mar. Geol. 163(1-4), 241-256.

Andreoli, R.V., et al. 2012. Seasonal anomalous rainfall in the central and eastern Amazon and associated anomalous oceanic and atmospheric patterns. Int. J. Climatol. 32, 1193-1205.

Beal, L.M., et al. 2011. On the role of the Agulhas system in ocean circulation and climate. Nature 472, 429-436.

Böhm, E., et al. 2015. Strong and deep Atlantic meridional overturning circulation during the last glacial cycle. Nature, 517, 73-76.

Bond, G., et al. 1993. Correlations between climate records from North Atlantic sediments and Greenland ice. Nature 365, 143-147.

Chang, P., et al. 2008. Oceanic link between abrupt changes in the North Atlantic Ocean and the African monsoon. Nat. Geosci. 1, 444-448.

Cheng, H., et al. 2013b. Climate change patterns in Amazonia and biodiversity. Nat. Commun. 4(1411), doi: 10.1038/ncomms2415.

Cheng, W., Chiang, J.C.H., and Zhang, D. 2013a. Atlantic Meridional Overturning Circulation (AMOC) in CMIP5 models: RCP and historical simulations. J. Climate 26, 7187-7197.

Ciais, P., et al. 2013. Carbon and Other Biogeochemical Cycles. In: Climate Change 2013: The Physical Science Basis. Contribution of Working Group I to the Fifth Assessment Report of the Intergovernmental Panel on Climate Change (Cambridge University Press).

Cunningham, S.A., Marsh R., 2010. Observing and modeling changes in the Atlantic MOC. WIREs Climate Change 1, 180-191.

Curry, R., and Mauritzen, C. 2005. Dilution of the northern North Atlantic in recent decades. Science 308, 1772-1774.

Dansgaard, W. et al. 1993. Evidence for general instability of past climate from a 250-kyr ice-core record. Nature 364, 218-220.

Deplazes, G., et al. 2013. Links between tropical rainfall and North Atlantic climate during the last glacial period. Nat. Geosci. 6, 213-217.

Eva, H.D., et al. 2004. A land cover map of South America. Glob. Chang Biol. 10, 731-744.

Feldpausch, T.R., et al. 2012. Tree height integrated into pantropical forest biomass estimates. Biogeosciences 9, 3381-3403.

Ganopolski, A., and Rahmstrof, S. 2001. Rapid changes of glacial climate simulated in a coupled climate model. Nature 409, 153-158.

Gatti, L.V., et al. 2014. Drought sensitivity of Amazonian carbon balance revealed by atmospheric measurements. Nature 506, 76-80.

Jackson, L.C., et al. 2015. Global and European climate impacts of a slowdown of the AMOC in a high resolution GCM. Clim. Dyn. 45, 3299-3316.

Jaeschke, A., et al. 2007. Coupling of millennial-scale changes in sea surface temperature and precipitation off northeastern Brazil with high-latitude climate shifts during the last glacial period. Paleoceanography 22(4), doi:10.1029/2006PA001391.

Johns, W.E., et al. 2011. Continuous, array-based estimates of Atlantic Ocean heat transport at 26.5°N. J. Climate 24, 2429-2449.

Kageyama, M., et al. 2013. Climatic impacts of fresh water hosing under Last Glacial Maximum conditions a multi-model study. Clim. Past 9, 935-953.

Kanner, L.C., et al. 2012. High latitude forcing of the South American Summer Monsoon during the Last Glacial. Science 335, 570-573.

Kayano, M.T., de Oliveira, C.P., Andreoli, R.V. 2009. Interannual relations between South American rainfall and tropical sea surface temperature anomalies before and after 1976. Int. J. Climatol. 29(10), 1439-1448.

Kirtman, B., et al. 2013. Near-term Climate Change: Projections and Predictability. In: Climate Change 2013: The Physical Science Basis. Contribution of Working Group I to the Fifth Assessment Report of the Intergovernmental Panel on Climate Change (Cambridge University Press).

Knutti, R., et al. 2004. Strong hemispheric coupling of glacial climate through freshwater discharge and ocean circulation. Nature 430, 851-856.

Levermann, A., et al. 2005. Dynamic sea level changes following changes in the thermohaline circulation. Clim. Dyn. 24, 347-354.

Manabe, S., and Stouffer, R.J. 1995. Simulation of abrupt climate change induced by freshwater input to the North Atlantic Ocean. Nature 378, 165-167.

Marengo, J.A. 2004. Interdecadal variability and trends of rainfall across the Amazon basin. Theor. Appl. Climatol. 78, 79-96.

Marshall, J., & Speer, K. 2012. Closure of the meridional overturning circulation through Southern Ocean upwelling. Nat. Geosci. 5, 71-180.

Merkel, U., Prange, M., Schulz, M., 2010. ENSO variability and teleconnections during glacial climates. Quat. Sci. Rev. 29, 86-100.

Mosblech, N.A.S., et al. 2012. North Atlantic forcing of Amazonian precipitation during the last ice age. Nat. Geosci. 5, 817-820.

Mulitza, S., et al. 2013. Response of Amazon sedimentation to deforestation, land use and climate variability. Cruise No. MSM20/3 (February 19 - March 11, 2012), Recife (Brazil) - Bridgetown (Barbados). MARIA S. MERIAN-Berichte, MSM20/3, 86 pp., DFG Senatskommission für Ozeanographie, doi:10.2312/cr_msm20_3.

Nace, T.E., et al. 2014. The role of North Brazil Current transport in the paleoclimate of the Brazilian Nordeste margin and paleoceanography of the western tropical Atlantic during the late Quaternary. Palaeogeogr. Palaeoclimatol. Palaeoecol. 415, 3-13.

Ohshima, K.I., et al. 2013. Antarctic Bottom Water production by intense sea-ice formation in the Cape Darnley polynya. Nat. Geosci. 6, 235-240.

Peterson, L.C., et al. 2000. Rapid changes in the hydrologic cycle of the tropical Atlantic during the Last Glacial. Science 290, 1947-1951.

Phillips, O.L., et al. 2009. Drought sensitivity of the Amazon rainforest. Science 323, 1344-1347.

Rahmstorf, S. 2003. The current climate. Nature 421, 699.

Rahmstorf, S., et al. 2015. Exceptional twentieth-century slowdown in Atlantic Ocean overturning circulation. Nature Climate Change 5, 475-480.

Rühlemann, C., et al. 1999. Warming of the tropical Atlantic Ocean and slowdown of thermohaline circulation during the last deglaciation. Nature 402, 511-514.

Schmidt, M.W., et al. 2012. Impact of abrupt deglacial climate change on tropical Atlantic subsurface temperatures. Proc. Natl. Acad. Sci. USA 109, 14348-14352.

Stouffer, R.J., et al. 2006. Investigating the Causes of the Response of the Thermohaline Circulation to Past and Future Climate Changes. J. Climate 19, 1365-1387.

Sutton, R.T., and Hodson, D.L.R. 2005. Atlantic Ocean forcing of North American and European summer climate. Science 309, 115-118.

Vellinga, M., and Wood, R.A. 2008. Impacts of thermohaline circulation shutdown in the twenty-first century. Climatic Change 91, 43-63.

Vellinga, M., Wood, R.A. 2002. Global climatic impacts of a collapse of the Atlantic thermohaline circulation. Climate Change 54, 251-267.

Villar, J.C., et al. 2009. Spatio-temporal rainfall variability in the Amazon basin countries (Brazil, Peru, Bolivia, Colombia, and Ecuador). Int. J. Climatol. 29, 1574-1594.

Wang, X., et al. 2004. Northeastern Brazil wet periods linked to distant climate anomalies and rainforest boundary changes. Nature 432, 740-743.

Wang, X., et al. 2006. Interhemispheric anti-phasing of rainfall during the last glacial period. Quat. Sci. Rev. 25(23-24), 3391-3403.

Wu, L., et al. 2007. Atmospheric Teleconnections of Tropical Atlantic Variability: Interhemispheric, Tropical-Extratropical, and Cross-Basin Interactions. J. Climate 20, 856-870.

Wunsch, C. 2002. What is the thermohaline circulation? Science 298, 1179-1181.

Yoon, J.H., and Zeng, N. 2010. An Atlantic influence on Amazon rainfall. Clim. Dyn. 34, 249-264.

Zhang, X., et al. 2014a. Abrupt glacial climate shifts controlled by ice sheet changes. Nature 512, 290-294.

Zhang, X., et al. 2014b. Instability of the Atlantic overturning circulation during Marine Isotope Stage 3. Geophys. Res. Lett. 41, doi:10.1002/2014GL060321.

Zhang, X., et al. 2015. Spatial fingerpring and magnitude of changes in the Atlantic meridional overturning circulation during Marine Isotope Stage 3. Geophys. Res. Lett. 42, doi:10.1002/2014GL063003.

Zweng, M.M, et al. 2013. World Ocean Atlas 2013. 2, Salinity. S. Levitus, Ed., A. Mishonov Technical Ed.; NOAA Atlas NESDIS 74, 39 pp.

Chapter Ⅱ

Origin of increased terrigenous supply to the NE South American continental margin during Heinrich Stadial 1 and the Younger Dryas

Yancheng Zhang[1*], Cristiano M. Chiessi[2], Stefan Mulitza[1], Matthias Zabel[1], Ricardo I. F. Trindade[3], Maria H. B. M. Hollanda[4], Elton L. Dantas[5], Aline Govin[1 a], Ralf Tiedemann[6], Gerold Wefer[1]

[1] MARUM - Center for Marine Environmental Sciences, University of Bremen, Germany

[2] School of Arts, Sciences and Humanities, University of São Paulo, Brazil

[3] Institute of Astronomy, Geophysics and Atmospheric Sciences, University of São Paulo, Brazil

[4] Institute of Geosciences, University of São Paulo, Brazil

[5] Institute of Geosciences, University of Brasília, Brazil

[6] Alfred Wegener Institute for Polar and Marine Research, Bremerhaven, Germany

* Corresponding author: Y. Zhang (yzhang@marum.de)

[a] Present address: IPSL/LSCE, Laboratoire des Sciences du Climat et de l'Environnement (CEA-CNRS-UVSQ), Gif sur Yvette, France

(Published in *Earth and Planetary Science Letters 432,493-500*)

Own contribution:

a) Calculated and complied sedimentation rates of the 108 sediment cores

b) Analysed cores GeoB16206-1 and GeoB16224-1: ^{14}C, XRF and EDP-XRF data

c) Summarized Nd radiogenic isotopes of terrestrial materials from Amazon Basin, and compared to the same proxies of cores GeoB16206-1 and GeoB16224-1

d) Wrote the draft of this manuscript

2.1. Abstract

We investigate the redistribution of terrigenous materials in the northeastern (NE) South American continental margin during slowdown events of the Atlantic Meridional Overturning Circulation (AMOC). The compilation of stratigraphic data from 108 marine sediment cores collected across the western tropical Atlantic shows an extreme rise in sedimentation rates off the Parnaíba River mouth (about 2°S) during Heinrich Stadial 1 (HS1, 18-15 ka). Sediment core GeoB16206-1, raised offshore the Parnaíba River mouth, documents relatively constant $^{143}Nd/^{144}Nd$ values (expressed as $\varepsilon_{Nd(0)}$) throughout the last 30 ka. Whereas the homogeneous $\varepsilon_{Nd(0)}$ data support the input of fluvial sediments by the Parnaíba River from the same source area directly onshore, the increases in Fe/Ca, Al/Si and Rb/Sr during HS1 indicate a marked intensification of fluvial erosion in the Parnaíba River drainage basin. In contrast, the $\varepsilon_{Nd(0)}$ values from sediment core GeoB16224-1 collected off French Guiana (about 7°N) suggest Amazon-sourced materials within the last 30 ka. We attribute the extremely high volume of terrigenous sediments deposited offshore the Parnaíba River mouth during HS1 to (i) an enhanced precipitation in the catchment region and (ii) a reduced North Brazil Current, which are both associated with a weakened AMOC.

2.2. Introduction

The North Brazil Current (NBC) constitutes an important conduit for the transfer of warm and salty surface waters into the high latitudes of the North Atlantic (Fig.2-1), balancing the southward export of North Atlantic Deep Water (NADW) (Johns et al., 1998). The NBC is also responsible for the northwestward transport of an enormous amount of freshwater and terrigenous sediment delivered to the ocean by the Amazon River that amount to about 2×10^6 m^3/s and 40 t/s, respectively (Lentz, 1995; Allison et al., 2000). Instrumental data and model simulations showed that the NBC transport is positively correlated with the strength of the Atlantic Meridional Overturning Circulation (AMOC) on decadal timescales (Zhang et al., 2011). Based on stable isotope and Mg/Ca records, other studies (i.e. Arz et al.,1999; Wilson et al., 2011) also suggested a marked decrease

in the NBC strength related to millennial-scale AMOC slowdown events of the last deglaciation, such as the Younger Dryas (YD, 13-11.5 ka) and Heinrich Stadial 1 (HS1, 18-15 ka). Modeling simulations of freshwater input into the high latitudes of the North Atlantic were even able to trigger a reversal of the NBC under both present-day (Chang et al., 2008) and Last Glacial Maximum (LGM, 23-19 ka) conditions (Schmidt et al., 2012).

Millennial-scale abrupt changes in AMOC strength during the last deglaciation greatly influenced the South American Monsoon System (SAMS) and the mean position of the Intertropical Convergence Zone (ITCZ). For example, northeastern (NE) Brazil, which is today characterized by a semi-arid climate, experienced wet conditions during HS1 and the YD in response to a southward displacement of the tropical rainbelt. Enhanced rainfall over NE Brazil associated with slowdown of the AMOC was documented by terrestrial archives like stalagmite isotopic records (i.e. Wang et al., 2004; Cruz et al., 2009) and also simulated by freshwater-hosing experiments with different coupled climate models (i.e. Zhang and Delworth, 2005; Jaeschke et al., 2007). The large increase in terrigenous sediments offshore NE Brazil during HS1 and the YD, observed in geochemical and palynological data of marine sediment cores, was interpreted as the product of massive fluvial input from the adjacent continent (Arz et al., 1998; Jennerjahn et al., 2004; Dupont et al., 2010). However, the role of the NBC (in particular its potential reversal) in the redistribution and deposition of terrigenous sediments on the NE South American continental margin remains unknown. If the NBC indeed reversed during slowdown events of the AMOC, the Amazon sediment discharge could be transported southeastwards rather than northwestwards and thus impedes robust interpretation of oceanic paleorecords offshore NE Brazil.

Here we reconstruct the provenance and distribution of terrigenous sediments off NE South America over the last 30 ka. We mainly focus on HS1, which was characterized by the longest perturbation in the AMOC of the last 30 ka (Böhm et al., 2015). First, we map the distribution of sedimentation rates off NE South America during the LGM and HS1 based on 108 marine sediment cores. Second, by using two marine sediment cores located under the influence of the NBC to the northwest and to the southeast of the Amazon River

mouth, we analyze neodymium (Nd) isotopic compositions to determine changes in sediment provenance throughout the last 30 ka. We verify that (i) the terrigenous sediments deposited offshore NE Brazil during the last 30 ka are not compatible with an Amazon origin, and (ii) the NBC was very unlikely reversed during HS1. Furthermore, major element compositions from the two cores allow insight into the relationship between changes in continental climate and weathering patterns.

2.3. Materials and methods

2.3.1. Calculation of sedimentation rates in compiled marine stratigraphies

Sedimentation rates for the western tropical Atlantic were calculated using stratigraphic data of 105 published marine sediment cores collected between 30°S and 20°N, 75°W and 25°W, and 472 and 5426 m water depth (Table S2-1 in Supplementary Material, hereafter 'SM'), and three marine sediment cores retrieved during RV Maria S. Merian cruise MSM20/3 (see section 2.3.2 below) (Mulitza et al., 2013).

Among these selected cores, 70 chronologies were constrained by radiocarbon ages, 24 by stable isotope stratigraphy (based on planktonic or benthic foraminifera, Fig.S2-1) and 14 by stratigraphic alignment of various downcore properties (i.e. lithology, magnetic susceptibility, Fig.S2-2). For each core location, we estimated the sedimentation rates during the LGM and HS1 (expressed as centimeters per thousand years, cm/ka). We used Monte-Carlo resampling to estimate chronological uncertainties by calculating about 10000 possible age models for each core. For all individual age models, ages were linearly interpolated to obtain the upper and lower depth corresponding to the LGM and HS1 time slices. This approach enabled us to derive mean sedimentation rates for the LGM and HS1, and 95% confidence intervals for the two time slices (see SM for further details). For all simulations, raw ^{14}C ages were recalibrated with the IntCal13 calibration curve (Reimer et al., 2013) and a reservoir age correction of 400 ± 100 (2σ error) years (Bard, 1988). Moreover, a constant dating uncertainty of 1500 years (2σ error) was assumed for age control points based on stable isotope stratigraphy or stratigraphic alignment of downcore properties.

2.3.2. New sediment cores from cruise MSM20/3

The two unpublished gravity cores used here were collected off NE South America under the influence of the NBC (Table 2-1) during RV MS Merian cruise MSM20/3 (Mulitza et al., 2013).

To the southeast and to the northwest of the Amazon River mouth, cores GeoB16206-1 and GeoB16224-1 were raised off the Parnaíba River mouth and off French Guiana, respectively (Fig.2-1). In addition, near-core-top sediments (at a core depth of 10 cm) of other 12 gravity cores raised along the NE South American continental margin during MSM20/3 were also included in this study (see section 2.3.2.3 below). We used near-core-top samples because multicores are not available for all investigated sites (Mulitza et al., 2013).

Table 2-1. Sediment cores and near-core-top samples from MSM20/3 used in this study

Sediment core	Latitude	Longitude	Water depth (m)	Nd isotope Analysis*
GeoB16203-1	2°02.11' S	41°43.11' W	1591	10 cm [a]
GeoB16204-2	1°59.75' S	42°20.31' W	1211	10 cm [a]
GeoB16205-4	1°21.11' S	43°05.80' W	1955	10 cm [a]
GeoB16206-1	1°34.75' S	43°01.42' W	1367	Downcore [a, b]
GeoB16211-3	2°52.69' N	49°20.98' W	56	10 cm [a]
GeoB16212-3	3°06.27' N	49°23.28' W	75	10 cm [a]
GeoB16216-3	6°14.43' N	51°15.34' W	2833	10 cm [a]
GeoB16217-2	6°04.17' N	51°17.41' W	2440	10 cm [a]
GeoB16218-4	4°46.17' N	51°31.33' W	41	10 cm [a]
GeoB16219-2	4°45.15' N	51°31.27' W	38	10 cm [a]
GeoB16220-1	4°43.41' N	51°30.82' W	31	10 cm [a]
GeoB16222-1	6°09.31' N	51°41.60' W	1749	10 cm [a]
GeoB16223-2	6°37.63' N	52°06.99' W	2253	10 cm [a]
GeoB16224-1	6°39.38' N	52°04.99' W	2510	Downcore [b]

* The Nd isotope analyses were performed at the (a) Laboratory of Geochronology, University of Brasília and the (b) Center of Geochronological Research (CPGeo), University of São Paulo.

Fig.2-1. Location of terrestrial samples in the Amazon and Parnaíba River drainage basins, as well as marine sediment cores used in this study (key to symbols are given in Fig.2-4). The red and blue dots represent sediment cores GeoB16206-1 and GeoB16224-1, respectively. The schematic position of the Intertropical Convergence Zone (ITCZ) (black dashed line) during June-July-August (JJA) and December-January-February (DJF) and surface currents (grey arrows) in the western tropical Atlantic Ocean are also shown (Johns et al., 1998). BC: Brazil Current, GC: Guiana Current, NBC: North Brazil Current, NEC: North Equatorial Current, NECC: North Equatorial Counter Current, RNBC: Retroflection of the North Brazil Current, SEC: South Equatorial Current. The map was plotted using the Ocean Data View software (version 4.6.2) (Schlitzer, R., http://odv.awi.de, 2014).

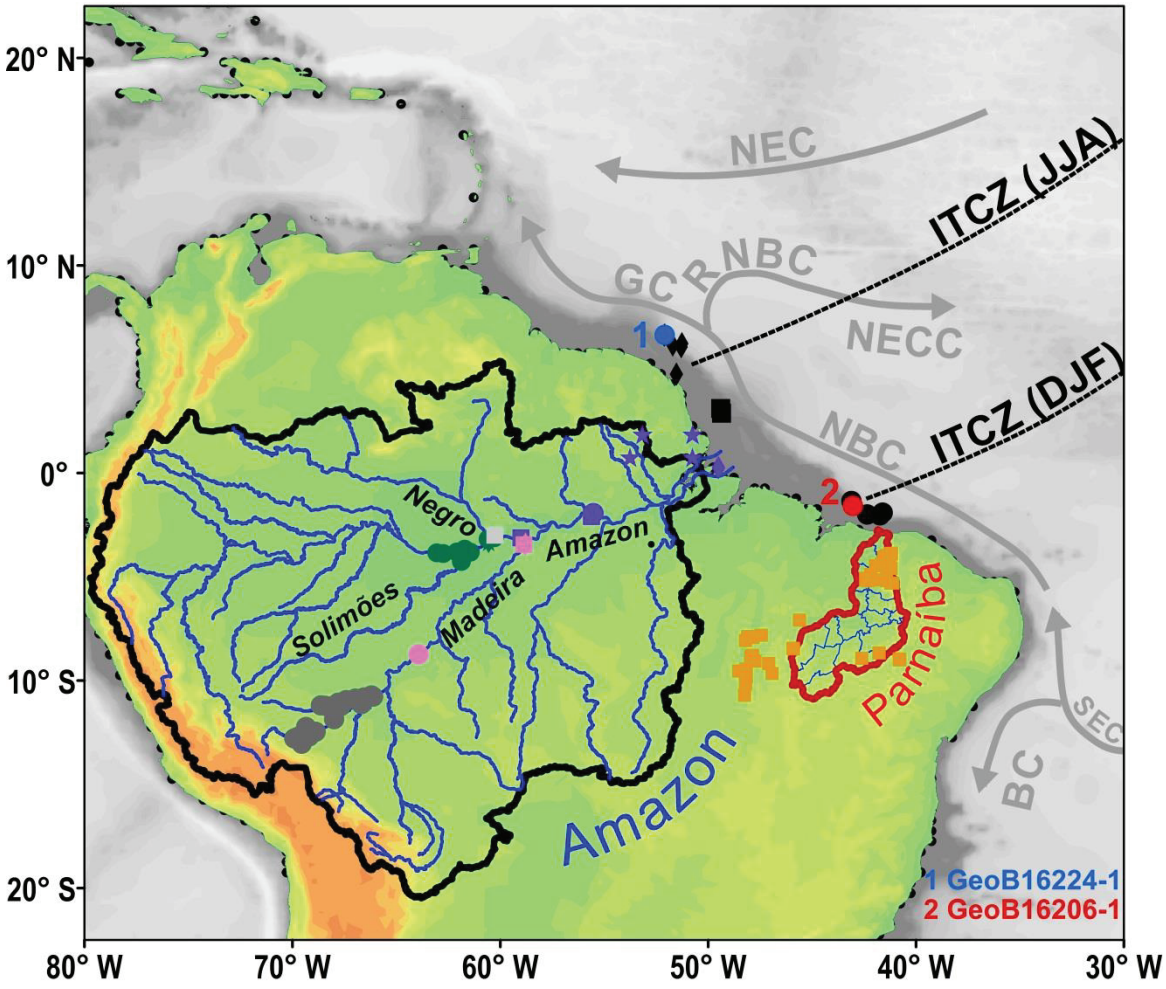

2.3.2.1. Age models of gravity cores GeoB16206-1 and GeoB16224-1

Age models for cores GeoB16206-1 and GeoB16224-1 from MSM20/3 were based on AMS radiocarbon analyses performed predominantly on samples of *Globigerinoides*

sacculifer or/and *Globigerinoides ruber*, and subordinately on samples of mixed planktonic foraminifera. Twelve and fifteen radiocarbon samples were taken in cores GeoB16206-1 and GeoB16224-1, respectively (Table 2-2). About 10 ml wet sediment was sampled, freeze-dried and washed over a 125 µm sieve. At least 7 mg of planktonic foraminifera specimens were hand-picked for ^{14}C measurements, which were conducted at the Poznan Radiocarbon Laboratory (Poland) or the Beta Analytic Inc. (USA). Raw radiocarbon ages were calibrated by using the Marine13 curve (Reimer et al., 2013) in the Calib 7.0 software (Stuiver and Reimer, 1993). Ages were linearly interpolated between calibrated ^{14}C dates. Furthermore, the ages of the 12 near-core-top samples were roughly estimated (i.e. mid or late Holocene, Table S2-2).

2.3.2.2. Major element composition

Elemental intensities of cores GeoB16206-1 and GeoB16224-1 were obtained by scanning the split core surfaces of the archive halves with an AVAATECH X-Ray Fluorescence (XRF) core-scanner at the MARUM, University of Bremen (Germany). The XRF data were measured downcore every 2 cm in core GeoB16206-1 and every 4 cm in core GeoB16224-1 (Table S2-3; detailed analytical information is provided in the SM). To calibrate the scanner intensities, we also analyzed elemental concentrations on bulk sediment samples at the MARUM too. In total, 37 and 50 discrete bulk sediment samples were taken from the working halves of cores GeoB16206-1 and GeoB16224-1, respectively, and analyzed with a PANalytical Epsilon3-XL XRF spectrometer (Table S2-3; detailed analytical techniques is provided in the SM). The powdered measurements and scanner data were combined to derive high-resolution calibrated proportions of elements with a log-ratio regression approach (Weltje and Tjallingii, 2008), in which Ca was commonly used as the denominator element (R^2 was 0.99 and 0.73 for the sediment cores GeoB16206-1 and GeoB16224-1, respectively; Fig.S2-3).

Table 2-2. Raw ^{14}C data and calibrated ages of cores GeoB16206-1 and GeoB16224-1.

Sediment core	Depth (cm)	Species	Lab. No.*	^{14}C AMS ages ± 1σ error (yr BP)	Calibrated ages ± 2σ error (yr BP)
GeoB16206-1	6	*G. sacculifer*	Poz-50178	1180 ± 30	705 ± 36
GeoB16206-1	70	*G. sacculifer*	Poz-52812	7610 ± 40	8013 ± 58
GeoB16206-1	135	*G. sacculifer*	Poz-52740	8210 ± 50	8588 ± 139
GeoB16206-1	200	*G. sacculifer*	Poz-50179	9690 ± 60	10438 ± 164
GeoB16206-1	360	*G. sacculifer*	Poz-52741	11630 ± 50	13104 ± 97
GeoB16206-1	400	*G. sacculifer*	Poz-50180	12840 ± 70	14587 ± 399
GeoB16206-1	500	*G. sacculifer*	Poz-52742	13490 ± 70	15671 ± 289
GeoB16206-1	600	*G. sacculifer*	Poz-50182	14630 ± 80	17323 ± 248
GeoB16206-1	665	*G. sacculifer*	Poz-52744	16060 ± 80	18920 ± 187
GeoB16206-1	705	*G. sacculifer*	Poz-52813	20390 ± 100	24050 ± 281
GeoB16206-1	735	*G. sacculifer*	Poz-52814	21840 ± 100	25754 ± 200
GeoB16206-1	800	*G. sacculifer*	Poz-52815	25790 ± 150	29462 ± 457
GeoB16224-1	6	*G. sacculifer, G. ruber*	Poz-49098	4910 ± 35	5126 ± 80
GeoB16224-1	50	*G. sacculifer, G. ruber*	Beta-356373	5920 ± 30	6318 ± 38
GeoB16224-1	66	Mixed planktonic foraminifera	Beta-377698	11110 ± 30	12635 ± 77
GeoB16224-1	82	Mixed planktonic foraminifera	Beta-377699	12220 ± 40	13667 ± 152
GeoB16224-1	100	*G. sacculifer, G. ruber*	Beta-356374	12760 ± 50	14420 ± 300
GeoB16224-1	150	Mixed planktonic foraminifera	Poz-49099	14090 ± 70	16537 ± 277
GeoB16224-1	200	*G. sacculifer, G. ruber*	Beta-356375	15790 ± 60	18660 ± 137
GeoB16224-1	250	*G. sacculifer, G. ruber*	Beta-356376	17980 ± 70	21245 ± 267
GeoB16224-1	300	*G. sacculifer, G. ruber*	Beta-356377	19640 ± 80	23193 ± 272
GeoB16224-1	350	*G. sacculifer, G. ruber*	Beta-356378	21820 ± 90	25740 ± 189
GeoB16224-1	400	*G. sacculifer, G. ruber*	Beta-356379	23980 ± 120	27700 ± 204
GeoB16224-1	450	Mixed planktonic foraminifera	Beta-356380	26930 ± 140	30792 ± 254
GeoB16224-1	500	Mixed planktonic foraminifera	Beta-377700	30110 ± 180	33854 ± 310
GeoB16224-1	550	Mixed planktonic foraminifera	Beta-377701	31950 ± 180	35428 ± 463
GeoB16224-1	600	Mixed planktonic foraminifera	Beta-377702	37070 ± 320	41222 ± 634

* Poz: Poznan Radiocarbon Laboratory (Poland); Beta: Beta Analytic Inc. (USA)

2.3.2.3. Nd isotopic composition

The Nd isotopic ratios of gravity cores GeoB16206-1 and GeoB16224-1 as well as of the near-core-top sediments of 12 gravity cores (Table 2-1) were measured at the Laboratory of Geochronology, University of Brasília (Brazil) or the Center of Geochronological Research (CPGeo), University of São Paulo (Brazil) (Table S2-2; detailed analytical information is provided in the SM). Additionally, a set of 49 sediment samples collected from different geological units in the Parnaíba River drainage basin and nearby region was analyzed for Nd isotopic composition at the CPGeo (Table S2-4). We combined these geological Nd isotopic measurements with previously published Nd and strontium ($^{87}Sr/^{86}Sr$) isotope ratios of terrestrial sediments from the Amazon River drainage basin (Figs.2-1, 2-4) to trace the sedimentary provenance of sediments deposited along the NE South American continental margin. The $^{143}Nd/^{144}Nd$ values were normalized to $^{146}Nd/^{144}Nd = 0.7219$ (De Paolo, 1981). We expressed the $^{143}Nd/^{144}Nd$ values using the $\varepsilon_{Nd(0)}$ notation, which was calculated according to the equation:

$$\varepsilon_{Nd(0)} = \frac{(^{143}Nd/^{144}Nd)_{sample}}{(^{143}Nd/^{144}Nd)_{CHUR}} \times 10^4$$

where the present-day chondritic uniform reservoir (CHUR) $^{143}Nd/^{144}Nd$ value is 0.512638 (Jacobsen and Wasserburg, 1980).

2.4. Results

2.4.1. Spatial distribution of marine sedimentation rates during the LGM and HS1

Generally, core sites from the abyssal depths show lower sedimentation rates (below ca. 10 cm/ka) than those from the continental margin under both the LGM and HS1 conditions (Fig.2-2 and Table S2-1). During the LGM (Fig.2-2a), sedimentation rates on the continental slope in the Cariaco Basin off Venezuela and off the Amazon River mouth reach 30-60 cm/ka (ca. 170 cm/ka in the specific case of core site CDH5), but stay below ca. 25 cm/ka in other regions. During HS1 (Fig.2-2b), sedimentation rates exhibit minor changes on the continental slope of the Cariaco Basin if compared to the LGM values, and a large decrease off the Amazon River mouth (15-30 cm/ka, with the exception of core site CDH5 where HS1 sedimentation rate still amounts to ca. 65 cm/ka). In contrast,

Fig.2-2. Sedimentation rates (SR, in cm/ka) during (a) the Last Glacial Maximum (LGM, 23-19 ka) and (b) Heinrich Stadial 1 (HS1, 18-15 ka). Dots denote ^{14}C-dated sediment cores and diamonds mark sediment cores dated by stable isotope stratigraphy or stratigraphic alignment (section 2.3.1). The dot colors and size of crosses within the dots or diamonds indicate SR values and errors respectively (Table S2-1), for every site. The Amazon and Parnaíba River drainage basins are outlined as in Fig.2-1.

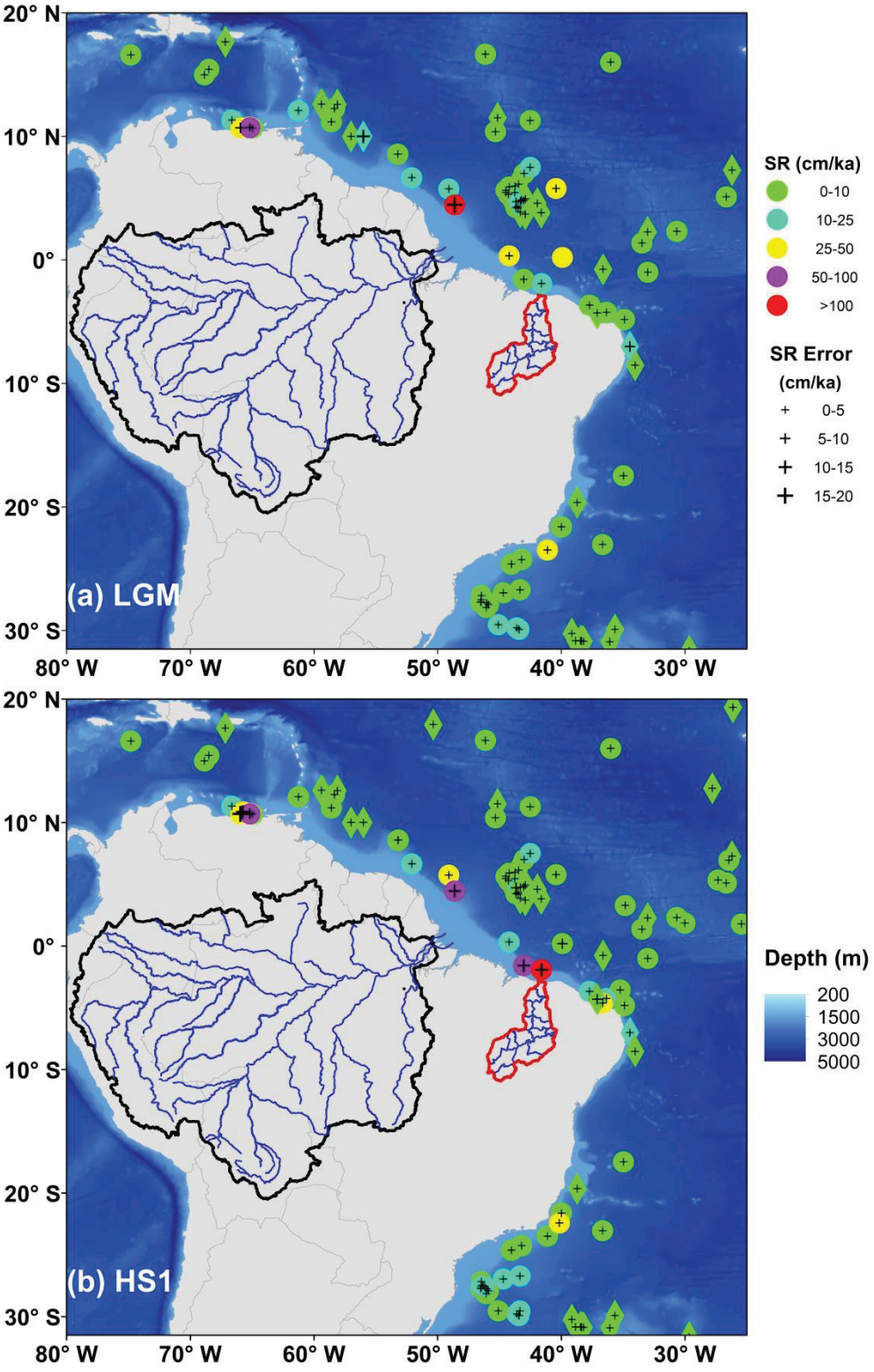

sedimentation rates on the continental slope off southern Brazil (between 25°S and 27°S) and off NE Brazil increase from ca. 10 cm/ka during the LGM to ca. 25 cm/ka during HS1. Yet, the most remarkable rise in sedimentation rates from the LGM to HS1 occurs off the Parnaíba River mouth, where HS1 sedimentation rates amount to ca. 80 cm/ka (about 65 cm/ka at core site GeoB16206-1 and 100 cm/ka at another nearby core site; Table S2-1) compared with ca. 10 cm/ka during the LGM. Notably, the core GeoB16206-1 also documents high sedimentation rate (ca. 60 cm/ka) during the YD (Fig.2-3c).

2.4.2. Downcore elements and Nd isotopic compositions of gravity cores from MSM20/3

2.4.2.1. Gravity core GeoB16206-1

The Fe/Ca ratio from sediment core GeoB16206-1, raised to the southeast of the Amazon River mouth, shows large increases during HS1 and the YD (Fig.2-3c). Elemental Al/Si and Rb/Sr ratios are also elevated during the same periods (Fig.2-3c and Table S2-3), and coincide with increased sedimentation rates. Apparently, the Fe/Ca, Al/Si and Rb/Sr values vary within similar ranges during Heinrich Stadial 2 (HS2, 25-24 ka), but the sedimentation rate (about 15 cm/ka) is markedly lower than during HS1 and the YD (about 60-80 cm/ka). In contrast to the elemental records, the $\varepsilon_{Nd(0)}$ values from sediment core GeoB16206-1 show little variation over the last 30 ka, ranging between -16.50 and -18.50 (Fig.2-3a and Table S2-2).

2.4.2.2. Gravity core GeoB16224-1

The Fe/Ca record from sediment core GeoB16224-1 (raised to the northwest of the Amazon River mouth) exhibits a moderate increase during HS1, while Al/Si and Rb/Sr variations show relatively small-amplitudes throughout the last 30 ka (Fig.2-3b). The sedimentation rates at this core site are generally higher during the glacial and deglacial periods (prior to ca. 13 ka) than during the Holocene, which is, notably, constrained only by two ^{14}C AMS dates (Fig.2-3b and Table 2-2). The $\varepsilon_{Nd(0)}$ values of core GeoB16224-1 show very little variation over the last 30 ka (from -11.11 to -12.22) (Fig.2-3a and Table

S2-2). However, these values are obviously higher than those of core GeoB16206-1 (around -17.45 ± 1.0 (mean ± 2σ)).

Fig.2-3. Downcore records of marine sediment cores GeoB16206-1 and GeoB16224-1 over the last 30 ka. (a) $\varepsilon_{Nd(0)}$ values of cores GeoB16206-1 (red) and GeoB16224-1 (blue). Elemental records of cores (b) GeoB16224-1 and (c) GeoB16206-1: sedimentation rate (black), ln(Fe/Ca) (blue), Al/Si ratio (red) and Rb/Sr ratio (orange). Triangles depict the calibrated ^{14}C-AMS ages (mean ± 2σ errors) for cores GeoB16206-1 (red) and GeoB16224-1 (blue). BA: Bølling-Allerød, HS1: Heinrich Stadial 1, HS2: Heinrich Stadial 2, LGM: Last Glacial Maximum, YD: Younger Dryas.

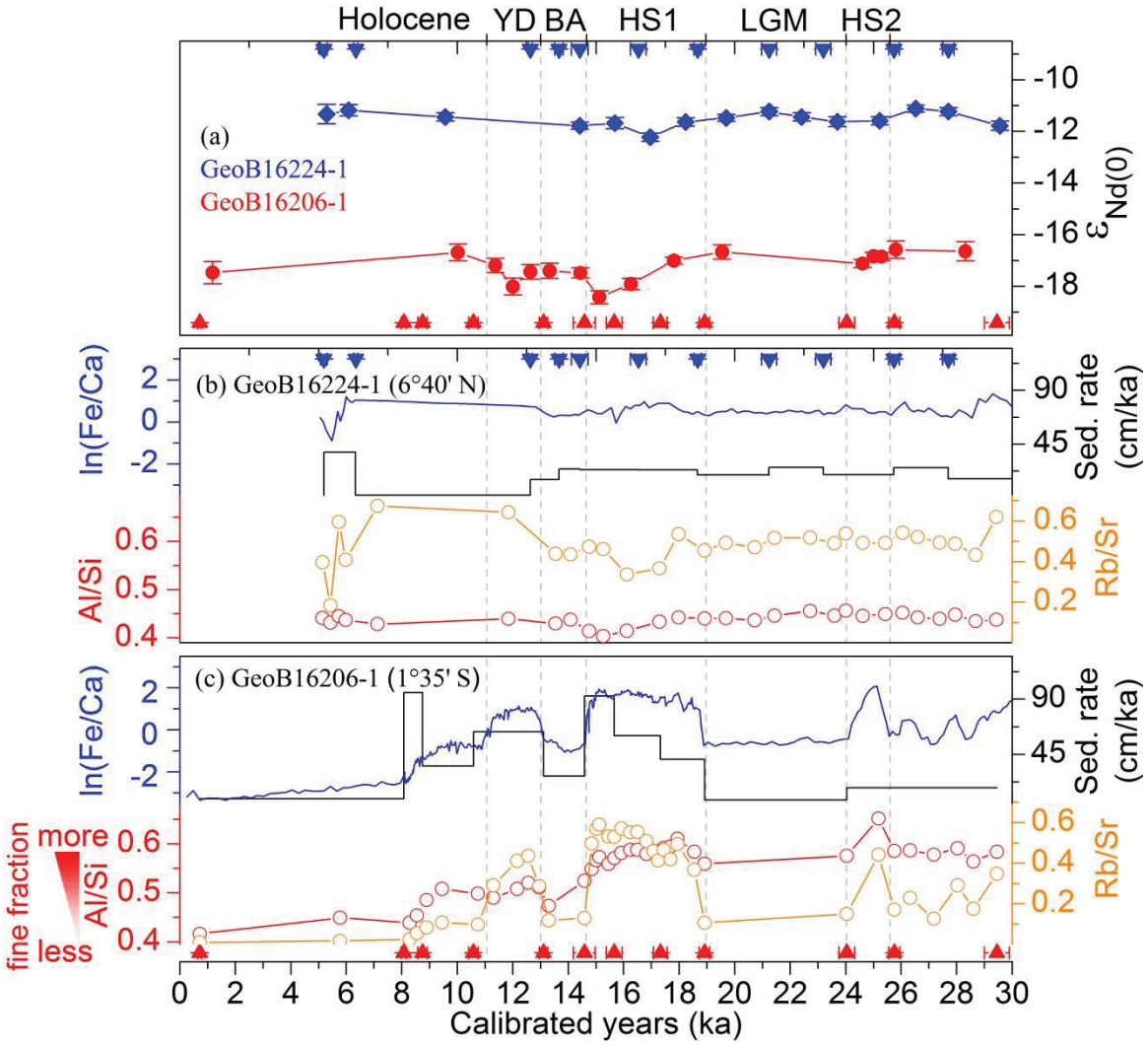

2.4.3. Nd isotopic compositions of marine near-core-top sediments, and samples from the Parnaíba River drainage basin and nearby region

The three near-core-top sediment samples collected offshore the Parnaíba River mouth show $\varepsilon_{Nd(0)}$ values ranging between -16.42 and -17.46 (Table S2-2; Fig.2-4, black dots). These values are homogeneous and similar to the values obtained downcore for GeoB16206-1.

The 49 samples characterizing different geological units from the Parnaíba River drainage basin and nearby region (orange squares in Figs.2-1, 2-4) document $\varepsilon_{Nd(0)}$ values between -15.55 and -18.56 (Table S2-4), which are also comparable with the $\varepsilon_{Nd(0)}$ data from the near-core-top and downcore sediments offshore the Parnaíba River mouth (Fig.2-4).

The two near-core-top samples collected off the Amazon River mouth (with $\varepsilon_{Nd(0)}$ values between -9.07 and -11.15, Table S2-2) and the seven near-core-top samples collected off French Guiana ($\varepsilon_{Nd(0)}$ values between -8.96 and -11.41, Table S2-2) show less negative $\varepsilon_{Nd(0)}$ values than those observed offshore the Parnaíba River mouth and from the Parnaíba River drainage basin and nearby region (Fig.2-4). Besides, the $\varepsilon_{Nd(0)}$ values of the near-core-top sediments collected off the Amazon River mouth and French Guiana are close to the $\varepsilon_{Nd(0)}$ data in sediment core GeoB16224-1 over the last 30 ka (Fig.2-4).

2.5. Discussion

The sedimentation rates off the Parnaíba River mouth during HS1 are 3-5 times higher than those of previously published sediment cores off NE Brazil (Arz et al., 1999; Jaeschke et al., 2007) (Table S2-1). Combined with the large increase in Fe/Ca record (Fig.2-3c), as a robust indicator of terrigenous (vs. marine biogenic) input (i.e. Zabel et al., 1999; Govin et al., 2012), such high sedimentation rates indicate an enhanced supply of terrigenous material to the continental margin during HS1. Although there was a southward migration (or expansion) of the Sahara-Sahel desert (Collins et al., 2013) and a strengthening of the northeast trade winds during this period (Bouimetarhan et al., 2012),

the markedly different $\varepsilon_{Nd(0)}$ values in African dust aerosols and core ODP 658C on the NW African continental slope (between -12.00 and -15.18), if compared to $\varepsilon_{Nd(0)}$ values offshore the Parnaíba River mouth (-17.45 ± 1.0; Fig.S2-4), suggest that the aeolian supply of Saharan dust has not significantly contributed to the high sedimentation rates off NE Brazil. Hence, we discuss three factors that may have caused the extremely high sedimentation rates off the Parnaíba River mouth during HS1: (i) changes in sea level (section 2.5.1); (ii) sediment supply from the Amazon River drainage basin (section 2.5.2); and (iii) changes in continental climate and erosion over the Parnaíba River drainage basin (section 2.5.3).

Fig.2-4. Summarized Nd and Sr isotopic ratios of terrestrial samples from the Amazon River drainage basin (previously published data), and those of geological terranes in the Parnaíba River drainage basin and marine sediments from MSM20/3 used in this study (see Fig.2-1 for their locations). The $\varepsilon_{Nd(0)}$ values of sediments from the Parnaíba River drainage basin were averaged by the 49 values in Table S4 (with standard error). Note that the $^{87}Sr/^{86}Sr$ on horizontal axis applies only for terrestrial samples from the Amazon Basin, and not for marine sediments from MSM20/3 (as marked by 'NA', not available).

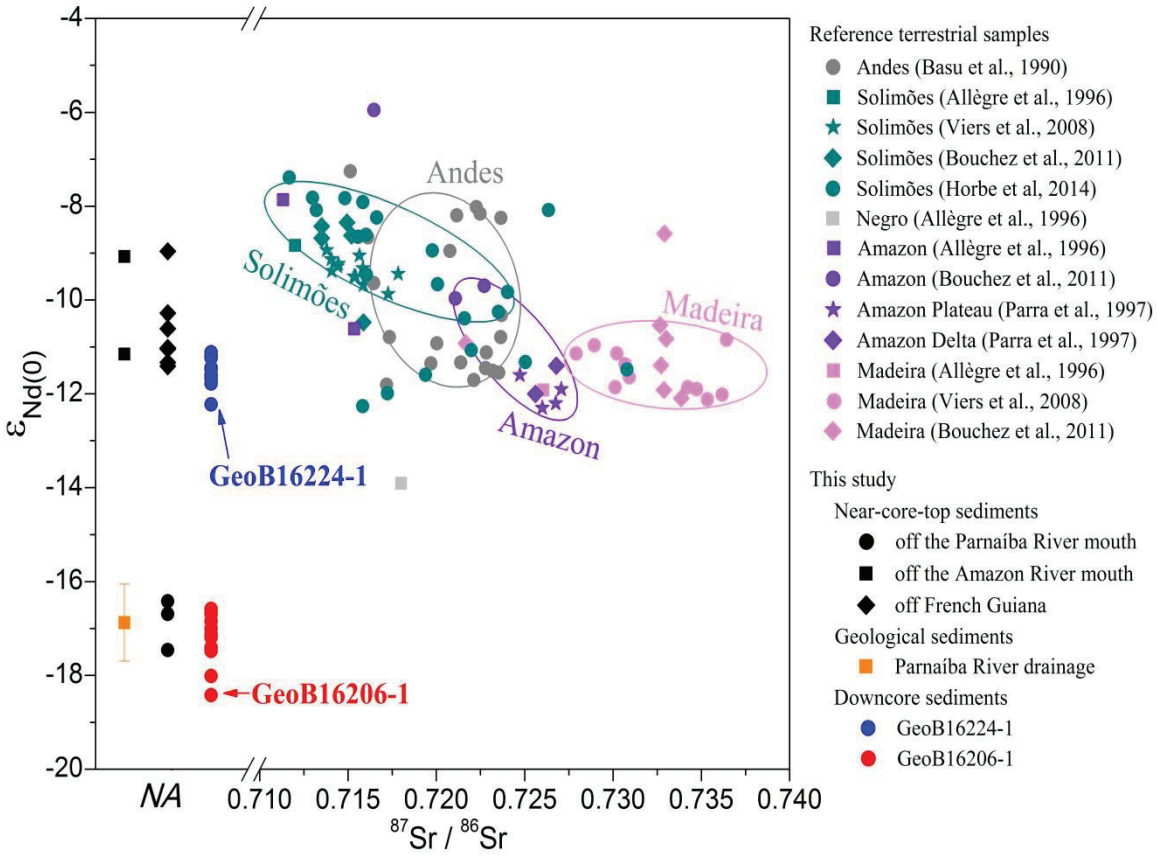

2.5.1. Changes in sea level and sedimentation rates off NE Brazil

During the last glacial period, riverine detritus were directly channeled down the continental slope and caused sedimentation rate increases in the deep Amazon Fan by 20-1000 times when sea level was ca. 120 m lower than today (i.e. Maslin et al., 2006). In contrast to the large amplitude (ca. 120 m) of glacial-interglacial sea level changes, the influence of millennial-scale sea level variations on the slope sedimentation of both large and small river systems over South America remains unclear. Aspects like (i) shift of depocenter to the continental shelf (Maslin et al., 1998), (ii) 'avulsion event' on the submarine fans (Nittrouer et al., 1995; Maslin et al., 2006) and (iii) variation of sediment discharge (i.e. Jegou et al., 2008) still require further investigation. Thus, we are only able to qualitatively assess the control of sea level changes on the sedimentation rates between the LGM and HS1, assuming similar effects of sea level changes on sediment deposition at glacial-interglacial and millennial timescales.

The increase in eustatic sea level (ca. 15 m) during HS1 (Clark et al., 2009), which largely resulted from ice sheets melting in high northern latitudes (Yokoyama et al., 2000), would tend to decrease sedimentation rates on the middle-lower continental slope off NE South America. In fact, we observe decreases of sedimentation rates in the middle-lower continental slope off southeastern Brazil (between 21°S and 23°S) and off the Amazon River mouth during HS1 (Fig.2-2b and Table S2-1). A similar situation was also reported for the continental slope off SE South America under the influence of the La Plata River drainage basin (Chiessi et al., 2008; Lantzsch et al., 2014). Conversely, the sedimentation rates off NE Brazil clearly exhibit an increase between the LGM and HS1 in both previously published (Arz et al., 1999; Jaeschke, et al., 2007) and our new data (Table S2-1). This result implies that changes in sea level are unlikely to be responsible for the large increase in sedimentation rates deposited off the Parnaíba River mouth during HS1.

2.5.2. Delivery of Amazon sediment discharge and sedimentation rates off NE Brazil

A reduction (Arz et al., 1999; Chang et al., 2008) or reversal (Schmidt et al., 2012; Nace et al., 2014) of the NBC along with a weakened AMOC might have caused Amazon sediments to be transported southeastwards, in opposition to its modern direction. Compared with the modern Amazon sediment discharge that is transported northwestwards by the NBC (ca. 8 t/s), the sediment supply from the Parnaíba River is between one to two orders of magnitude lower (ca. 0.2 t/s, Allison et al., 2000; Nace et al., 2014). To clarify if the Amazon sediments could be responsible for the marked increase in sedimentation rates offshore NE Brazil during HS1, we summarize previously published Nd and Sr isotopic ratios of terrestrial materials from different geological settings in the Amazon River drainage basin, such as fluvial sands from the Andean foreland basin, suspensions and bedloads from various Amazon River tributaries (Figs.2-1, 2-4).

The $\varepsilon_{Nd(0)}$ values at core site GeoB16224-1 and seven near-core-top samples also collected off French Guiana as well as two near-core-top samples collected off the Amazon River mouth are compatible with those from the Amazon River drainage basin (Fig.2-4) (Basu et al., 1990; Allègre et al., 1996; Parra et al., 1997; Viers et al., 2008; Bouchez et al., 2011; Horbe et al., 2014). This result confirms that the Amazon-sourced terrigenous component dominates the marine sediments deposited off the Amazon River mouth and French Guiana, but our $\varepsilon_{Nd(0)}$ data alone are insufficient to further differentiate between Amazonian sub-regions such as the Solimões River and the Madeira River. Interestingly, the $\varepsilon_{Nd(0)}$ values between -16.50 and -18.50 at core site GeoB16206-1 and three near-core-top samples (with late Holocene ages) collected offshore the Parnaíba River mouth are significantly different from those of samples collected to the northwest of the Amazon River mouth (-11.65 ± 0.5) (Fig.2-4). It is worthy of note that marine carbonates may influence the $\varepsilon_{Nd(0)}$ values of bulk sediment. However, due to the high terrigenous content of the analyzed bulk sediments and the low rare earth elements concentrations of marine carbonates, this effect is very limited (i.e. less than 1 ε unit generally; Bayon et al., 2002). Nevertheless, the large difference between $\varepsilon_{Nd(0)}$ values of

cores GeoB16224-1 (-11.65 ± 0.5) and GeoB16206-1 (-17.45 ± 1.0) marks the most remarkable geochemical feature of sediments deposited to the northeast and the southeast of the Amazon River mouth over the last 30 ka (Fig.2-3a). We thus suggest that the terrigenous sediments deposited off NE Brazil (i.e. at our core site GeoB16206-1) are not affected by an Amazonian source.

Instead, the $\varepsilon_{Nd(0)}$ values of core GeoB16206-1 and three near-core-top sediments collected off the Parnaíba River mouth are compatible with those from different lithostratigraphic units within the Parnaíba River drainage basin and nearby region (Fig.2-4 and Table S2-4). Because the contribution of Amazon sediments can be convincingly excluded, it seems that the Parnaíba River drainage basin is the main source of terrigenous materials deposited at core site GeoB16206-1.

2.5.3. Climate changes and erosion patterns in the Parnaíba River drainage basin and sedimentation rates off NE Brazil

$\varepsilon_{Nd(0)}$ was broadly used to determine the origin of riverine sediments and its relationship with past climate changes (i.e. Jung et al., 2004; Colin et al., 2006; Cole et al., 2009; Ali et al., 2015). At core site GeoB16206-1 off the Parnaíba River mouth, the small variability of $\varepsilon_{Nd(0)}$ values throughout the last 30 ka indicates no significant changes in the origin of terrigenous materials. However, Al/Si and Rb/Sr ratios from the same core are increased during HS1 and the YD (Fig.2-3c and Table S2-3), i.e. at times when conditions over NE Brazil were wetter (Wang et al., 2004; Jacob et al., 2007). We propose that the increases in Al/Si and Rb/Sr ratios are probably associated with the changes of fluvial processes in the Parnaíba River drainage basin during such millennial-scale intervals.

Al/Si ratios in riverine sediments are related to the relative content of clay (enriched in Al) and coarser quartz (enriched in Si), and can hence be used as proxy for grain size distribution (i.e. McLennan et al., 1993). Rb/Sr ratios also increase with decreasing particle size, because the mica-enriched clay fraction is characterized by high Rb/Sr, and coarser feldspar-enriched sediments by low Rb/Sr values (Hemming, 2007). Overall,

strengthening of physical sorting increase both the Al/Si and Rb/Sr ratios in the fine grained fractions, reflecting a high amount of clays relative to other minerals (Cole et al., 2009).

Therefore, the increased Al/Si and Rb/Sr ratios from core GeoB16206-1 during HS1 and the YD (Fig.2-3c and Table S2-3) indicate an increased proportion of fine-grained sediments within the extremely high fluvial input delivered by the Parnaíba River. Unlike HS1, we note only one (zero) sample during HS2 (the LGM) measured for Al/Si and Rb/Sr ratios, which hinders a full discussion of changes over HS2 (the LGM) (Fig.2-3c and Table S2-3). The sediment core GeoB16224-1 collected to the northwest of the Amazon River mouth exhibits minor Al/Si and Rb/Sr changes over the last 30 ka (Fig.2-3b and Table S2-3), which suggest minor past changes in the relative proportions of fine vs. coarse-grained sediments transported by the Amazon River. Since the westernmost Amazon probably underwent increased precipitation during HS1 (i.e. Mosblech et al., 2012), it is hence likely that, before reaching our core site, the climate signals imprinted in the Al/Si and Rb/Sr proxies were blurred by grain-sorting through the long distance transport pathway from the eastern Andes to the western tropical Atlantic (i.e. Roddaz et al., 2005; Bouchez et al., 2011).

In summary, we propose that increased precipitation strengthened the fluvial processes (i.e. physical erosion, sediment sorting) in the Parnaíba River drainage basin (and possibly also in other smaller drainage basins in NE Brazil) during HS1 and the YD. During such intervals, the AMOC reduction, probably in relation to meltwater input into the high latitudes of the North Atlantic (i.e. Bond et al., 1992; Gherardi et al. 2009), induced a steeper latitudinal temperature gradient (i.e. Maslin et al., 2011) by cooling surface waters of the northern North Atlantic (i.e. Bard et al., 2000) and warming surface waters of the tropical Atlantic (i.e. Rühlemann et al., 1999). This steeper temperature gradient led to a strengthening in the zonal component of the northeast trade winds and a southward displacement of the tropical rainbelt (i.e. the ITCZ mean position), which, as a result, increased terrestrial precipitation in NE Brazil (Wang et al., 2004; Cruz et al., 2009). It subsequently caused an intensification of physical erosion over the continent and

an enhancement of fluvial sediment input to the western tropical South Atlantic (Arz et al., 1998; Dupont, et al., 2010). Meanwhile, a reduced NBC during such periods, triggered by a weakened AMOC, most probably also allowed the enhanced input of terrigenous materials to settle down in the continental margin offshore NE Brazil, resulting in the extraordinarily high sedimentation rates.

2.6. Conclusions

We show that a depocenter with extremely high sedimentation rates of terrigenous materials existed directly offshore the Parnaíba River mouth (NE Brazil) during HS1 and the YD. Sediments from this depocenter show homogeneous $\varepsilon_{Nd(0)}$ values (from -16.50 to -18.50) during the last 30 ka, which are characteristic of terrigenous material derived from the Parnaíba River drainage basin. In contrast, $\varepsilon_{Nd(0)}$ values of the sediments off French Guiana range between -11.11 and -12.22, and are characteristic of terrigenous material from the Amazon River drainage basin. Although the development of the depocenter off NE Brazil might have been promoted by a more sluggish transport with the NBC, our $\varepsilon_{Nd(0)}$ results do not support a southeastward transport of Amazon suspension to the NE Brazilian continental margin, as expected due to a reversal of the NBC. Without a major change in the source area throughout the last 30 ka, increased Fe/Ca ratios in sediment cores off the Parnaíba River mouth during HS1 and the YD must be interpreted as increased river suspension input. Increased Al/Si and Rb/Sr ratios suggest an intensification of fluvial physical sorting in the Parnaíba River drainage basin, probably in response to increased terrestrial precipitation over NE Brazil.

2.7. Acknowledgements

We thank three anonymous Reviewers and Dr. M. Frank (Editor) for constructive comments that greatly improved this manuscript. We sincerely appreciate the technical support from Dr. M. Segl for ^{14}C AMS measurements, S. Pape for the EDP-XRF analyses, Dr. U. Röhl and V. Lukies for the XRF scanning, as well as I.R. Uriarte for Nd isotopic measurements. We acknowledge the Department of Geosciences and the GeoB Core

Repository at MARUM - University of Bremen for supplying sediment samples. All the data presented in this paper are archived in Pangaea (www.pangaea.de). This work was funded by the Deutsche Forschungsgemeinschaft through the DFG Research Centre/Cluster of Excellence 'The Ocean in the Earth System'. C.M.C. was also supported by FAPESP (grant 2012/17517-3) and the Hanse Institute for Advanced Study in Delmenhorst, Germany.

2.8. References

Ali, S., et al. 2015. South Asian monsoon history over the past 60 kyr recorded by radiogenic isotopes and clay mineral assemblages in the Andaman Sea. Geochem. Geophys. Geosyst., 16, 505-521.

Allègre, C.J., et al. 1996. Sr-Nd-Pb isotope systematics in Amazon and Congo River systems: Constraints about erosion processes. Chem. Geol. 131, 93-112.

Allison, M.A., et al. 2000. Origin of Amazon mudbanks along the northeastern coast of South America. Mar. Geol. 163(1-4), 241-256.

Arz, H.W., Pätzold, J., Wefer, G., 1998. Correlated millennial-scale changes in surface hydrography and terrigenous sediment yield inferred from last-glacial marine deposits off northeastern Brazil. Quaternary Res. 50, 157-166.

Arz, H.W., Pätzold, J., Wefer, G., 1999. The deglacial history of the western Tropical Atlantic as inferred from high resolution stable isotope records off northeastern Brazil. Earth Planet. Sci. Lett. 167, 105-117.

Bard, E., 1988. Correction of accelerator mass spectrometry ^{14}C ages measured in planktonic foraminifera: Paleoceanographic implications. Paleoceanography 3(6), 635-645.

Bard, E., et al. 2000. Hydrological Impact of Heinrich Events in the Subtropical Northeast Atlantic. Science 289, 1321-1324.

Basu, A.R., Sharma, M., DeCelles, P.G., 1990. Nd, Sr-isotopic provenance and trace element geochemistry, Bolivia and Peru. Earth Planet. Sci. Lett. 100(1-3), 1-17.

Bayon, G., et al. 2002. An improved method for extracting marine sediment fractions and its application to Sr and Nd isotopic analysis. Chem. Geol. 187, 179-199.

Böhm, E., et al. 2015. Strong and deep Atlantic meridional overturning circulation during the last glacial cycle. Natrue 517, 73-76.

Bond, G.C., et al. 1992. Evidence for massive discharges of icebergs into the North Atlantic ocean during the last glacial period. Nature 360, 245-249.

Bouchez, J., et al. 2011. Grain size control of river suspended sediment geochemistry: Clues from Amazon River depth profiles. Geochem. Geophys. Geosyst. 12, Q03008, doi: 10.1029/2010gc003380.

Bouimetarhan, I., et al. 2012. Sahel megadrought during Heinrich Stadial 1: Evidence for a three-phase evolution of the low- and mid-level West African wind system. Quat. Sci. Rev. 58, 66-76.

Chang, P., et al. 2008. Oceanic link between abrupt changes in the North Atlantic Ocean and the African monsoon. Nat. Geosci. 1, 444-448.

Chiessi, C.M., et al. 2008. South Atlantic interocean exchange as the trigger for the Bølling warm event. Geology 36 (12), 919-922.

Clark, P.U., et al. 2009. The Last Glacial Maximum. Science 325, 710-714.

Cole, J.M., et al. 2009. Contrasting compositions of Saharan dust in the eastern Atlantic Ocean during the last deglaciation and African Humid Period. Earth Planet. Sci. Lett. 278, 257-266.

Colin, C., et al. 2006. Evolution of weathering patterns in the Indo-Burman Ranges over the last 280 kyr: Effects of sediment provenance on $^{87}Sr/^{86}Sr$ ratios tracer. Geochem. Geophys. Geosyst.,7, Q03007, doi:10.1029/2005GC000962.

Collins, J.A., et al. 2013. Abrupt shifts of the Sahara-Sahel boundary during Heinrich Stadials. Clim. Past 9, 1181-1191.

Cruz, F.W., et al. 2009. Orbitally driven east-west antiphasing of South American precipitation. Nat. Geosci. 2, 210-214.

De Paolo, D.J., 1981. Neodymium isotopes in the Colorado Front Range and implications for crust formation and mantle evolution in the Proterozoic. Nature 291, 193-197.

Dupont, L.M., et al. 2010. Two-step vegetation response to enhanced precipitation in Northeast Brazil during Heinrich event 1. Global Change Biol. 16, 1647-1660.

Gherardi, J., et al. 2009. Glacial-interglacial circulation changes inferred from $^{231}Pa/^{230}Th$ sedimentary record in the North Atlantic region. Paleoceanography 24, PA2204, doi:10.1029/2008pa001696.

Govin, A., et al. 2012. Distribution of major element ratios in Atlantic surface sediments (36°N-49°S): imprint of terrigenous input and continental weathering. Geochem. Geophys. Geosyst. 13, Q01013, doi: 10.1029/2011gc003785.

Hemming, S.R., 2007. Terrigenous sediments. In: Elias, S.A. (Ed.), Encyclopedia of Quaternary Science, 3. Elsevier, Oxford, pp. 1776-1785.

Horbe, A.M.C., et al. 2014. Provenance of quaternary and modern alluvial deposits of the Amazonian floodplain (Brazil) inferred from major and trace elements and Pb-Nd-Sr isotopes. Palaeogeogr. Palaeoclimatol. Palaeoecol. 411, 144-154.

Jacob, J., et al. 2007. Paleohydrological changes during the last deglaciation in Northern Brazil. Quat. Sci. Rev. 26, 1004-1015.

Jacobsen, S.B., and Wasserburg, G.J., 1980. Sm-Nd isotopic evolution of chondrites. Earth Planet. Sci. Lett. 50, 139-155.

Jaeschke, A., et al. 2007. Coupling of millennial-scale changes in sea surface temperature and precipitation off northeastern Brazil with high-latitude climate shifts during the last glacial period. Paleoceanography 22(4), doi:10.1029/2006PA001391.

Jegou, I., et al. 2008. Channel-mouth lobe complex of the recent Amazon Fan: The missing piece. Mar. Geol. 252, 62-77.

Jennerjahn, T.C., et al. 2004. Asynchronous terrestrial and marine signals of climate change during Heinrich Events. Science 306(5705), 2236-2239.

Johns, W.E., et al. 1998. Annual cycle and variability of the North Brazil Current. J. Phys. Oceanogr. 28(1), 103-128.

Jung, S.J.A., et al. 2004. Stepwise Holocene aridification in NE Africa deduced from dust-borne radiogenic isotope records. Earth Planet. Sci. Lett. 221, 27-37.

Lantzsch, H., et al. 2014. The high-supply, current-dominated continental margin of southeastern South America during the late Quaternary. Quaternary Res. 81, 339-354.

Lentz, S.J., 1995. Seasonal variations in the horizontal structure of the Amazon Plume inferred from historical hydrographic data, J. Geophys. Res.-Oceans, 100, 2391-2400.

Maslin, M., et al. 1998. Sea-level- and gas-hydrate-controlled catastrophic sediment failures of the Amazon Fan. Geology , 26 (12), 1107-1110.

Maslin, M.A., et al. 2011. Dynamic boundary-monsoon intensity hypothesis: evidence from the deglacial Amazon River discharge record. Quat. Sci. Rev. 30, 3823-3833.

Maslin, M.A., Knutz, P.C., Ramsay, T., 2006. Millennial-scale sea-level control on avulsion events on the Amazon Fan. Quat. Sci. Rev. 25, 3338-3345.

McLennan, S.M., et al. 1993. Geochemical approaches to sedimentation, provenance, and tectonics. Geol. Soc. Am. Spec. Pap. 284, 21-40.

Mosblech, N.A.S., et al. 2012. North Atlantic forcing of Amazonian precipitation during the last ice age. Nat. Geosci. 5, 817-820.

Mulitza, S., et al. 2013. Response of Amazon sedimentation to deforestation, land use and climate variability. Cruise No. MSM20/3 (February 19 - March 11, 2012), Recife (Brazil) - Bridgetown (Barbados). MARIA S. MERIAN-Berichte, MSM20/3, 86 pp., DFG Senatskommission für Ozeanographie, doi:10.2312/cr_msm20_3.

Nace, T.E., et al. 2014. The role of North Brazil Current transport in the paleoclimate of the Brazilian Nordeste margin and paleoceanography of the western tropical Atlantic during the late Quaternary. Palaeogeogr. Palaeoclimatol. Palaeoecol. 415, 3-13.

Nittrouer, C.A., et al. 1995. An introduction to the geological significance of sediment transport and accumulation on the Amazon continental shelf. Mar. Geol. 125(3-4), 177-192.

Parra, M., et al. 1997. Sr-Nd isotopes as tracers of fine-grained detrital sediments the South-Barbados during the last 150 kyr. Mar. Geol. 136(3-4), 225-243.

Reimer, P.J., et al. 2013. IntCal13 and Marine13 radiocarbon age calibration curves 0-50,000 years cal BP. Radiocarbon 55(4), 1869-1887.

Roddaz, M., Viers, J., Brusset, S., Baby, P., Hérail, G., 2005. Sediment provenances and drainage evolution of the Neogene Amazonian foreland basin. Earth Planet. Sci. Lett. 239(1-2), 57-78.

Rühlemann, C., et al. 1999. Warming of the tropical Atlantic Ocean and slowdown of thermohaline circulation during the last deglaciation. Nature 402, 511-514.

Schmidt, M.W., et al. 2012. Impact of abrupt deglacial climate change on tropical Atlantic subsurface temperatures. Proc. Natl. Acad. Sci. USA. 109, 14348-14352.

Stuiver, M., Reimer, P. J., 1993. Extended ^{14}C database and revised CALIB radiocarbon calibration program. Radiocarbon 35, 215-230.

Viers, J., et al. 2008. Seasonal and provenance controls on Nd-Sr isotopic compositions of Amazon rivers suspended sediments and implications for Nd and Sr fluxes exported to the Atlantic Ocean. Earth Planet. Sci. Lett. 274(3-4), 511-523.

Wang, X., et al. 2004. Northeastern Brazil wet periods linked to distant climate anomalies and rainforest boundary changes. Nature 432, 740-743.

Weltje, G.J., and Tjallingii, R., 2008. Calibration of XRF core scanners for quantitative geochemical logging of sediment cores: Theory and application. Earth Planet. Sci. Lett. 274(3-4), 423-438.

Wilson, K.E., Maslin, M.A., Burns, S.J., 2011. Evidence for a prolonged retroflection of the North Brazil Current during glacial stages. Palaeogeogr. Palaeoclimatol. Palaeoecol. 301, 86-96.

Yokoyama, Y., et al. 2000. Timing of last glacial maximum from observed sea level minima. Nature 406, 713-716.

Zabel, M., et al. 1999. Significance of the sedimentary Al/Ti ratio as an indicator for variations in the circulation patterns of the equatorial North Atlantic. Paleoceanography 14(6), 789-799.

Zhang, D., et al. 2011. Multidecadal variability of the North Brazil Current and its connection to the Atlantic meridional overturning circulation. J. Geophys. Res. 116, C04012, doi: 10.1029/2010JC006812.

Zhang, R., and Delworth, T.L., 2005. Simulated tropical response to a substantial weakening of the Atlantic thermohaline circulation. J. Climate. 18, 1853-1860.

2.9. Supplementary Material

2.9.1. Chronologies of the cores dated by stable isotope stratigraphy or stratigraphic alignment of downcore properties

We describe here the chronologies of sediment cores defined by stable isotope stratigraphy (24) or stratigraphic alignment of downcore properties (14), all of which refer to the published age model of the selected cores (see Table S2-1 for reference of each individual core in details).

For the cores with stable isotope stratigraphy, their chronologies were constrained by oxygen ($\delta^{18}O$) record of planktonic (i.e. *G. ruber*, *G. sacculifer*) or benthic (i.e. *P. wuellerstorfi*, *C. wuellerstorfi*, *Cibicidoides spp.*) foraminifera (see Fig.S2-1 below). To determine the quality of the published age models, we compare the planktonic or benthic $\delta^{18}O$ record of each selected core with that of the reference core respectively (Fig. S1). For core RC16-66, we show the sedimentation rates obtained by the same age model of planktonic $\delta^{18}O$ alignment (which was not available at PANGAEA and NOAA/NCDC database). Chronologies of reference cores were based on (i) ^{14}C dates (cores GIK16458-2, V19-30, KNR110-82), (ii) the alignment of $\delta^{18}O$ records to the astronomically tuned SPECMAP stack (core RC11-120, Martinson et al., 1987), (iii) astronomical tuning for the SPECMAP planktonic $\delta^{18}O$ stack (Imbrie et al., 1984) and (iv) orbital tuning for the LR04 benthic $\delta^{18}O$ stack (Lisiecki and Raymo 2005).

For the cores dated by stratigraphic alignment of downcore properties (Fig.S2-2 below), used proxies include XRF data, carbonate data and planktonic $\delta^{18}O$ records for cores GeoB3117-1, GeoB3176-1, GeoB3229-2 and V16-20 (see Fig. S2-2 for planktonic $\delta^{18}O$ data of cores GeoB3229-2 and V16-20, since the XRF or carbonate data are unavailable), magnetic susceptibility of core GeoB2822-2 and ODP sites 925-929, terrigenous fraction of cores V19-303, V20-241, V25-44 and V26-41. Chronologies of their reference cores were based on (i) ^{14}C ages (core GeoB3104-1, M13289-2, GeoB3129-1/GeoB3911-3), (ii) orbital tuning of susceptibility (core GeoB2821-1, Gingele, et al. 1999), (iii) astronomical tuning for the SPECMAP $\delta^{18}O$ curve (ODP 677, Mix et al., 1995).

Fig.S2-1. Published age models of the cores (24 in total) dated by stable isotope stratigraphy in this study (planktonic or benthic foraminifera, number of each core is the same as given in Table S2-1). The sediment core (black) and its target curve (orange, triangles mark available ^{14}C dates) are showed individually.

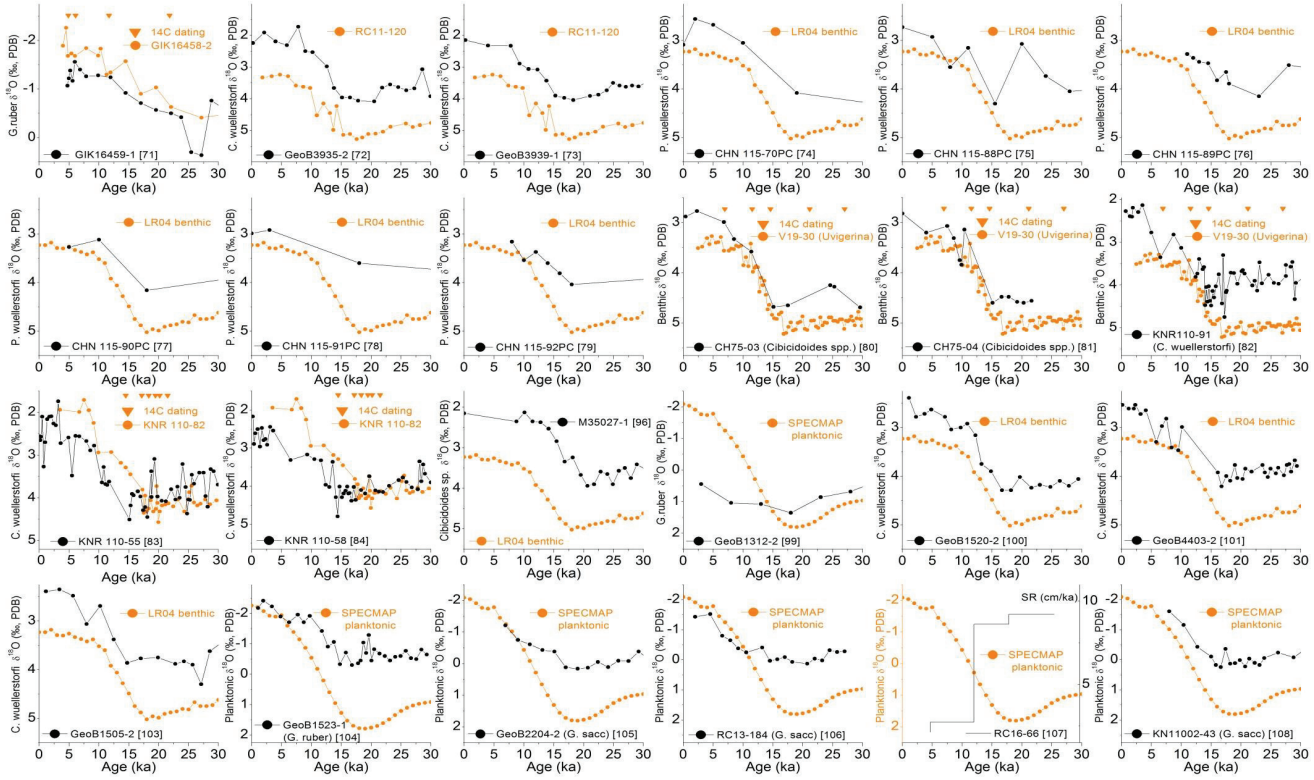

Fig.S2-2. The same as Fig.S2-1 but for those (14 in total) dated by stratigraphic alignment of various downcore properties (i.e. lithology, magnetic susceptibility). The sediment core (black) and its target curve (orange, triangles mark available ^{14}C dates) are showed individually.

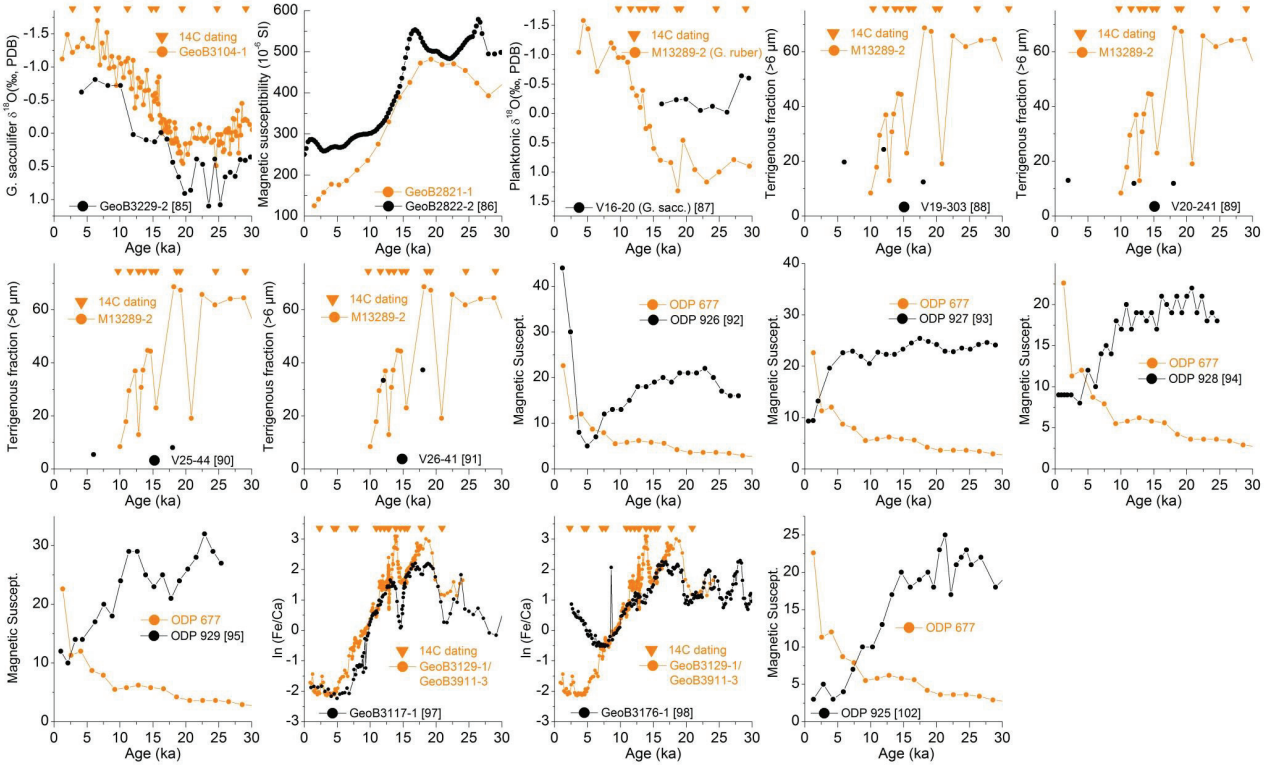

In general, age models of the selected sediment cores constrained by stratigraphic alignment of downcore properties were less precise than those dated by stable isotope stratigraphy. However, these increased age uncertainties have little influence on sedimentation rate estimates during HS1 and the LGM (see below).

2.9.2. Estimation of LGM and HS1 sedimentation rates and error propagation (95% uncertainties) in MATLAB algorithm

To assess the uncertainty in the thickness of the sediment layer deposited during the LGM and HS1, we produced about 10,000 age models for each core based on the available dating approach through Monte Carlo resampling (Blaauw, 2010). For cores with radiocarbon dates, calibrated 95% probability age distributions were recalculated using the IntCal13 calibration curve (Reimer et al. 2013) and standard calibration methods (Stuiver and Reimer, 1993). For age control points not derived by radiocarbon dating (i.e. based on stable isotope stratigraphy or graphic correlation of downcore proxies), we assumed a constant error of 1500 years (2σ). Random samples were drawn from the probability distributions to produce about 10,000 realizations of the age-depth relationship. Runs with age reversals were discarded. For each core within Monte Carlo run, the thickness of the LGM (23-19 ka) and HS1 (18-15 ka) period was calculated through linear interpolation. From all estimates of the LGM and HS1 thickness for a given core, we calculated the mean and the 95% non-parametric error through the 2.5 and 97.5 percentiles.

Among the radiocarbon dated sediment cores (as in Table S2-1), we note that the ^{14}C-AMS ages of the cores from CLIMAP (1976) were based on the measurements of carbonates rather than foraminifera. To estimate the sedimentation rates of these cores, we supposed an increased reservoir age value (i.e. 1500 years) instead of 400 ± 100 years for their ^{14}C -AMS age control points. The large age uncertainties of chronologies in sediment cores dated by stratigraphic alignment of downcore properties (i.e. magnetic susceptibility, terrigenous fraction) have little influence on the estimation of sedimentation rates during the LGM and HS1, because the sediment deposition at these

sites was very low (<5 cm/ka) over the last 30 ka at least (see Table S2-1 for further details).

2.9.3. Major element composition

2.9.3.1. The XRF scanning

At the XRF-scanning laboratory (MARUM, University of Bremen), The split core surface was covered with a 4 μm thin SPEXCerti Prep Ultralene1 foil to avoid contamination of the measurement unit and desiccation of the sediment. The XRF core-scanner uses a Canberra X-PIPS Silicon Drift Detector (Model SXD 15C-150-500) with 150eV X-ray resolution, a Canberra Digital Spectrum Analyzer DAS 1000, and an Oxford Instruments 50W XTF5011 X-Ray tube with rhodium (Rh) target material. The XRF data (expressed as counts per second, cps) were collected downcore over an area of 0.15 cm^2 with generator settings of 10 kV, a current of 0.40 mA, and a sampling time of 20 seconds. Raw data were processed by the analysis of X-ray spectra by the Iterative Least square software package (WIN AXIL) from Canberra Eurisys.

2.9.3.2. EDP-XRF measurement

At room temperature, bulk sediment samples were taken with 10-ml cut syringes in the working halves of cores GeoB16206-1 and GeoB16224-1, respectively. Samples were freeze-dried, powdered and homogenized using an agate mortar, and prepared for measurement by energy dispersive polarization XRF (EDP-XRF) spectroscopy at the Inorganic Geochemistry laboratory (MARUM, University of Bremen). Measurements were performed with a PANalytical Epsilon3-XL XRF spectrometer equipped with a rhodium tube, several filters and a SSD5 detector. The precision and accuracy of measurements were assessed by repeated analyses of the certified standard reference material MAG-1 (Govindaraju, 1994), and the standard deviation of replicated sediment samples was in our case less than 1.5%.

Fig.S2-3. The comparison between XRF intensity and EDP-XRF data of two sediment cores. Downcore ln(Fe/Ca) variations obtained from the XRF-scanning major element proportions (grey line) and the EDP-XRF measurements (crossed dots) are presented versus depth for cores: A. GeoB16224-1 (R^2=0.73), B. GeoB16206-1(R^2=0.99). The R^2 value is the mean R^2 of all element/Ca log-ratio regressions (Weltje and Tjallingii, 2008).

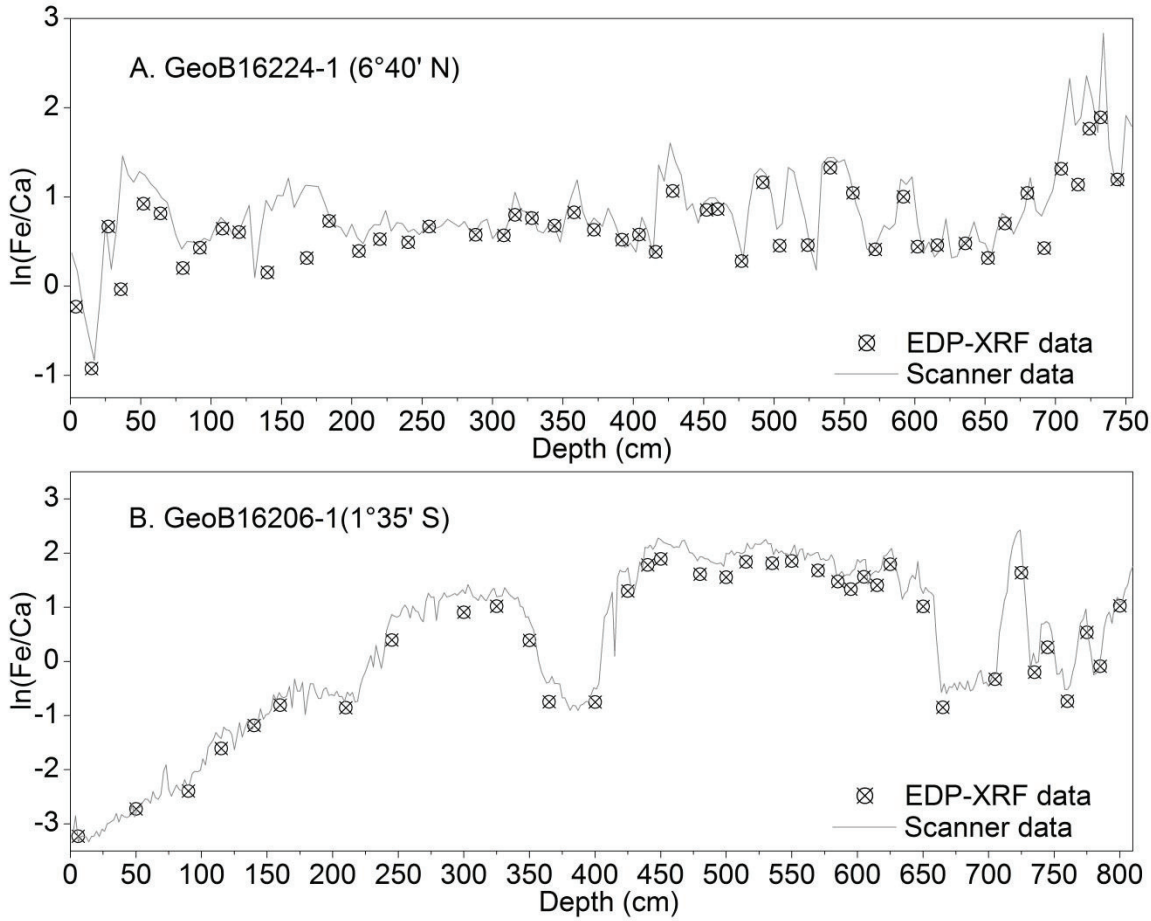

2.9.4. $^{143}Nd/^{144}Nd$ isotopic composition

At CPGeo (Center for Geochemical Research, University of São Paulo), all chemical procedures were carried out in an ultra-clean laboratory class 10,000, equipped with laminar flow fumes class 100. The sediment powder was dissolved by acid digestion using HNO_3 + HF and HCl (purified in the sub-boiling device Distiller STD-1000 at low temperatures) in discrete steps in teflon beakers (Savillex®), at a temperature of 100º C. The Nd was separated from other rare earths firstly by a specific resin (RE-Spec) and secondly by the resin Ln-Spec. Then, Nd samples were deposited in rhenium parallel filaments with the addition of ultra-pure H_2O. The $^{143}Nd/^{144}Nd$ ratios were obtained by

thermal ionization mass spectrometry (TIMS), using the spectrometer Finnigan Triton. Replicate analysis of JNdi standard (n=19) yielded $^{143}Nd/^{144}Nd$ = 0.512093 ± 0.000009 (1σ). Nd procedure blanks were about 70 pg.

At the Laboratory of Geochronology, University of Brasília, the analysis of Nd isotopic ratios were implemented by similar techniques. The sediment powder was dissolved in teflon beakers (Savillex®) by diluted acetic acid (0.5 N) for carbonate components of the samples. Nd extraction from the sample dissolution was conducted by cation exchange columns loaded with HDEHP (di-2-ethylhexeyl phosphoric acid) supported on teflon resin. Then, Nd samples were loaded onto Re evaporation filaments of a double filament assembly and the isotopic ratios were analyzed by a Finningan MAT-262 multi-collector mass spectrometer in static mode. The uncertainties in the individual analyses of $^{143}Nd/^{144}Nd$ ratios were lower than 0.005% (2σ), based on repeated analyses of the BHVO-1 standard.

Fig.S2-4. Comparison of $\varepsilon_{Nd(0)}$ and $^{87}Sr/^{86}Sr$ data between dust/aerosol from the Sahara/Sahel region and marine sediments off western Africa and those in Fig.4 (with the same symbols).

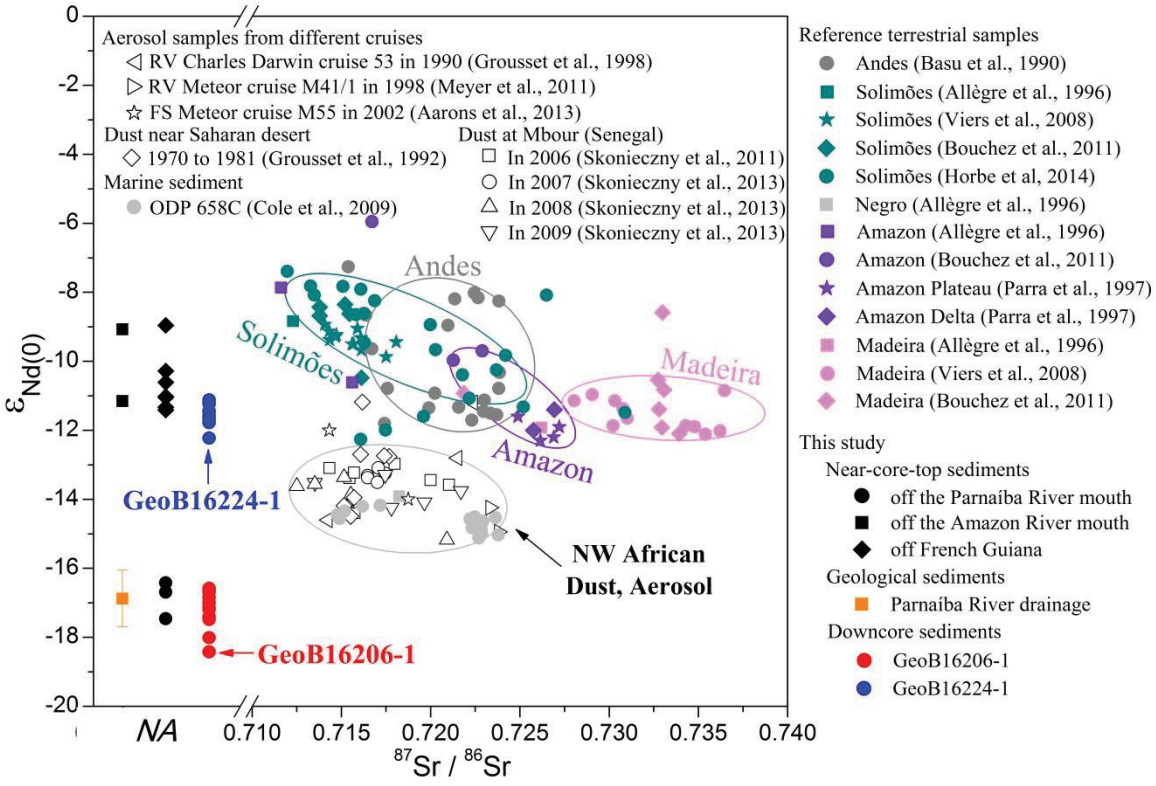

2.9.5. References

Aarons, S.M., Aciego, S.M., Gleason, J.D., 2013. Variable Hf-Sr-Nd radiogenic isotopic compositions in a Saharan dust storm over the Atlantic: Implications for dust flux to oceans, ice sheets and the terrestrial biosphere. Chem. Geol. 349-350, 18-26.

Allègre, C.J., et al. 1996. Sr-Nd-Pb isotope systematics in Amazon and Congo River systems: Constraints about erosion processes. Chem. Geol. 131, 93-112.

Basu, A.R., Sharma, M., DeCelles, P.G., 1990. Nd, Sr-isotopic provenance and trace element geochemistry, Bolivia and Peru. Earth Planet. Sci. Lett. 100(1-3), 1-17.

Blaauw, M., 2010. Methods and code for 'classical' age-modelling of radiocarbon sequences. Quaternary Geochronology 5, 512-518.

Bouchez, J., et al. 2011. Grain size control of river suspended sediment geochemistry: Clues from Amazon River depth profiles. Geochem. Geophys. Geosyst. 12, Q03008, doi: 10.1029/2010gc003380.

CLIMAP Project Members. 1976. The surface of the ice-age earth. Science, 191, 1131-1144.

Cole, J.M., et al. 2009. Contrasting compositions of Saharan dust in the eastern Atlantic Ocean during the last deglaciation and African Humid Period. Earth Planet. Sci. Lett. 278, 257-266.

Gingele, F., et al. 1999. Terrigenous flux in the Rio Grande Rise area during the last 1.5 Ma: evidence of deepwater advection or rapid response to continental rainfall patterns. Paleoceanography, 14(1), 84-95.

Govindaraju, K., 1994. 1994 Compilation of working values and sample description for 383 geostandards. Geostand. Newsl. 18, 1-158.

Grousset, F.E., et al. 1998. Saharan wind regimes traced by the Sr-Nd isotopic composition of subtropical Atlantic sediments: Last Glacial Maximum vs today. Quat. Sci. Rev. 17(4-5), 395-409.

Grousset, F.E., et al. 1992. Origins of peri-Saharan dust deposits traced by their Nd and Sr isotopic composition. Palaeogeogr. Palaeoclimatol. Palaeoecol. 93(3-4), 203-212.

Horbe, A.M.C., et al. 2014. Provenance of quaternary andmodern alluvial deposits of theAmazonian floodplain (Brazil) inferred from major and trace elements and Pb-Nd-Sr isotopes. Palaeogeogr. Palaeoclimatol. Palaeoecol. 411, 144-154.

Imbrie et al., 1984. The orbital theory of Pleistocene climate: Support from a revised chronology of the marine $\delta^{18}O$ record. In A.L. Berger (Ed.), et al., Milankovitch and Climate, Part 1, Reidel, The Netherlands pp. 269-305.

Lisiecki, L.E., and Raymo., M.E., 2005. A Pliocene-Pleistocene stack of 57 globally distributed benthic $\delta^{18}O$ records. Paleoceanography, Vol. 20, PA1003, doi:10.1029/2004PA001071.

Martinson, D.G., et al. 1987. Age Dating and the orbital theory of the ice ages: development of a high-resolution 0 to 300,000-year chronostratigraphy. Quaternary Research, 27, 1-29

Meyer, I., et al. 2011. Grain size control on Sr-Nd isotope provenance studies and impact on paleoclimate reconstructions: An example from deep-sea sediments offshore NW Africa. Geochem. Geophys. Geosyst. 12, Q03005, doi:10.1029/2010GC003355.

Mix, A.C., et al. 1995. Benthic foraminifer stable isotope record from Site 849 (0-5 Ma): local and global climate changes. In: Pisias, NG; Mayer, LA; Janecek, TR; Palmer-Julson, A; van Andel, TH (eds.), Proceedings of the Ocean Drilling Program, Scientific Results, College Station, TX (Ocean Drilling Program), 138, 371-412.

Parra, M., et al. 1997. Sr-Nd isotopes as tracers of fine-grained detrital sediments the South-Barbados during the last 150 kyr. Mar. Geol. 136(3-4), 225-243.

Reimer, P.J., et al. 2013. IntCal13 and Marine13 radiocarbon age calibration curves 0-50,000 years cal BP. Radiocarbon 55(4), 1869-1887.

Skonieczny, C., et al. 2011. The 7-13 March 2006 major Saharan outbreak: Multiproxy characterization of mineral dust deposited on the West African margin. J. Geophys. Res. 116, D18210, doi: 10.1029/2011JD016173.

Skonieczny, C., et al. 2013. A three-year time series of mineral dust deposits on the West African margin: Sedimentological and geochemical signatures and implications for interpretation of marine paleo-dust records. Earth Planet. Sci. Lett. 364, 145-156.

Stuiver, M, Reimer, PJ, 1993. Extended 14C database and revised CALIB radiocarbon calibration program. Radiocarbon 35, 215-230.

Viers, J., et al. 2008. Seasonal and provenance controls on Nd-Sr isotopic compositions of Amazon rivers suspended sediments and implications for Nd and Sr fluxes exported to the Atlantic Ocean. Earth Planet. Sci. Lett. 274(3-4), 511-523.

Weltje, G.J., and Tjallingii, R., 2008. Calibration of XRF core scanners for quantitative geochemical logging of sediment cores: Theory and application. Earth Planet. Sci. Lett. 274(3-4), 423-438.

Chapter III

Equatorial Pacific forcing of western Amazonian precipitation during Heinrich Stadial 1

Yancheng Zhang[1*], Xu Zhang[2], Cristiano M. Chiessi[3], Stefan Mulitza[1], Xiao Zhang[1†], Gerrit Lohmann[2], Matthias Prange[1], Hermann Behling[4], Matthias Zabel[1], Aline Govin[5], André O. Sawakuchi[6], Francisco W. Cruz[6], Gerold Wefer[1]

[1] MARUM – Center for Marine Environmental Sciences, University of Bremen, Germany

[2] Alfred Wegener Institute for Polar and Marine Research, Bremerhaven, Germany

[3] School of Arts, Sciences and Humanities, University of São Paulo, São Paulo, Brazil

[4] Department of Palynology and Climate Dynamics, Albrecht-von-Haller-Institute for Plant Sciences, University of Göttingen, Germany

[5] IPSL/LSCE, Laboratoire des Sciences du Climat et de l'Environnement (CEA-CNRS-UVSQ), Université Paris Saclay, Gif sur Yvette, France

[6] Institute of Geosciences, University of São Paulo, São Paulo, Brazil

[†] Present address: School of Atmospheric Science, Nanjing University of Information Science and Technology, Nanjing, China

[*] Corresponding author: Y. Zhang (yzhang@marum.de)

(Submitted to *Scientific Reports*)

Own contribution:

a) Reviewed and completed compilation of the 107 hydroclimate records

b) Designed (together with modelling scientists) the sensitivity experiments

c) Interpreted the results from both paleorecords and numerical simulations

d) Wrote the draft (and led the write-up) of this manuscript

3.1. Abstract

Abundant hydroclimatic evidence from western Amazonia and the adjacent Andes documents wet conditions during Heinrich Stadial 1 (HS1, 18-15 ka), a cold period in the high latitudes of the North Atlantic. This precipitation anomaly was always attributed to a strengthening of the South American summer monsoon due to a change in the Atlantic interhemispheric sea surface temperature (SST) gradient. However, the physical viability of this mechanism has never been rigorously tested. We address this issue by combining a thorough compilation of tropical South American paleorecords and a set of atmosphere model sensitivity experiments. Our results show that the Atlantic SST variations alone, although leading to dry conditions in northern South America and wet conditions in northeastern Brazil, cannot produce increased precipitation over western Amazonia and the adjacent Andes during HS1. Instead, an eastern equatorial Pacific SST increase (i.e., 0.5-1.5°C), in response to the slowdown of the Atlantic Meridional Overturning Circulation during HS1, is crucial to generate the wet conditions in these regions. The mechanism works via anomalous low sea level pressure over the eastern equatorial Pacific, which promotes a regional easterly low-level wind anomaly and moisture recycling from central Amazonia towards the Andes.

3.2. Introduction

Amazonia, host of the richest terrestrial biomes on Earth (ter Steege et al., 2013; Silva et al., 2015; Winemiller et al., 2016), plays a fundamental role in the tropical water cycle (Werth et al., 2002). Future possible changes of Amazonian precipitation that bear direct consequences on Amazon ecosystems (Malhi et al., 2008, 2009) and carbon storage (Gatti et al., 2014; Brienen et al., 2015; Chazdon et al., 2016) are of great concern (e.g., Collins et al., 2013). Analysis of observational data demonstrated a strong dependence of western Amazonian precipitation (e.g., the 2005 drought) on the Atlantic meridional sea surface temperature (SST) gradient (Cox et al., 2008), but equatorial Pacific climate anomalies have also been related to Amazonian droughts and floods (Lopes et al., 2015; Marengo et

al., 2016). Potential decreases in the strength (by ca. 20-40%; Weaver et al., 2012) of the Atlantic Meridional Overturning Circulation (AMOC) under climate warming, which involve variations in both the Atlantic meridional SST gradient (Zhang et al., 2013a) and the tropical eastern Pacific SSTs (Timmermann et al., 2007), are rationally expected to affect Amazonian precipitation in the future. Past intervals when the AMOC underwent substantial reduction, such as Heinrich Stadial 1 (HS1, 18-15 ka before present, BP), provide valuable information on the response of South American precipitation to a weakened AMOC.

The HS1 was characterized as the strongest AMOC perturbation over the last glacial period (Böhm et al., 2015) and significantly influenced tropical South American climate (e.g., Hessler et al., 2010; Handiani et al., 2013; Stríkis et al., 2015; Mohtadi et al., 2016). For example, a southward migration of the Intertropical Convergence Zone (ITCZ) during HS1, if compared to the Last Glacial Maximum (LGM, 23-19 ka BP), resulted in a considerable decrease of precipitation over northernmost South America (Peterson et al., 2000; Deplazes et al., 2013) and a substantial increase over northeastern (NE) Brazil (Wang et al., 2004; Jaeschke et al., 2007; Zhang et al., 2015). To explain wet conditions over the Andes (e.g., Mosblech et al., 2012; Kanner et al., 2012; Cheng et al., 2013) and southeastern (SE) Brazil (e.g., Stríkis et al., 2015) during HS1, some authors proposed a strengthening of the South American summer monsoon (SASM). Various freshwater-hosing experiments with climate models of different complexity levels (under both the LGM (Kageyama et al., 2013) and modern (Stouffer et al., 2006) boundary conditions) successfully simulated the Atlantic ITCZ shift, but exhibited a large spread of rainfall patterns across western Amazonia. Moreover, a growing number of studies also suggested a correlation between increased precipitation along the Andes and the El Niño Southern Oscillation (ENSO) during HS1 (Placzek et al., 2006; Gayo et al., 2012; Bekaddour et al., 2014).

Here, we integrate (i) a quality-flagged compilation of 107 published hydroclimate records from tropical South America and (ii) a suite of sensitivity experiments in an Atmospheric General Circulation Model (AGCM) to evaluate the impacts of HS1

(relative to the LGM) SST anomalies on tropical South American precipitation (see Materials and Methods). Our results show that SST changes over the eastern equatorial Pacific rather than the Atlantic are responsible for the increased precipitation over western Amazonia and the adjacent Andes during HS1.

3.3. Material and Methods

Paleomoisture (precipitation) difference between HS1 and the LGM over tropical South America was determined by compiling 107 published terrestrial hydroclimate records between 30°S-10°N and 80°W-35°W, including 53 lacustrine sediment cores, 10 alluvial deposits, 9 speleothems, 9 moraine landforms, 9 fauna remains, 7 shoreline deposits, 5 paleosol sequences, 3 paleodune profiles as well as 2 ice cores. Chronologies and proxies of all these paleorecords were used directly from their original references. To evaluate the dating quality of the selected hydroclimate records, we applied a chronological reliability index (CRI) based on (i) age model properties and (ii) sampling resolution of each record (Prado et al., 2013; detailed description is given in Supplementary Information). Higher CRI values indicate more reliable hydroclimate records (see Supplementary Fig.S3-1). By referring to interpretations of proxies in each record individually, we identified four types of paleomoisture (precipitation) anomalies between HS1 and the LGM as: drier, wetter, similar or unclear (Supplementary Fig.S3-2, Table S3-1 and Supplementary Information).

To evaluate different regional contributions of climatological SST changes to South American precipitation anomalies between the LGM and HS1 (Supplementary Figs.S3-3, S3-4), an atmospheric general circulation model (AGCM), the ECHAM5 (L19/T31, i.e., 19 vertical levels and 3.75° × 3.75° horizontal resolution) was employed (Roeckner et al., 2003). Because freshwater perturbation was the major forcing of the AMOC slowdown during HS1 (e.g., Liu et al., 2009; Kageyama et al., 2013), we used the LGM boundary conditions (i.e., orbital parameters, topography land-sea mask, ice sheet and greenhouse gas concentrations) to operate the experiments in this study. The LGM and HS1 control runs in the AGCM were forced by climatology monthly mean SST and sea ice cover from experiment LGMW and hosing experiment LGMW-0.2Sv of the fully coupled general

circulation model COSMOS (see Zhang et al. (2013b) for further details), respectively. To investigate the individual contributions of SST changes over different basins to South American precipitation anomalies during HS1, we conducted another three sensitivity experiments in which regional SST fields from the experiment LGMW-0.2Sv (Zhang et al., 2013b) were imposed upon the LGMW SST background, such as the Atlantic basin (30°S-80°N) (ATL), the eastern equatorial Pacific (180°E-~70°W, 25°S-25°N) (EEP) and a combination of ATL and EEP (ATL+EEP). The atmosphere model was integrated for 50 years for each experiment and the last 30 years were taken to calculate climatological fields.

3.4. Results

3.4.1. Compilation of hydroclimate records

Our compilation of paleomoisture difference between HS1 and the LGM indicates dry conditions to the north of the equator, but widespread wet conditions over the Andes, western Amazonia, NE and SE Brazil (Fig.3-1b). Enhanced precipitation (or moisture) extends from the Ecuadorian Andes (e.g., Santiago Cave at ca. 3°S; Mosblech et al., 2012) to the northern Chilean Andes (e.g., central Atacama Desert at 22°S-24°S; Betancourt et al., 2000). The few available records from central Amazonia, characterized by low CRI values, exhibited in general dry climate during HS1 (see Supplementary Information).

Fig.3-1. Precipitation and low level atmospheric circulation (a) and paleodata compilation for tropical South America (b). (a) Long-term (1981-2010) monthly averaged terrestrial precipitation (color scale) from the University of Delaware (available online at linkage, http://climate.geog.udel.edu/~climate/) and 850hPa wind field (vectors) from the NOAA/OAR/ESRL PSD (available online at linkage, http://www.esrl.noaa.gov/psd/) during austral summer (December-January-February, DJF). Thick green arrows mark the South American low level jet (SALLJ). (b) Compilation of hydroclimate records, expressed as the difference between Heinrich Stadial 1 (HS1, 18-15 ka) and the Last Glacial Maximum (LGM, 23-19 ka). Symbol color indicates drier (red), wetter (blue), similar (grey) and unclear (white) conditions during HS1 in comparison to the LGM. Symbol size denotes the quality of the age model based on the chronological reliability index (CRI) (details see Supplementary Information). Paleoclimate records with CRI

values > 1 are numbered (Supplementary Table S3-1). Black dashed lines mark the location of the Intertropical Convergence Zone (ITCZ) during DJF and austral winter (June-July-August, JJA). Black solid line in both (a) and (b) outline the Amazon River drainage basin.

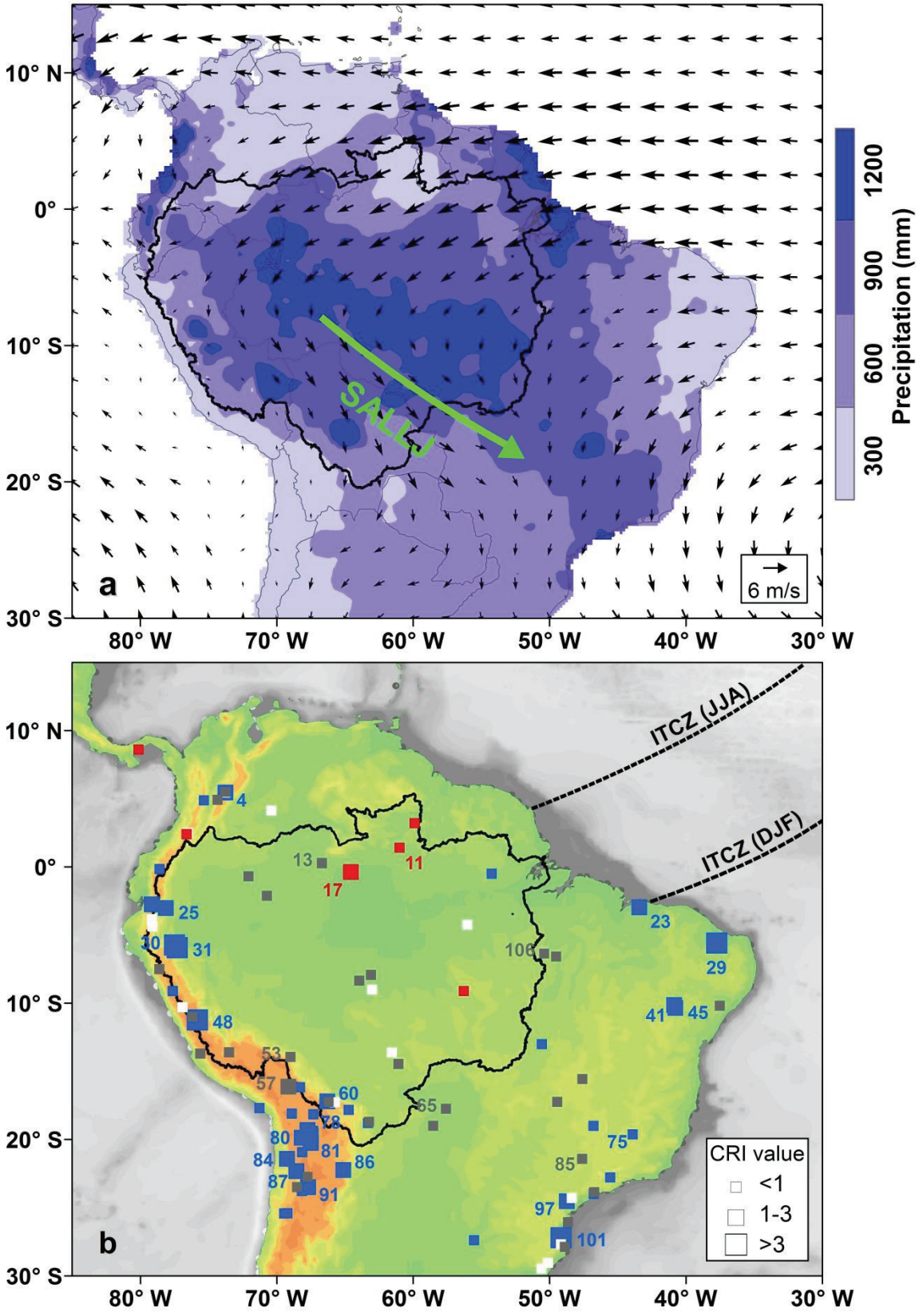

3.4.2. Atmosphere model sensitivity experiments

Driving the atmosphere general circulation model with global HS1 SST anomalies (see Supplementary Fig.S3-4) in the GLB SST experiment (Fig.3-2d) shows similar rainfall regimes as the ones simulated by the fully coupled atmosphere-ocean model (Zhang et al., 2013b; Supplementary Fig.S3-3). The ATL SST experiment, forced by only Atlantic HS1 SST anomalies, simulates a southward migration of the ITCZ as evidenced by decreased rainfall over northernmost South America and increased rainfall over NE Brazil (Fig.3-2a), but apparently fails to generate the wet conditions over western Amazonia. The EEP SST experiment (by applying only eastern equatorial Pacific HS1 SST anomalies) produces enhanced rainfall over western Amazonia together with the intensification of the northeast trade winds over central Amazonia and the South American Low Level Jet (SALLJ) (Fig.3-2b), while the ITCZ displays no evident shift. The ATL+EEP SST experiment, in which we superimposed the eastern equatorial Pacific SST anomalies upon the Atlantic interhemispheric SST gradient, exhibits increased rainfall and easterly wind anomalies over western Amazonia (Fig.3-2c), although dry conditions over SE Brazil are in contradiction to the GLB SST and the EEP SST experiments (Fig.3-2b, d) as well as to our hydroclimate compilation (Fig.3-1b).

Fig.3-2. Results of atmospheric model sensitivity experiments. Differences of simulated (ECHAM5) annual mean climate variables between Heinrich Stadial 1 (18-15 ka) and the Last Glacial Maximum (23-19 ka) for the (a) Atlantic (ATL) SST experiment, (b) eastern equatorial Pacific (EEP) SST experiment, (c) ATL+EEP experiment and (d) global (GLB) SST experiment (Supplementary Information). Climate variables include rainfall (shaded, mm/day), 850hPa wind field (vectors, m/s) and sea level pressure (contours, Pa).

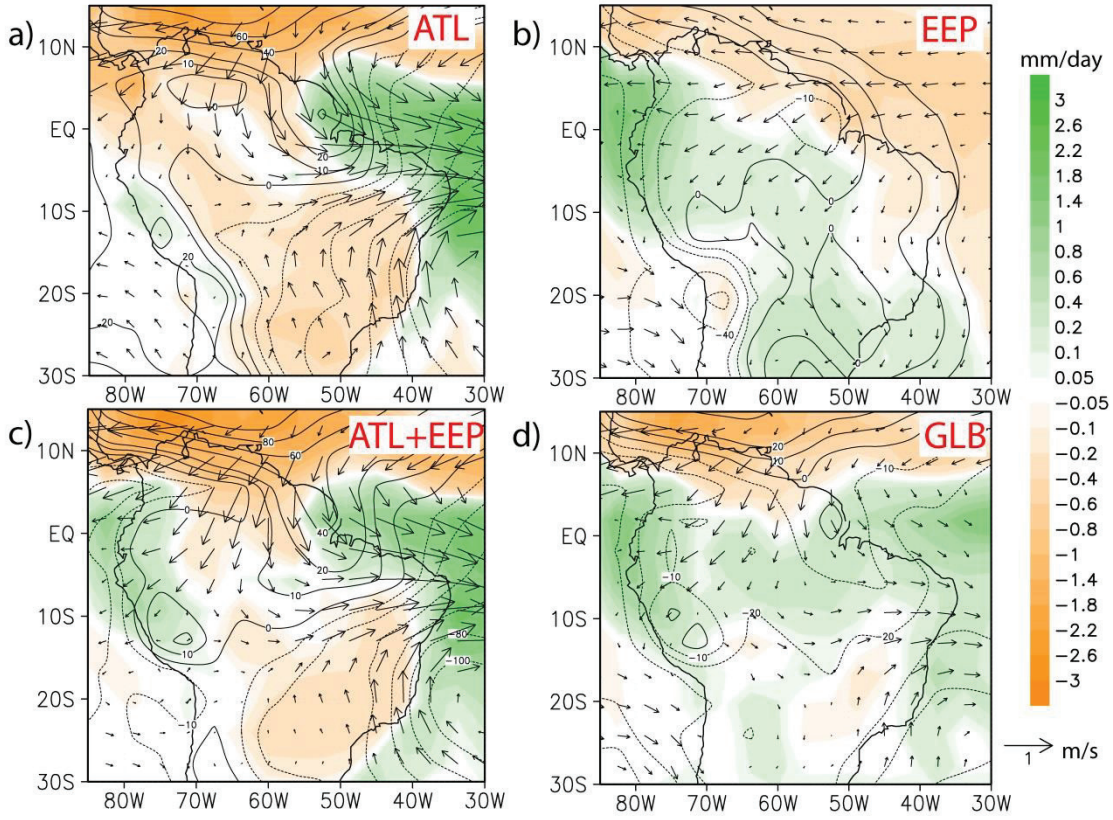

3.5. Discussion

During HS1, a stronger SASM associated with a change in the Atlantic interhemispheric SST gradient was commonly assumed to have triggered increased precipitation over the Amazonian Andes (Mosblech et al., 2012; Kanner et al., 2012; Cheng et al., 2013). By contrast, our ATL SST experiment shows that the change in Atlantic interhemispheric SST gradient actually weakens the northeast trade winds over central Amazonia and the SALLJ (Fig.3-2a), such that less moisture is transported from tropical Atlantic towards western Amazonia and the adjacent Andes (Fig.3-2a). Decreased precipitation over these areas as reproduced by the ATL SST experiment (Fig.3-2a), however, conflicts with the prevailing wet conditions derived from our compilation (Fig.3-1b). Thus, the Atlantic interhemispheric SST gradient alone is insufficient to explain the wet conditions over western Amazonia and the adjacent Andes during HS1, and contributions from other oceanic regions (e.g., tropical Pacific) should be taken into account.

The EEP SST experiment demonstrates that positive climatological SST anomalies over the eastern equatorial Pacific (Supplementary Fig.S3-4) are able to cause increased precipitation over western Amazonia and the adjacent Andes during HS1, probably in relation to enhanced northeast trade winds over central Amazonia and the SALLJ (Fig.3-2b). The northeast trade winds over central Amazonia, importantly, are also clearly identified in the ATL+EEP SST experiment (Fig.3-2c). Remarkably, the wind field pattern over the western tropical Atlantic from the ATL+EEP SST experiment rather resembles that of the ATL SST experiment than of the EEP SST experiment (Fig.3-2a, b, c). This result implies that in the ATL+EEP SST experiment, western Amazonia and the adjacent Andes still experienced an increased rainfall, although less equatorial Atlantic moisture was transported towards the Andes. These features agree well with the overall characteristics of our compilation (Fig.3-1b), in particular with the presence of dry conditions over central Amazonia during HS1.

If the Atlantic meridional SST gradient was not the only driver for an increased rainfall over the Amazonian Andes (Vuille et al., 2005; Lee et al., 2009; Baker et al., 2015), other processes must be involved. We turn to the SST increases of around 0.5-1.5°C in the eastern equatorial Pacific during HS1, with the exception of minor SST decreases over coastal regions (Koutavas et al., 2008; Shakun et al., 2012; Supplementary Fig.S3-4 and Table S3-2). These SST variations tend to yield low-pressure anomalies over the eastern equatorial Pacific, which then deepens the zonal sea level pressure (SLP) gradient between the Atlantic and the Pacific and strengthens the easterly flow anomaly over western Amazonia and the adjacent Andes (Fig.3-2b, c, d). Such easterly wind anomalies together with the northeast trade winds over central Amazonia subsequently promote moisture recycling from central Amazonia towards the Andes, enhancing the evaporation-condensation along its pathway (e.g., Vizy et al., 2007). In fact, this mechanism was previously suggested to account for wet Andean conditions during the LGM (e.g., Vizy et al., 2007). The extent to which enhanced moisture recycling contributed to the wet conditions over the Amazonian Andes remains elusive, but our interpretation coincides with abundant evidence across the central Andes that supported increased proportions of regional-sourced moisture over HS1 and the LGM (Thompson et al., 1998; Betancourt et

al., 2000; Ammann et al., 2001; Godfrey et al., 2003; Placzek et al., 2006; Kull et al., 2008; Gayo et al., 2012; Bekaddour et al., 2014).

Seasonal-scale SST changes in the eastern equatorial Pacific were often assigned to the ENSO activity (Stott et al., 2002). Because reconstructions of the ENSO variability across HS1 and the LGM are not well established from both numerical simulations (Merkel et al., 2010; Liu et al., 2014) and proxy data (Koutavas et al., 2002; Felis et al., 2012; Ford et al., 2015), it is difficult to quantify the ENSO impact on South American precipitation during HS1. For instance, rainfall over NE Brazil and SE Brazil, which are typically in strong negative and positive relationship with El Niño events today (Grimm et al., 2009), indeed experienced similar wet patterns during HS1 (Fig.3-1b). Analyses of instrumental data also suggested that climatological conditions over the eastern equatorial Pacific (e.g., related to ENSO; Ford et al., 2015) may be linked to Atlantic climate forcing (Wu et al., 2007; Dima et al., 2015). Eastern equatorial Pacific SST variations, probably a response to the weakened AMOC during HS1, are, nevertheless, crucial for triggering wet conditions over western Amazonia and the adjacent Andes (Fig.3-1b).

Our ATL and ATL+EEP SST experiments (Fig.3-2a, c) are unable to reproduce increased SE Brazilian rainfall as seen in the paleodata during HS1 (Fig.3-1b). Interestingly, the GLB SST experiment (Fig.3-2d), although forced by global SST anomalies (see Supplementary Fig.S3-4), still cannot capture the wet conditions over SE Brazil. We realize that the SALLJ is weakened in both the GLB SST and the ATL+EEP SST experiments (relative to the EEP SST experiment), and thus seems unlikely to transport equatorial Atlantic moisture towards SE Brazil. In a recent paper, Kageyama et al. (2013) compared eleven freshwater-hosing experiments (under the LGM conditions) with six different fully coupled climate models, none of which, notably, showed increased rainfall over SE Brazil. Therefore, additional investigations on paleoclimate records and model simulations are necessary to clarify this point.

3.6. Conclusion

Comparing hydroclimate records compilation and atmosphere model sensitivity experiments provides a deeper understanding of the influence of glacial North Atlantic climate on South American precipitation during HS1. An anomalous Atlantic meridional SST gradient, due to AMOC slowdown, drove a southward ITCZ shift leading to decreased precipitation over northernmost South America and increased precipitation over NE Brazil. The concomitant variations in eastern equatorial Pacific SST produced a negative SLP anomaly over the eastern tropical Pacific, which then deepened the SLP gradient between the Atlantic and the Pacific. As a result, it strengthened the northeasterly winds over the central and western Amazonia, enhancing the moisture recycling over western Amazonia and the adjacent Andes.

Our results highlight that future changes in the eastern equatorial Pacific SST, as the AMOC weakens, will be of vital importance to affect western Amazonian precipitation. Depending on the magnitude of the AMOC slowdown under different global warming scenarios (e.g., Weaver et al., 2012; Collins et al., 2013), consideration of both eastern equatorial Pacific and Atlantic SST variations would allow more accurate insights into the possible changes of Amazonian precipitation in the future.

3.7. Acknowledgements

This work was funded by the Deutsche Forschungsgemeinschaft through the DFG Research Centre/Cluster of Excellence 'The Ocean in the Earth System' and the Helmholtz Climate Initiative REKLIM. We thank Dr. Dunia H. Urrego for constructive discussion. X.Z.(Xu) was supported by Helmholtz funding through the Polar Regions and Coasts in the Changing Earth System (PACES) programme of Alfred Wegener Institute Helmholtz Centre for Polar and Marine Research (AWI) in Bremerhaven, Germany. C.M.C. was supported by FAPESP (grant 2012/17517-3) and CAPES (grants 1976/2014 and 564/2015). A.O.S. was supported by FAPESP (grant 2011/06609-1). The compilation of paleodata presented in this paper will be archived in PANGAEA (www.pangaea.de).

3.8. References

Ammann, C., et al. 2001. Late Quaternary Glacier response to humidity changes in the arid Andes. Palaeogeogr. Palaeoclimatol. Palaeoecol. 172, 313-326.

Baker, P. A., et al. 2015. Nature and causes of Quaternary climate variation of tropical South America. Quat. Sci. Rev. 124, 31-47.

Bekaddour, T., et al. 2014. Paleo erosion rates and climate shifts recorded by Quaternary cut-and-fill sequences in the Pisco valley, central Peru. Earth Planet. Sci. Lett. 390, 103-115.

Betancourt, J.L., et al. 2000. A 22,000-year record of monsoonal precipitation from northern Chile's Atacama desert. Science 289, 1542-1546.

Böhm, E., et al. 2015. Strong and deep Atlantic meridional overturning circulation during the last glacial cycle. Nature 517, 73-76.

Brienen, R.J.W., et al. 2015. Long-term decline of the Amazon carbon sink. Nature 519, 344-348.

Chazdon, R.L., et al. 2016. Carbon sequestration potential of second-growth forest regeneration in the Latin American tropics. Sci. Adv. 2, doi:10.1126/sciadv.1501639.

Cheng, H., et al. 2013. Climate change patterns in Amazonia and biodiversity. Nat. Commun. 4, doi: 10.1038/ncomms2415.

Collins, M., et al. 2013. in Climate Change 2013: The Physical Science Basis. Contribution of Working Group I to the Fifth Assessment Report of the Intergovernmental Panel on Climate Change. Ch. 12, 1029-1136 (Cambridge University Press).

Cox, P., et al. 2008. Increasing risk of Amazonian drought due to decreasing aerosol pollution. Nature 453, 212-215.

Deplazes, G., et al. 2013. Links between tropical rainfall and North Atlantic climate during the last glacial period. Nat. Geosci. 6, 213-217.

Dima, M., et al. 2015. Possible North Atlantic origin for changes in ENSO properties during the 1970s. Clim. Dyn. 44, 925-935.

Felis, T., et al. 2012. Pronounced interannual variability in tropical South Pacific temperatures during Heinrich Stadial 1. Nat. Commun. 3, doi:10.1038/ncomms1973.

Ford, H.L., et al. 2015. Reduced El Niño-Southern Oscillation during the Last Glacial Maximum. Science 347, 255-258.

Gatti, L.V., et al. 2014. Drought sensitivity of Amazonian carbon balance revealed by atmospheric measurements. Nature 506, 76-80.

Gayo, E.M., et al. 2012. Late Quaternary hydrological and ecological changes in the hyperarid core of the northern Atacama Desert (~21°S). Earth-Science Reviews 113, 120-140.

Godfrey, L.V., et al. 2003. Stable isotope constraints on the transport of water to the Andes between 22° and 26°S during the last glacial cycle. Palaeogeogr. Palaeoclimatol. Palaeoecol. 194, 299-317.

Grimm, A.M., et al. 2009. ENSO and extreme rainfall events in South America. J. Climate 22, 1589-1609.

Handiani, D., et al. 2013. Tropical vegetation response to Heinrich Event 1 as simulated with the UVic ESCM and CCSM3. Clim. Past 9, 1683-1696.

Hessler, I., et al. 2010. Millennial-scale changes in vegetation records from tropical Africa and South America during the last glacial. Quaternary Sci. Rev. 29, 2882-2899.

Jaeschke, A., et al. 2007. Coupling of millennial-scale changes in sea surface temperature and precipitation off northeastern Brazil with high-latitude climate shifts during the last glacial period. Paleoceanography 22, doi:10.1029/2006PA001391.

Kageyama, M., et al. 2013. Climatic impacts of fresh water hosing under Last Glacial Maximum conditions a multi-model study. Clim. Past 9, 935-953.

Kanner, L.C., et al. 2012. High latitude forcing of the South American Summer Monsoon during the Last Glacial. Science 335, 570-573.

Koutavas, A., et al. 2002. El Niño-like pattern in Ice Age Tropical Pacific sea surface temperature. Science 297, 226-230.

Koutavas, A., et al. 2008. Northern timing of deglaciation in the eastern equatorial Pacific from alkenone paleothermometry. Paleoceanography 23, doi:10.1029/2008PA001593.

Kull, C., et al. 2008. Late Pleistocene glaciation in the Central Andes Temperature versus humidity control - A case study from the eastern Bolivian Andes (17°S) and regional synthesis. Global Planet. Change 60, 148-164.

Lee, J.E., et al. 2009. Precipitation over South America during the Last Glacial Maximum An analysis of the “amount effect” with a water isotope-enabled general circulation model. Geophys. Res. Lett. 36, doi:10.1029/2009GL039265.

Liu, Z., et al. 2009. Transient simulation of Last Deglaciation with a new mechanism for Bølling-Allerød warming. Science 325, 310-314.

Liu, Z., et al. 2014. Evolution and forcing mechanisms of El Niño over the past 21,000 years. Nature 515, 550-553.

Lopes, A.V., et al. 2016. Trend and uncertainty in spatial-temporal patterns of hydrological droughts in the Amazon basin. Geophys. Res. Lett. 43, 3307-3316.

Malhi, Y., et al. 2008. Climate change, deforestation, and the fate of the Amazon. Science 390, 169-172.

Malhi, Y., et al. 2009. Exploring the likelihood and mechanism of a climate-change-induced dieback of the Amazon rainforest. Proc. Natl. Acad. Sci. USA 106, 20610-20615.

Marengo, J.A., et al. 2016. Extreme seasonal droughts and floods in Amazonia: causes, trends and impacts. Int. J. Climatol. 36, 1033-1050.

Merkel, U., et al. 2010. ENSO variability and teleconnections during glacial climates. Quat. Sci. Rev. 29, 86-100.

Mohtadi M., et al. 2016. Palaeoclimatic insights into forcing and response of monsoon rainfall. Nature 533, 191-199.

Mosblech, N.A.S., et al. 2012. North Atlantic forcing of Amazonian precipitation during the last ice age. Nat. Geosci. 5, 817-820.

Peterson, L.C., et al. 2000. Rapid changes in the hydrologic cycle of the tropical Atlantic during the Last Glacial. Science 290, 1947-1951.

Placzek, C., et al. 2006. Geochronology and stratigraphy of late Pleistocene lake cycles on the southern Bolivian Altiplano Implications for causes of tropical climate change. GSA Bulletin 118, 515-532.

Prado, L. F., et al. 2013. A mid-Holocene climate reconstruction for eastern South America. Clim. Past 9, 2117-2133.

Roeckner, E., et al. 2003. The atmospheric general circulation model ECHAM 5, Part I: Model description. Report 349. Max-Planck Institut für Meteorologie: Hamburg, Germany.

Shakun, J.D., et al. 2012. Global warming preceded by increasing carbon dioxide concentrations during the last deglaciation. Nature 484, 49-54.

Silva, J.M.C., et al. 2015. The fate of the Amazonian areas of endemism. Conservation Biology 19, 689-694.

Stott, L., et al. 2002. Super ENSO and Global Climate Oscillations at Millennial Time Scales. Science 297, 222-226.

Stouffer, R. et al. 2006. Investigating the causes of the response of the thermohaline circulation to past and future climate changes. J. Climate 19, 1365-1387.

Stríkis, N.M., et al. 2015. Timing and structure of Mega-SACZ events during Heinrich Stadial 1. Geophys. Res. Lett. 42, 5477-5484.

ter Steege, H., et al. 2013. Hyperdominance in the Amazonian tree flora. Science 342, doi:10.1126/science.1243092.

Thompson, L.G., et al. 1998. A 25,000-year tropical climate history from Bolivian ice cores. Science 282, 1858-1864.

Timmermann, A., et al. 2007. The influence of a weakening of the Atlantic meridional overturning circulation on ENSO. J. Climate 20, 4899-4019.

Vizy, E.K., et al. 2007. Relationship between Amazon and high Andes rainfall. J. Geophys. Res. 112, doi:10.1029/2006JD007980.

Vuille, M., et al. 2005. Stable isotopes in precipitation recording South American summer monsoon and ENSO variability: observations and model results. Clim. Dyn. 25, 401-413.

Wang, X., et al. 2004. Northeastern Brazil wet periods linked to distant climate anomalies and rainforest boundary changes. Nature 432, 740-743.

Weaver, A.J., et al. 2012. Stability of the Atlantic meridional overturning circulation: A model intercomparison. Geophys. Res. Lett. 39, doi:10.1029/2012GL053763.

Werth, D., et al. 2002. The local and global effects of Amazon deforestation. J. Geophys. Res. 107, doi:10.1029/2001JD000717.

Winemiller, K. O., et al. 2016. Balancing hydropower and biodiversity in the Amazon, Congo, and Mekong. Science 351, 128-129.

Wu, L., et al. 2007. Atmospheric teleconnections of tropical Atlantic variability: interhemispheric, tropical-extratropical, and cross-basin interactions. J. Climate 20, 856-870.

Zhang, L., et al. 2013a. Multidecadal North Atlantic sea surface temperature and Atlantic meridional overturning circulation variability in CMIP5 historical simulations. J. Geophys. Res. 118, 5772-5791.

Zhang, X., et al. 2013b. Different ocean states and transient characteristics in the Last Glacial Maximum simulations and implications for deglaciation. Clim. Past 9, 2319-2333.

Zhang, Y., et al. 2015. Origin of increased terrigenous supply to the NE-South American continental margin during Heinrich Stadial 1 and the Younger Dryas. Earth Planet. Sci. Lett. 432, 493-500.

3.9. Supplementary materials

3.9.1. Compilation of the the hydroclimate records

For the compilation of published paleoclimatic records across tropical South America, we included the following archives: 53 lacustrine sediment cores (geochemistry, palynology and mineralogy), 10 alluvial deposits (geomorphology, palynology), 9 moraine deposits (glacial landforms), 9 speleothems (oxygen stable isotopes), 9 fauna remains (fossil rodent middens, palynology), 7 shoreline deposits (mollusc shells), 5 paleosol sequences (palynology, geochemistry), 3 paleodune profiles (geomorphology, luminescence ages), as well as 2 ice cores (oxygen stable isotopes) (Supplementary Fig.S3-1). Chronologies (e.g., using ^{14}C, U-Th, luminescence dating methods, as provided in Supplementary Table S3-1) and interpretation of the hydroclimate records agree to the original reference (Supplementary Table S3-1).

Fig.S3-1. Categorization of the 107 hydroclimate records based on their chronological reliability index (CRI) values (data and detailed information are given in Supplementary Table S3-1).

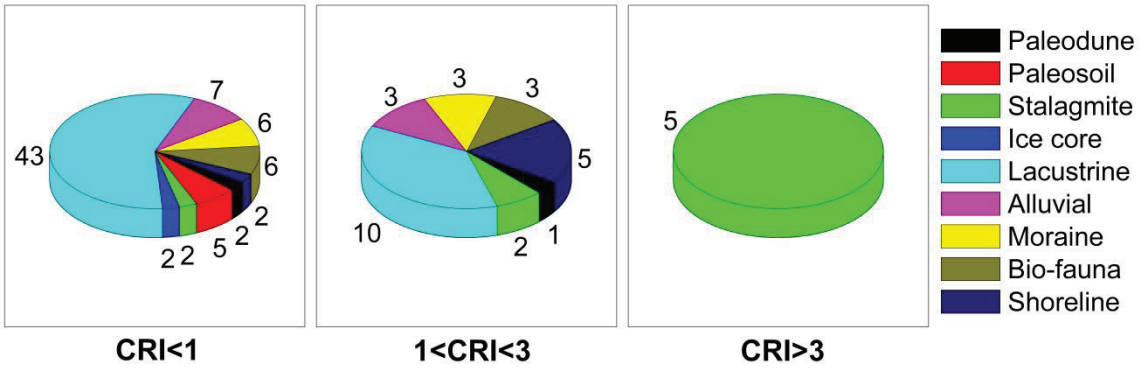

We used the time windows of 18-15 ka (Sanchez Goñi et al., 2010) and 23-19 ka (MARGO Project, 2009) to define the Heinrich Stadial 1 (HS1) and the Last Glacial Maximum (LGM), respectively. For paleorecords with uncalibrated ^{14}C ages, the intervals of 15-12 ka ^{14}C ages and 20-16 ka ^{14}C ages were used to outline the HS1 and the LGM. Based on the chronological reliability index (CRI) (see below), we mainly used the paleorecords with CRI values over 1 to determine the overall pattern of the paleomoisture difference between HS1 and LGM. We acknowledge that the age controls based on

uncalibrated ^{14}C ages may have large uncertainty, because the radiocarbon reservoir correction of terrestrial archives like sediment cores from lacustrine environment are less accurate due to local water-air CO_2 exchange (e.g., Grosjean et al., 2001). In the compilation, we included 28 paleoclimate records constrained by uncalibrated ^{14}C ages (with large age uncertainty as mentioned above), but note that only two of them are characterized by CRI values higher than 1 (e.g., sites No.85 and No.91 in Supplementary Table S3-1). Thus, the consideration of these paleorecords with uncalibrated ^{14}C ages does not modify our conclusions based on the compilation of South American hydroclimate records (Supplementary Fig.S3-2).

To calculate the CRI values, we employed the function established by Prado et al. (2013) as follows:

$$\mathrm{CRI} = \frac{\mathrm{CA} + \mathrm{D} + \mathrm{R}}{3}$$

where CA (calibration) equals 1 (or 0) if age control points were (or not) calibrated; D (dating) is the number of age control points within HS1 and LGM, divided by 10; R (resolution) refers to the mean number of total samples per entire core length ratio, as given:

$$\mathrm{R} = \begin{cases} 0.1 \text{ for ratio between } 0.01 \text{ and } 0.1 \\ 0.2 \text{ for ratio between } 0.11 \text{ and } 0.2 \\ \qquad \ldots\ \ldots \\ 11.0 \text{ for ratio between } 10.01 \text{and } 11.00 \end{cases}$$

Among the selected paleoclimate records, most speleothem records have high CRI values (≥3), while paleoclimatic archives from lacustrine environments (e.g., peat bog, peatland, swamp) or alluvial and moraine deposits generally show low CRI values (Supplementary Table S3-1, Fig.S3-1). Based on the interpretation of each paleorecord (Supplementary Table S3-1 for further details), we identify the paleomoisture (precipitation) anomalies between HS1 and LGM with three categories: ‘drier’, ‘wetter’ and ‘similar’. For the paleorecords whose references did not allow a clear comparison (e.g., no information available on paleohydrology variations, or/and no age points available within HS1 or the LGM), we distinguish them as ‘unclear’ (Supplementary Fig.S3-2, detailed description is given in Supplementary Table S3-1).

Fig.S3-2. Types of South American hydroclimatic archives used to determine the difference between Heinrich Stadial 1 (HS1) and the Last Glacial Maximum (LGM) (data are provided in Supplementary Table S3-1). Red (blue) symbols denote a drier (wetter) HS1 than the LGM, while grey (white) symbols represent similar (unclear) conditions. Symbol sizes relate to the quality level established by chronological reliability index (CRI) (Supplementary Fig.S3-1). Numbers mark those records with CRI values > 1 (Supplementary Table S3-1) that constitute the base for the determination of paleomoisture difference between HS1 and the LGM.

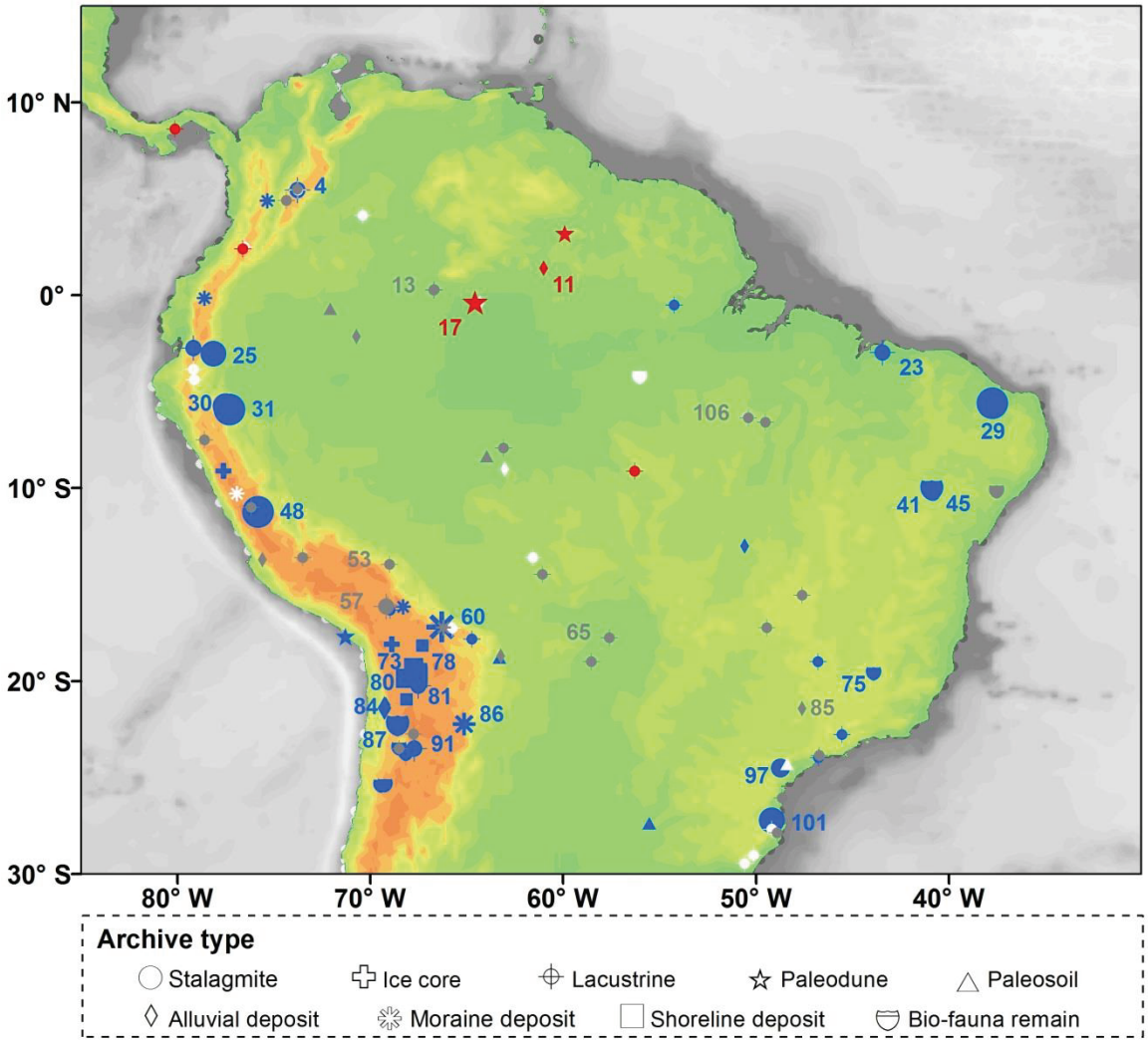

3.9.2. General dry HS1 vs. LGM conditions over central Amazonia

Based on palynological analyses, previous studies showed that the dry climate at Lagoa Verde (Hill of six lakes, site No.13; D'Apolito et al., 2013; Bush et al., 2004) and Lagoa da Cachoeira (site No.106; Hermanowski et al., 2012, 2015) was comparable between the LGM and HS1. The paleodune profile at Temedauí, Rio Negro (site No.17; Carneiro-

Filho et al., 2002) apparently demonstrated a slightly enhanced eolian activity during 17.2-16.4 ka compared to the period 22.8-22 ka, both periods being in intensified state relative to the Holocene. Similarly, the megafan at Viruá National Park (site No. 11, Rossetti et al., 2012) suggested a high water discharge in wet seasons during 24-20 ka, while an extensive dry season was associated with C4 grassland development between 20-5 ka (with a hiatus during HS1). Together with other paleorecords with low CRI values over central Amazonia (Supplementary Fig.S3-2, see also Supplementary Table S3-1 for detailed interpretations), we therefore suggest that central Amazonia underwent slightly drier conditions during HS1 relative to the LGM. A better understanding of this issue depends on new paleoclimate records with high CRI values (e.g., speleothem) from central Amazonia and nearby regions in the future.

Fig.S3-3. Climatological anomalies between the Heinrich Stadial 1 (HS1) and the Last Glacial Maximum (LGM), as derived from the experiments LGMW-0.2Sv and LGMW in the fully coupled AOGCM respectively (Zhang et al., 2013), including rainfall (shaded, mm/day), 850hPa wind field (vectors, m/s) and sea level pressure (contours, Pa). Good agreement between outputs of the fully coupled AOGCM and the AGCM (Fig.2d in the manuscript), e.g., dry conditions over northernmost South America and wet conditions over the Andes and NE Brazil, suggests that climatological SST variations are a major forcing of South American precipitation changes during HS1.

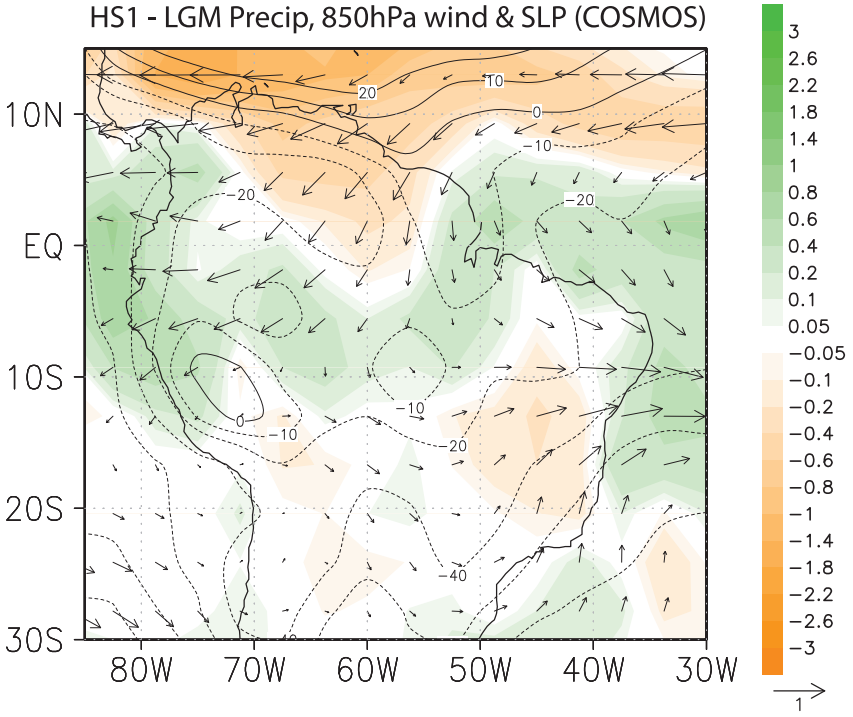

Fig.S3-4. The COSMOS simulated sea surface temperature (SST) anomalies in the freshwater- hosing experiment (°C) relative to the LGM background experiment (Zhang et al., 2013). The areas outlined within the pink (Atlantic) and black (Pacific) lines were used to perform the ATL SST and EEP SST sensitivity experiments, respectively. Filled circles in the eastern equatorial Pacific denote paleodata-reconstructed SST increases (red) and decreases (blue) during HS1 relative to LGM (data are given in Supplementary Table S3-2).

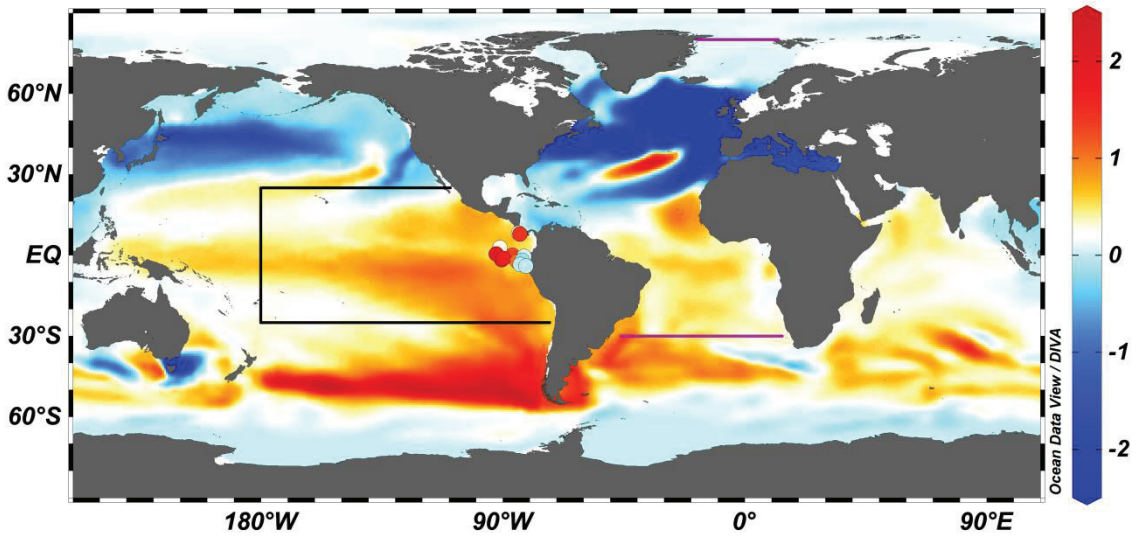

3.9.3. References

Bush, M.B., et al. 2004. Amazonian paleoecological histories: one hill, three watersheds. Palaeogeogr. Palaeoclimatol. Palaeoecol. 214, 359-393.

Carneiro-Filho, A., et al. 2002. Amazonian Paleodunes Provide Evidence for Drier Climate Phases during the Late Pleistocene–Holocene. Quaternary Res. 58, 205-209.

D'Apolito, C., et al. 2013. The Hill of Six Lakes revisited new data and re-evaluation of a key Pleistocene Amazon site. Quat. Sci. Rev. 76, 140-155.

Grosjean, M., et al. 2001. A 22,000 14C year BP sediment and pollen record of climate change from Laguna Miscanti (23°S), northern Chile. Global and Planetary Change 28(1-4), 35-51.

Hermanowski, B., et al. 2012. Environmental changes in southeastern Amazonia during the last 25,000 yr revealed from a paleoecological record. Quaternary Res. 77, 138-148.

Hermanowski, B., et al. 2015. Possible linkages of palaeofires in southeast Amazonia to a changing climate since the Last Glacial Maximum. Veget Hist Archaeobot 24, 279-292.

MARGO Project Members. 2009. Constraints on the magnitude and patterns of ocean cooling at the Last Glacial Maximum. Nature Geosciences 2, 127-132.

Prado, L.F., et al. 2013. A mid-Holocene climate reconstruction for eastern South America. Clim. Past 9, 2117-2133

Rossetti, D.F., et al. 2012. A Late Pleistocene–Holocene wetland megafan in the Brazilian Amazonia. Sedimentary Geology 282, 276-293.

Sanchez Goñi, M.F., et al. 2010. Millennial-scale climate variability and vegetation changes during the Last Glacial: Concepts and terminology. Quat. Sci. Rev. 29, 2823-2827.

Zhang, X., et al. 2013. Different ocean states and transient characteristics in the Last Glacial Maximum simulations and implications for deglaciation. Clim. Past 9, 2319-2333.

Chapter IV

Discriminating the impacts of Heinrich and Dansgaard-Oeschger stadials over tropical South America

Yancheng Zhang[1*], Cristiano M. Chiessi[2], Stefan Mulitza[1], André O. Sawakuchi[3], Matthias Zabel[1], Stefano Crivellari[3], Gerold Wefer[1]

[1] MARUM-Center for Marine Environmental Sciences, University of Bremen, Germany

[2] School of Arts, Sciences and Humanities, University of São Paulo, São Paulo, Brazil

[3] Institute of Geosciences, University of São Paulo, São Paulo, Brazil

[*] Corresponding author: Y. Zhang (yzhang@marum.de)

(Ready for submission to *Geophysical Research Letters*)

Own contribution:

a) Measured the downcore proxies in core GeoB16224-1

b) Selected other published high resolution paleorecoreds across Central and South America, and compared with core GeoB16224-1

c) Interpreted the data and discussed the hypothesis

d) Wrote the draft of this manuscript

4.1. Abstract

Detailed knowledge about responses of tropical South American precipitation to Heinrich Stadials (HS) and Dansgaard-Oeschger (DO) Stadials allows relevant insight into possible evolution of Amazonian biodiversity under future climate change. Sediment core GeoB16224-1 (ca. 7°N), raised from the continental slope offshore French Guiana in the western equatorial Atlantic, documents enhanced input of Amazonian Andes-sourced sediments during HS and DO Stadials from 13-41 ka. Combined with published high temporal resolution paleoprecipitation records from ca. 17°N to 4°S, we differentiate the influences of HS and DO Stadials on tropical South American precipitation. Our results show that both HS and DO Stadials resulted in decreased precipitation over northernmost South America whiles increased precipitation over the Andes. Notably, northeastern (NE) Brazilian precipitation underwent significant increases during HS, but was characterized by subtle changes across DO Stadials. Because DO Stadials involved smaller decreases in the strength of the Atlantic meridional overturning circulation (AMOC) in comparison to HS, we suggest that the southward shifts of the ITCZ mean position during DO Stadials were insufficient to reach NE Brazil, triggering no increase of terrigenous materials input to the adjacent continental margin. Future AMOC slowdown (ca. 20-50%) derived from model simulations is thus likely to affect precipitation over northernmost South America and western Amazon rather than NE Brazil.

4.2. Introduction

During the last glacial period, a succession of millennial-scale cold intervals in the Northern Hemisphere high latitudes was recognized as the Heinrich Stadials (HS, e.g., Heinrich, 1988) and the Dansgaard-Oeschger (DO) Stadials (e.g., Dansgaard et al., 1993). The HS were outlined by the massive deposition of ice-rafted debris (IRD) in the North Atlantic (e.g., Bond et al., 1992), while the DO Stadials were typically referred to cooling phases over Greenland when IRD layer did not occur (Svensson et al., 2006; Sanchez Goñi and Harrison, 2010). The HS and DO Stadials, although probably attributed to different mechanisms (e.g., Alvarez-Solas et al., 2010; Zhang et al., 2014a), were broadly

believed to involve decreases in the strength of the Atlantic meridional overturning circulation (AMOC) (Clark et al., 2002; Böhm et al., 2015). Such changes in AMOC strength, together with large scale ocean-atmosphere interactions, had a crucial role in major features of the global climate (e.g., Voelker 2002) like abrupt reorganizations of monsoon systems over Asia (Wang et al., 2001; Burns et al., 2003) and North America (Asmerom et al., 2010).

Precipitation over tropical South America, under the control of the South American summer monsoon (SASM) and the Intertropical Convergence Zone (ITCZ) (Fig.4-1a, b), was substantially affected by the millennial-scale AMOC variations. During HS when the AMOC was nearly shutdown (e.g., McManus et al., 2004; Böhm et al., 2015), annual mean precipitation decreased over northernmost South America (Peterson et al., 2000) while increased over northeastern (NE) (Wang et al., 2004) and southeastern (SE) Brazil (Wang et al., 2006) as well as western Amazon (Cheng et al., 2013a). Available proxy data however are still sparse to fully capture the regional structures of tropical South American precipitation during DO Stadials. Importantly, the simulated magnitudes of the AMOC reduction under anthropogenic greenhouse-gas-induced climate change scenarios, ca. 20-50% by the end of this century from various climate models (Cheng et al., 2013b; Rahmstorf et al., 2015), are comparable with the reconstructed AMOC slowdown during DO Stadials (Rahmstorf 2002; Zhang et al., 2014a, b, 2015a). Thus, understanding the responses of tropical South American precipitation to DO stadials sheds better insights into the possible changes of precipitation over tropical South America that bears strong consequence for Amazonian ecosystems (e.g., Malhi et al., 2008, 2009). For example, the Amazon flood cycle controls not only around 20% of freshwater fish species (Winemiller et al., 2016) but also flooded forests hosting many endemic species of birds and trees (Remsen and Parker, 1983, Wittmann et al., 2013).

Here we investigated the regional characteristics of tropical South American precipitation in response to HS and DO Stadials. First, based on sediment core GeoB16224-1 raised to the northwest of the Amazon River mouth, we documented the relationship between variations in terrigenous sediment input to the western equatorial Atlantic and the two

types of northern high latitude cold intervals from 13 to 41 ka. Second, we compiled other four high temporal resolution terrestrial paleoprecipitation records along a meridional transect across Central and South America between ca. 17°N and 4°S to study the spatial impacts of HS and DO Stadials. Our results highlight different manifestations of NE Brazilian precipitation in responses to HS and DO Stadials, probably in relation to the individual magnitudes of the AMOC slowdown.

4.3. Material and Methods

4.3.1. Core site

The 760 cm long gravity core GeoB16224-1 (6°39.38' N, 52°04.99' W, 2510 m water depth) was retrieved from the continental slope off French Guiana during RV MS Merian cruise MSM20/3 (Fig.4-1; Mulitza et al., 2013). At this core site, prominent seasonal variations of sea surface salinity (SSS) between austral summer (ca. 36 psu in March) and winter (ca. 34.5 psu in September) (Fig.4-1a, b) document the influence of the Amazon freshwater discharge (e.g., Müller-Karger et al., 1988; Lentz, 1995). With the North Brazil Current (NBC) large amounts of sediment delivered from the Amazon River are transported to the continental margin off French Guiana and beyond (e.g., Allison et al., 2000). Overall, the core site GeoB16224-1 is suitably located to determine variations of the Amazon discharge along with millennial-scale climate oscillations at northern high latitudes.

Fig.4-1. Environmental setting. Monthly averaged 1981-2010 continental precipitation from the University of Delaware (http://climate.geog.udel.edu/~climate/) and wind field from the NOAA/OAR/ESRL PSD (http://www.esrl.noaa.gov/psd/) and mean sea surface salinity (SSS) from the World Ocean Atlas 2013 (Zweng et al., 2013) are given in (a) austral summer (December-January-February (DJF) for precipitation, March for SSS) and (b) austral winter (June-July-August (JJA) for precipitation, September for SSS). The schematic position of the Intertropical Convergence Zone (ITCZ) during JJA and DJF (black dashed lines) and surface currents (grey arrows) in the western tropical Atlantic Ocean (Johns et al. 1998) are sketched in (c). Dots denote the location of sediment core GeoB16224-1 (site E) and other published paleoclimate records (red) discussed in the text (detailed information of each site was given in Table 4-1) as well as the suspended sediment samples (grey) used for endmember unmixing analysis (section 4.3.4).

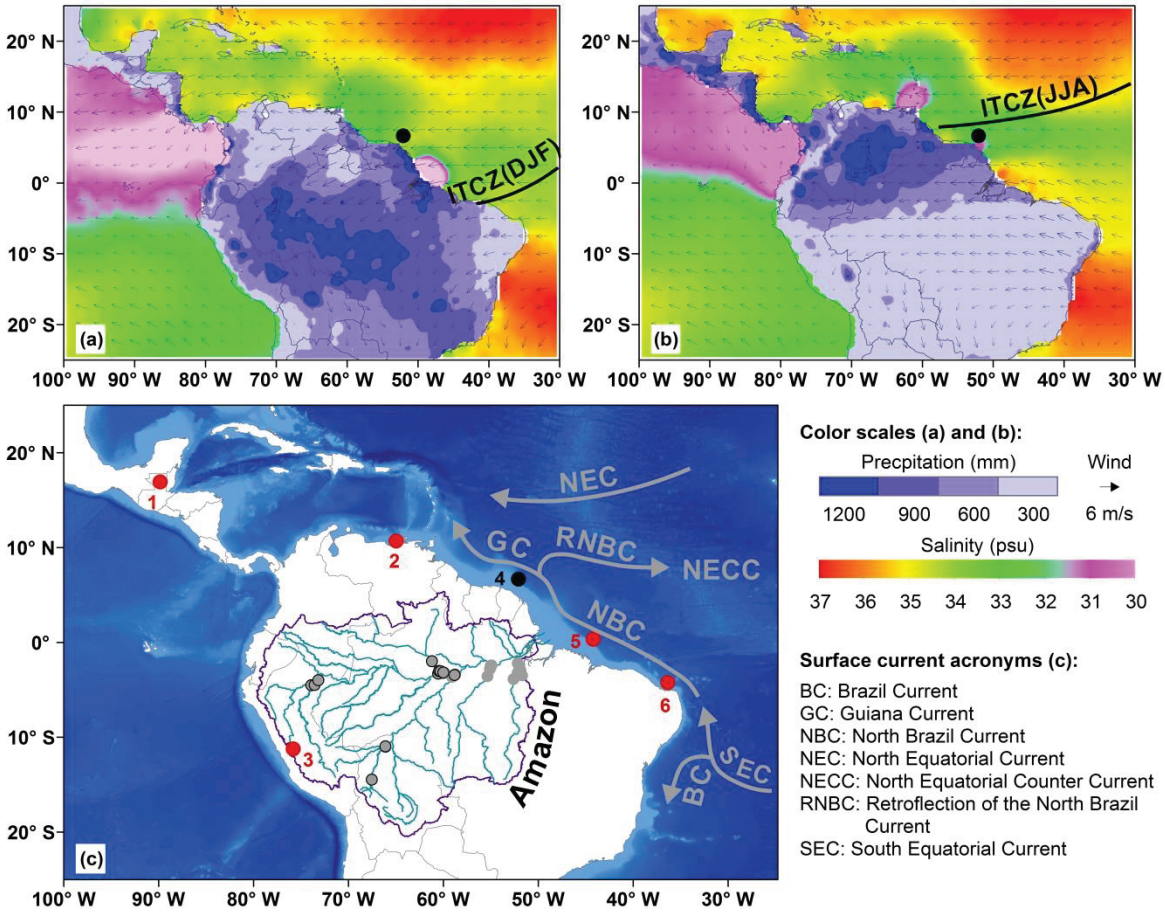

4.3.2. Age model

The upper 600 cm of sediment core GeoB16224-1 extends back to ca. 41 ka, based on fifteen radiocarbon (^{14}C) measurements performed on samples of mixed planktonic foraminifera (e.g., *G. ruber* and *G. sacculifer*; see Zhang et al., 2015b). With these ^{14}C dates, we established the age model and estimated the associated uncertainties (Fig.S4-1) by using the R script BACON version 2.2 (Blaauw and Christen 2011) and the IntCal13 calibration curve (Reimer et al., 2013) with a reservoir correction age of 400 ± 100 (2σ error) years. Default parameter settings, except for mem.mean (set to 0.4) and acc.shape (set to 0.5), were applied to constrain ages as drawn from a t-distribution with 9 degrees of freedom (t.a=9, t.b=10). The age-depth models also included analytical uncertainty of the raw ^{14}C ages by combining downcore Monte Carlo proxy time series realizations. We used the last 10000 age-depth realizations from 15000 iterations to calculate median age and the 2σ uncertainty at 5 mm resolution. The chronology of sediment core GeoB16224-1 enables us to mainly focus on the HS and the DO Stadials between 13-41 ka.

4.3.3. Major element composition

Major element intensities of core GeoB16224-1 were obtained by scanning the split core surface of the archive half at 5 mm step with a XRF core-scanner II (AVAATECH no.2) at MARUM, University of Bremen. The XFR data were collected with generator settings of 10 kV, a current of 0.40 mA, and a sampling time of 20 seconds. To calibrate the scanner intensities, we also analyzed elemental concentrations on bulk sediment samples from the working half. In total, 50 discrete samples of about 10 ml wet sediment were freeze-dried, powdered and homogenized using an agate mortar. Measurements were conducted by using a PANalytical Epsilon3-XL XRF spectrometer equipped with a rhodium tube, several filters and a SSD5 detector. The raw data were processed against certified sediment standards. Standard deviations for the single elements were <1%. The powdered measurements and scanner data were combined to derive high-resolution calibrated proportions of elements with a log-ratio regression approach (Weltje and Tjallingii, 2008), in which Ca was used as the denominator element (R^2 was 0.83, Fig.S4-2).

A set of 28 suspended sediment samples from different tributaries of the Amazon River (grey circles without outlines in Fig.4-1c, the data were provided in Table S4-1) was also measured for major element concentrations. First, we collected water samples using a submersible pump at the upper 60% water depth of river channel during the dry (Nov. 2011) and wet (May 2012) seasons. At least 4 l of water was filtered by using cellulose filters (0.2 μm), which were immediately dried and packed in plastic bags for transportation. Then, the sample materials (filter + suspended material, about 21-89 mg) were digested in Teflon liners with a microwave system (MLS, 1200 MEGA) by adding 7 ml HNO_3 (65%), 0.5 ml HF (40%), 0.5 ml HCl (30%) and 0.5 ml MilliQ. All acids were of suprapure quality. Finally, element concentrations (but Si was lost during total digestion procedure, Table S4-1) were measured with ICP-OES (Agilent 720; precision of 2%, standard deviation of 1-3%).

4.3.4. Endmember unmixing analysis

An endmember unmixing model (e.g., Mulitza et al., 2010; Collins et al., 2013) was applied for the suspended sediment samples and the downcore records to determine past changes in the relative input of different components. We included two terrigenous endmembers (e.g., Andes and lowland) as the source origin of fluvial material and one marine endmember as the biogenic fraction. The 28 new (grey circles without outlines in Fig.4-1c) and 18 published (greys circles with black outlines in Fig.4-1c; Sholkovitz et al., 1978; Bouchez et al., 2011, 2012; Govin et al., 2014) geochemical data of suspended materials from different tributaries of the Amazon River (Table S4-1, see Supplementary for details) were compiled to define the two terrigenous endmembers. For marine endmember we only considered Si and Ca compositions (Table S4-2). Because of small changes in palaeoproductivity over the western tropical Atlantic and low accumulation of biogenic opal in sediments (Govin et al., 2014), Si and Ca proportions were fixed to biogenic opal and carbonate measurements, respectively, from nearby sites (Table S4-2). Moreover, multiple iterations of the unmixing analysis allow the estimation of uncertainties in aspects like: (i) modern terrigenous endmember compositions (which were assumed as constant over time); (ii) different sets of lowland elemental proportions (Si concentrations, Table S4-1); and (iii) marine endmember compositions (Si and Ca proportions, Table S4-2). The endmember proportions are expressed as the median values of all iterations (Figs.4-2, 4-3) with non-parametric 95% confidence intervals (2.5th and 97.5th percentiles, not shown).

4.4. Results

The downcore Fe/Ca record of sediment core GeoB16224-1 increases significantly during HS 1-4 and DO Stadials (in particular during DO Stadials 5-8, Fig.4-2b). The Fe/K record also shows clearly elevated values during HS 1-4, while changes during DO Stadials are rather small (Fig.4-2c). The Al/Si values exhibits limited range throughout the whole record (Fig.4-2d). Endmember unmixing analysis shows that Andean and lowland components account for ca. 68% and ca. 26% on average of total materials at the core site,

respectively (Fig.4-2e). The proportion of Andean-sourced terrigenous sediment is also increased during HS 1-4 (although less prominent for HS 2) and DO Stadials 5-8 (Fig.4-3f).

Fig.4-2. Elemental compositions (b-d) and the endmember modeled components (e) of sediment core GeoB16224-1, e.g., ln(Fe/Ca) (b), ln(Fe/K) (c) and Al/Si ratio (d). Vertical bars represent Heinrich Stadials (HS) 1-4 (pink) and Dansgaard-Oeschger (DO) Stadials (cyan) as defined from the NGIRP ice core $\delta^{18}O$ record (a) (Rasmussen et al., 2014).

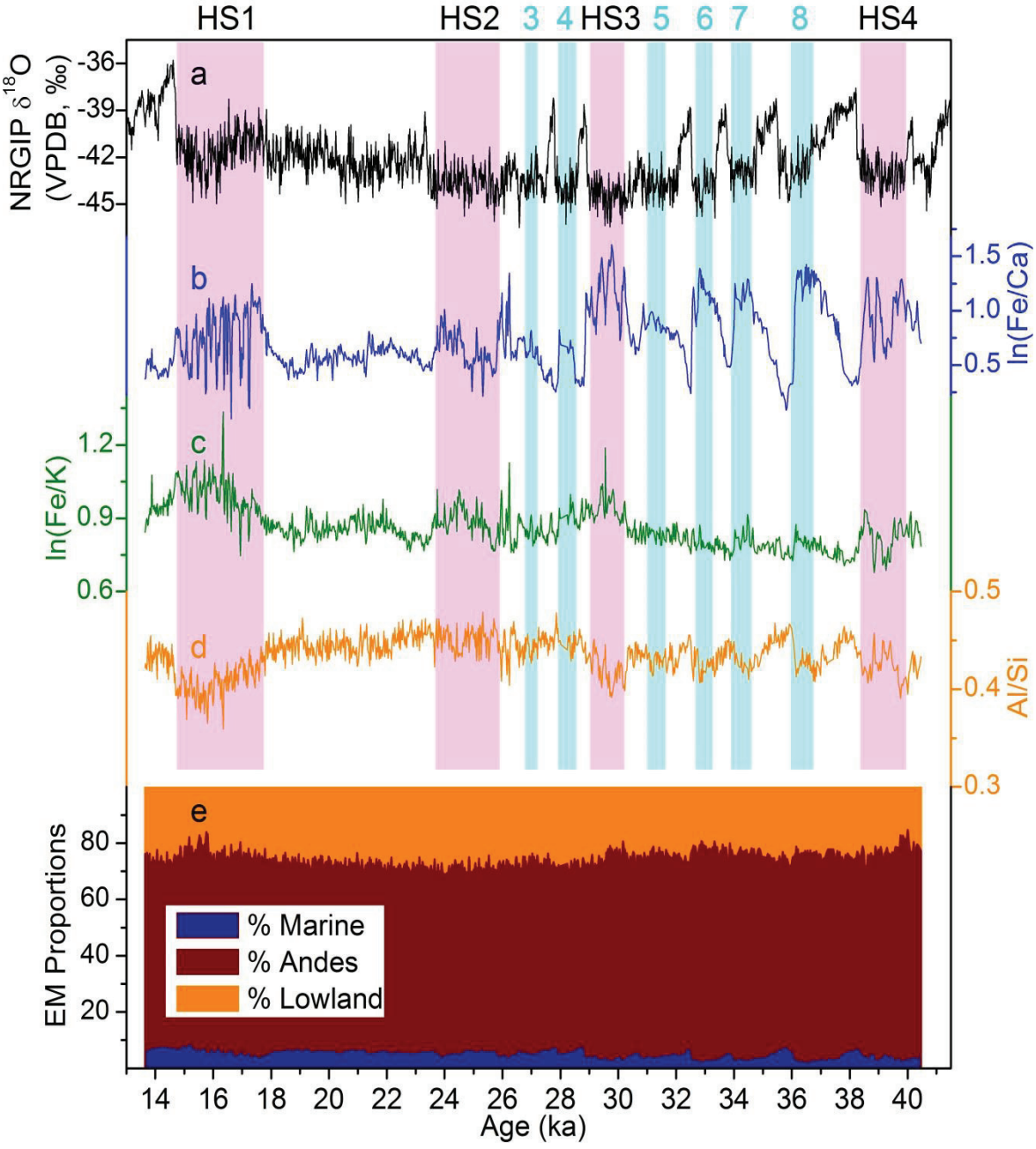

4.5. Discussion

The marked increases in the Fe/Ca record (Fig.4-2b) and Andean-component (Fig.4-3f), in conjunction with the Neodymium (Nd) isotopic composition from the same core GeoB16224-1 (Zhang et al., 2015b), indicate an enhanced supply of Andean-sourced terrigenous material from the Amazon River basin to the western equatorial Atlantic during HS and DO Stadials. Variations of the Fe/K record (Fig.4-2c) display recurrent intensifications in the strength of chemical weathering during HS relative to during DO Stadials. In view of the grain-size control on geochemistry in suspended sediments from the Amazon River (e.g., Bouchez et al., 2011), the small amplitude of changes in the Al/Si record reflects no significant modification of grain-size sorting on fluvial sediments through the long-distance transport pathway. The increased Fe/Ca values documented in core GeoB16224-1 (Fig.4-2b) are hence robust proxy to manifest enhanced precipitation in the source region. Indeed, this connection is apparently substantiated by the negative excursions of Amazonian Andes stalagmite $\delta^{18}O$ records during HS and DO Stadials, such as the Pacupahuain Cave (Kanner et al., 2012; Fig.4-3d) and the Santiago Cave (Mosblech et al., 2012).

Based on the in-phase relationship between the Pacupahuain $\delta^{18}O$ record and our Fe/Ca record (Figs.4-3d, e and 4-4c, d), it seems that there was virtually no delay for fine-grained sediments transport from the Andes to the western equatorial Atlantic. This agrees with previous studies (e.g., Meade et al., 1985) that claimed that fine-grained sediments from the Solimões and the Madeira Rivers (about 90% of total sediment discharge by the Amazon River) are mainly delivered downstream to the ocean within two months (March-April) after the austral summer season. By measuring uranium-series isotopes of suspended sediments in the Madeira River, Dosseto et al. (2006) suggested long-timescale storage for fine-grained sediments in Andean floodplains which implied ca. 17 ± 3 ka for transferring suspended sediment from the Andes to the confluence of the Madeira River with the Amazon River. A full discussion on this issue is unfortunately beyond the scope of this paper, since we have no direct proxy to constrain the residence time of suspended sediments within the basin. Nevertheless, our results highlights that an

Table 4-1. Coordinates and other information of sediment core GeoB16224-1 and published paleorecords in Figs.4-1, 4-3 and 4-4.

Site	Core ID	Latitude	Longitude	Altitude (m)	Dating	Proxy	Resolution (mm / year)*	Reference
1	PI-2/6	16.9° N	-89.8° W	-71	^{14}C	Magnetic susceptibility	10 / ca. 10	Escobar et al., 2012
2	MD03-2621	10.7° N	-65.0° W	-847	Match to ^{14}C	Total reflectance	0.07 / ca. 0.15	Deplazes et al., 2013
3	P09-PH12	11.2° S	-75.8° W	3800	U-Th	δ^{18}O	0.1-0.2 / ca. 32	Kanner et al., 2012
4	GeoB16224-1	6.7° N	-52.1° W	-2510	^{14}C	Fe/Ca	5 / ca. 26.5	This study
5	CDH86	0.3° N	-44.2° W	-3107	^{14}C	Ti/Ca	2 / ca. 7.5	Nace et al., 2014
6	GeoB3910-2	-4.2° S	-36.3° W	-2362	^{14}C	Ti/Ca	4 / ca. 40	Jaeschke et al., 2007

* Represents the measurement step (in mm) and the related temporal resolution (in year).

increased precipitation in the Andes during HS and DO Stadials accounts directly for an enhanced discharge of fine-grained Andean terrigenous sediments by the Amazon River.

Increased precipitation over the Amazonian Andes during both HS and DO Stadials was attributed to a stronger SASM, despite some elusive intervals, e.g., the HS 3 (Mosblech et al., 2012) and the DO Stadial 3 (Kanner et al., 2012). In fact, the SASM mainly dominates precipitation across the Amazon basin (Fig.4-1a), whiles the ITCZ is the main atmosphere feature that controls rainfall over northernmost South America and NE Brazil (Fig.4-1a, b). Comparing well-dated records along a north-south transect across Central and South America (Fig.4-1c and Table 4-1) enables us to disentangle regional responses of the SASM and the ITCZ to HS and DO Stadials. During HS, the compiled records indicate decreased rainfall to the north of our core site (namely PI-2/6 and MD03-2621; Fig.4-3b, c) (Escobar et al., 2012; Deplazes et al., 2013), but our core site GeoB16224-1 and the two cores to the south (CDH86 and GeoB3910-2; Fig.4-3e, h) showed increased precipitation (Jaeschke et al., 2007; Nace et al., 2014). Likewise, during DO Stadials, in particular for DO Stadials 5-8, we see the same antiphased relationship of terrestrial

Fig.4-3. Paleoprecipitation records from tropical Central and South America. Vertical bars represent HS (pink) and the DO Stadials (cyan) as defined from the NGIRP ice core $\delta^{18}O$ record (a) (Rasmussen et al., 2014). (b): Lake Petén Itzá (Escobar et al., 2012); (c): sediment core MD03-2621 (Deplazes et al., 2013); (d): Pacupahuain Cave (Kanner et al., 2012); (e) and (f): ln(Fe/Ca) and proportion of Andean material within terrigenous fraction in core GeoB16224-1; (g): sediment core CDH86 (Nace et al., 2014); (h): sediment core GeoB3910-2 (Jaeschke et al., 2007). Note the HS2 in core CDH86 (g) is misplaced since its age control for last 20 ka was aligned with another gravity core nearby.

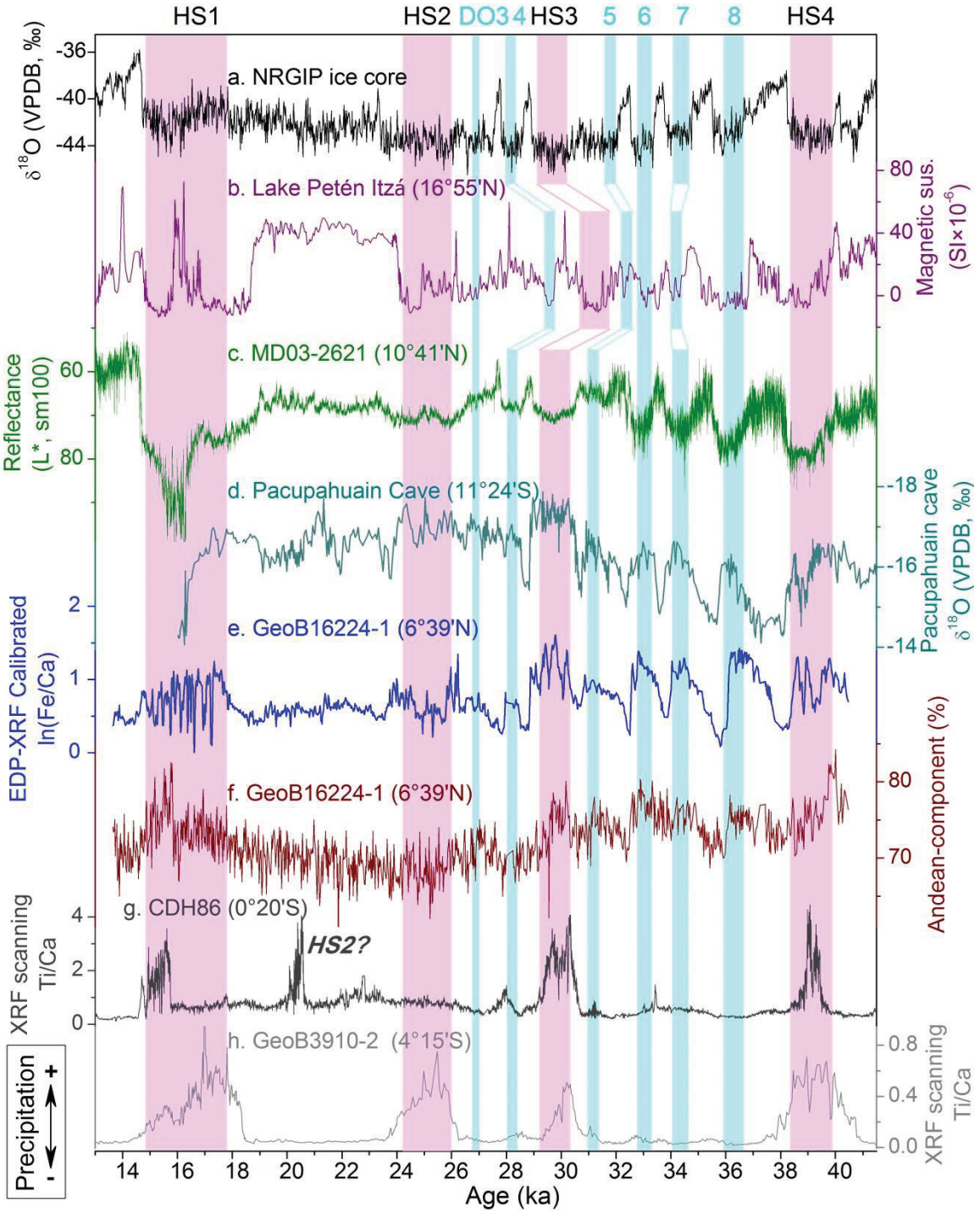

precipitation between core GeoB16224-1 and the two cores to the north (e.g., MD03-2621, Fig.4-4b, d; Deplazes et al., 2013). However, the two cores to the south of our core site (CDH86 and GeoB3910-2) document no systematic evidence for changes in terrigenous input across DO Stadials (Figs.4-3g, h and 4-4e) (Jaeschke et al., 2007; Nace et al., 2014). It is also worth noting that the temporal resolutions of the proxy records to the south of our core site (Table 4-1), e.g., cores CDH86 (ca. 8 years per sample, Fig.4-3g; Nace et al., 2014) and GeoB3910-2 (ca. 40 years per sample, Fig.4-3h; Jaeschke et al., 2007), are sufficiently high to resolve climatic signals associated with the DO Stadials.

Fig.4-4. Detailed comparison between paleoprecipitation records for tropical South America. Vertical bars represent HS (pink) and DO Stadials (cyan) as defined from the NGIRP ice core $\delta^{18}O$ record (a) (Rasmussen et al., 2014). (b): sediment core MD03-2621 (Deplazes et al., 2013), (c): Pacupahuain Cave (Kanner et al., 2012), (d): core GeoB16224-1, (e): sediment core CDH86 (Nace et al., 2014).

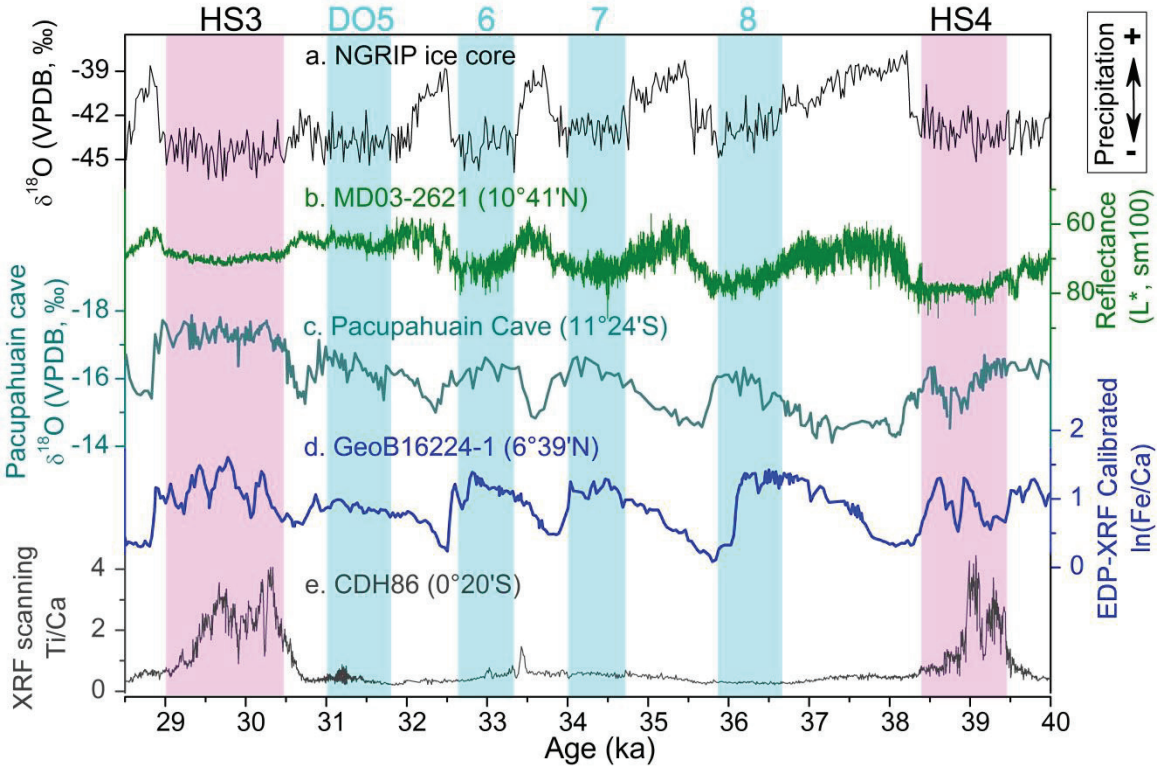

During HS, freshwater perturbation in the high latitudes of the North Atlantic and the subsequent slowdown of the AMOC (e.g., Böhm et al., 2015) led to a steeper latitudinal sea surface temperature gradient over the Atlantic. It, as a result, induced a strengthening of the SASM and a southward displacement of the ITCZ mean position which then

increased precipitation over the Andes (Kanner et al., 2012) and NE Brazil (Wang et al., 2004; Jaeschke et al., 2007) respectively. Accordingly, an enhanced input of fluvial sediments to the continental margin was determined at core site GeoB16224-1 and offshore NE Brazil (Arz et al., 1998; Jaeschke et al., 2007; Nace et al., 2014; Zhang et al., 2015b). By contrast, the DO Stadials only involved a moderate decrease (generally less than ca. 50%) in the strength of the AMOC (Zhang et al., 2014a, b), if compared to the significant slowdown (or even near shutdown) described for HS (McManus et al., 2004; Böhm et al., 2015). It also brought about an intensification of the SASM during DO Stadials, as evidenced by enhanced precipitation from Andean stalagmite $\delta^{18}O$ records (e.g., Kanner et al., 2012) and increased Fe/Ca values at core site GeoB16224-1. However, the moderate AMOC reduction was likely unable to shift the ITCZ mean position as far south as during HS, thus not influencing the supply of fluvial sediments to the continental margin off NE Brazil (e.g., Jaeschke et al., 2007; Nace et al., 2014). This interpretation is clearly consistent with model simulations (e.g., Zhang et al., 2014a) that confirmed little change in NE Brazilian precipitation between the DO Stadials and the DO interstadials.

Considering different behaviors of terrestrial precipitation changes to the north (Figs.4-3b, c and 4-4b) and the south of our core site (Figs.4-3g, h and 4-4e), it is also possible that the northern and southern boundaries of the ITCZ rainbelt responded to DO Stadials independently (such as the ITCZ shift was prominent over northernmost South America while inappreciable over NE Brazil). Such hypothesis, although applied to explain the characteristics of the ITCZ rainfall over tropical South America during HS1 (Maslin et al., 2011), remains equivocal for other HS based on our results (Figs.4-3, 4-4). Interestingly, we also note that precipitation changes during DO Stadials apparently displayed an opposite pattern between NE Brazil (dry) (Jaeschke et al., 2007; Nace et al., 2014) and the Andes (wet) (Kanner et al., 2012; this study). Previous studies reported an east-west antiphase of tropical South American precipitation (Cruz et al., 2009; Cheng et al., 2013a), the mechanism of which was attributed to the orbital forcing. It is still unknown whether the insolation played a role in the east-west antiphase of precipitation changes between NE Brazil and the Andes during DO Stadials. Hence, further investigation on this issue would improve our knowledge about the ITCZ shift under a moderate magnitude of the

AMOC, a particularly timely topic regarding the AMOC slowdown in the near future (e.g., Cheng et al., 2013b; Rahmstorf et al., 2015).

4.6. Conclusions

We determined the regional structures of tropical South American precipitation in response to HS and DO Stadials. Analyses of major element ratios together with Nd isotopic data indicate enhanced input of fine-grained Amazonian Andes sediments during HS and DO Stadials from 13-41 ka to the continental margin off French Guiana (ca. 7°N) in the western equatorial Atlantic. The comparison of these results to four previously published high temporal resolution sediment cores between ca. 17°N and 4°S across Central and South America show that both H and DO stadials led to a strengthening of the SASM and a southward migration of the ITCZ. However, NE Brazilian precipitation, which is today under the control of the ITCZ, experienced significant increases during HS but no evident changes during DO Stadials. We suggest that the moderate reduction of the AMOC during DO Stadials, in comparison to the nearly shutdown during HS, was unable to shift the ITCZ mean position enough to the south in order to substantially increase precipitation over NE Brazil.

4.7. Acknowledgements

We appreciate the technical support from S. Pape for the EDP-XRF analyses, Dr. U. Röhl and V. Lukies for the XRF scanning. We acknowledge the Department of Geosciences and the GeoB Core Repository at MARUM – University of Bremen for supplying sediment samples. We thank Dr. A. Govin and Dr. J. Just for constructive discussion. All the data presented in this paper will be archived in Pangaea (www.pangaea.de). This work was funded by the Deutsche Forschungsgemeinschaft through the DFG Research Centre/Cluster of Excellence 'The Ocean in the Earth System'. C.M.C. was supported by FAPESP (grant 2012/17517-3) and CAPES (grants 1976/2014 and 564/2015), as well as the Hanse Institute for Advanced Study in Delmenhorst, Germany. A.O.S. was supported

by CNPq (grant 309223/2014-8). Sampling suspended sediments in the Amazonian tributaries was also funded by FAPESP (grant 2011/06609-1).

4.8. References

Allison, M.A., et al. 2000. Origin of Amazon mudbanks along the northeastern coast of South America. Mar. Geol. 163(1-4), 241-256.

Alvarez-Solas, J., et al. 2010. Links between ocean temperature and iceberg discharge during Heinrich events. Nat. Geosci. 3, 122-126.

Arz, H.W., Pätzold, J., Wefer, G. 1998. Correlated millennial-scale changes in surface hydrography and terrigenous sediment yield inferred from last-glacial marine deposits off northeastern Brazil. Quaternary Res. 50(2), 157-166.

Asmerom, Y., et al. 2010. Variable winter moisture in the southwestern United States linked to rapid glacial climate shifts. Nat. Geosci. 3, 114-117.

Blaauw, M., Christen, J.A., 2011. Flexible Paleoclimate Age-Depth Models Using an Autoregressive Gamma Process. Bayesian Anal. 6, 457-474.

Böhm, E., et al. 2015. Strong and deep Atlantic meridional overturning circulation during the last glacial cycle. Natrue 517, 73-76.

Bond, G., et al. 1992. Evidence for massive discharges of icebergs into the North Atlantic ocean during the last glacial period. Nature 360, 245-249.

Bouchez, J., et al. 2011. Grain size control of river suspended sediment geochemistry: Clues from Amazon River depth profiles. Geochem. Geophys. Geosyst. 12, Q03008, doi: 10.1029/2010gc003380.

Bouchez, J., et al. 2012. Floodplains of large rivers: Weathering reactors or simple silos? Chem. Geol. 332–333, 166–184.

Burns, S.J., et al. 2003. Indian Ocean Climate and an Absolute Chronology over Dansgaard/Oeschger Events 9 to 13. Science 301, 1365-1367.

Cheng, H., et al. 2013a. Climate change patterns in Amazonia and biodiversity. Nat. Commun. 4(1411), doi:10.1038/ncomms2415.

Cheng, W., et al. 2013b. Atlantic Meridional Overturning Circulation (AMOC) in CMIP5 models: RCP and historical simulations. J. Climate 26, 7187-7197.

Clark, P.U., Pisias, N.G., Stocker, T.F., Weaver, A.J. 2002. The role of the thermohaline circulation in abrupt climate change. Nature 415, 863-869.

Collins, J.A., et al. 2013. Abrupt shifts of the Sahara-Sahel boundary during Heinrich stadials. Clim. Past 9, 1181-1191.

Cruz, F.W., et al. 2009. Orbitally driven east–west antiphasing of South American precipitation. Nat. Geosci. 2, 210-214.

Dansgaard, W., et al. 1993. Evidence for general instability of past climate from a 250-kyr ice-core record. Nature 364, 218-220.

Deplazes, G., et al. 2013. Links between tropical rainfall and North Atlantic climate during the last glacial period. Nat. Geosci. 6, 213-217.

Dosseto, A., et al. 2006. Weathering and transport of sediments in the Bolivian Andes: Time constraints from uranium-series isotopes. Earth Planet. Sci. Lett. 248, 759-771.

Escobar, J., et al. 2012. A ~43-ka record of paleoenvironmental change in the Central American lowlands inferred from stable isotopes of lacustrine ostracods. Quat. Sci. Rev. 37, 92-104.

Govin, A., et al. 2014. Terrigenous input off northern South America driven by changes in Amazonian climate and the North Brazil Current retroflection during the last 250 ka. Clim. Past 10, 843-862.

Heinrich, H. 1988. Origin and consequences of cyclic ice rafting in the northeast Atlantic ocean during the past 130,000 years. Quaternary Res. 29, 142-152.

Jaeschke, A., et al. 2007. Coupling of millennial-scale changes in sea surface temperature and precipitation off northeastern Brazil with high-latitude climate shifts during the last glacial period. Paleoceanography 22(4), doi:10.1029/2006PA001391.

Johns, W.E., et al. 1998. Annual cycle and variability of the North Brazil Current. J. Phys. Oceanogr. 28(1), 103-128.

Kanner, L.C., Burns, S.J., Cheng, H., Edwards, R.L. 2012. High latitude forcing of the South American Summer Monsoon during the Last Glacial. Science 335, 570-573.

Lentz, S.J. 1995. Seasonal variations in the horizontal structure of the Amazon Plume inferred from historical hydrographic data. J. Geophys. Res.-Oceans, 100, 2391-2400.

Malhi, Y., et al. 2008. Climate Change, Deforestation, and the Fate of the Amazon. Science 390, 169-172.

Malhi, Y., et al. 2009. Exploring the likelihood and mechanism of a climate-change-induced dieback of the Amazon rainforest. Proc. Natl. Acad. Sci. 106, 20610-20615.

Maslin, M.A., et al. 2011. Dynamic boundary-monsoon intensity hypothesis: evidence from the deglacial Amazon River discharge record. Quat. Sci. Rev. 30, 3823-3833.

McManus, J.F., et al. 2004. Collapse and rapid resumption of Atlantic meridional circulation linked to deglacial climate changes. Nature 428, 834-837.

Meade, R.H., et al. 1985. Storage and Remobilization of Suspended Sediment in the Lower Amazon River of Brazil, Science 228, 488-490.

Mosblech, N.A.S., et al. 2012. North Atlantic forcing of Amazonian precipitation during the last ice age. Nat. Geosci. 5, 817-820.

Mulitza, S., et al. 2010. Increase in African dust flux at the onset of commercial agriculture in the Sahel region. Nature 466, 226-228.

Mulitza, S., et al. 2013. Response of Amazon sedimentation to deforestation, land use and climate variability. Cruise No. MSM20/3 (February 19 – March 11, 2012), Recife (Brazil) – Bridgetown (Barbados). MARIA S. MERIAN-Berichte, MSM20/3, 86 pp., DFG Senatskommission für Ozeanographie, doi:10.2312/cr_msm20_3.

Müller-Karger, F.E., McClain, C.R., Richardson, P.L. 1988. The dispersal of the Amazon's water. Nature, 333, 56–59.

Nace, T.E., et al. 2014. The role of North Brazil Current transport in the paleoclimate of the Brazilian Nordeste margin and paleoceanography of the western tropical Atlantic during the late Quaternary. Palaeogeogr. Palaeoclimatol. Palaeoecol. 415, 3-13.

Peterson, L.C., et al. 2000. Rapid changes in the hydrologic cycle of the tropical Atlantic during the Last Glacial. Science 290, 1947-1951.

Rahmstorf, S. 2002. Ocean circulation and climate during the past 120,000 years. Nature 419, 207-214.

Rahmstorf, S., et al. 2015. Exceptional twentieth-century slowdown in Atlantic Ocean overturning circulation. Nature Climate Change 5, 475-480.

Rasmussen, S.O., et al. 2014. A stratigraphic framework for abrupt climatic changes during the Last Glacial period based on three synchronized Greenland ice-core records: refining and extending the INTIMATE event stratigraphy. Quat. Sci. Rev. 106, 14-28.

Reimer, P.J., et al. 2013. IntCal13 and Marine13 radiocarbon age calibration curves 0–50,000 years cal BP. Radiocarbon 55(4), 1869-1887.

Remsen Jr, J.V., & Parker III, T.A. 1983. Contribution of river-created habitats to bird species richness in Amazonia. Biotropica, 223-231.

Sanchez Goñi M.F., Harrison S.P. 2010. Millennial-scale climate variability and vegetation changes during the Last Glacial: Concepts and terminology. Quat. Sci. Rev. 29, 2823-2827.

Sholkovitz, E.R., van Grieken, R., Eisma, D., 1978. The major-element composition of suspended matter in the Zaire river and estuary, Netherlands Journal of Sea Research, 12, 407–413.

Svensson, A., et al. 2006. The Greenland Ice Core Chronology 2005, 15–42 ka. Part 2: comparison to other records. Quat. Sci. Rev. 25, 3258-3267.

Voelker, A.H.L. 2002. Global distribution of centennial-scale records for Marine Isotope Stage (MIS) 3: a database. Quat. Sci. Rev. 21, 1185-1212.

Wang, X., et al. 2004. Northeastern Brazil wet periods linked to distant climate anomalies and rainforest boundary changes. Nature 432, 740-743.

Wang, X., et al. 2006. Interhemispheric anti-phasing of rainfall during the last glacial period. Quat. Sci. Rev. 25(23-24), 3391-3403.

Wang, Y.J., et al. 2001. A High-Resolution Absolute-Dated Late Pleistocene Monsoon Record from Hulu Cave, China. Science 294, 2345-2348.

Weltje, G.J., Tjallingii, R. 2008. Calibration of XRF core scanners for quantitative geochemical logging of sediment cores: Theory and application. Earth Planet. Sci. Lett. 274, 423-438.

Winemiller, K.O., et al. 2016. Balancing hydropower and biodiversity in the Amazon, Congo, and Mekong. Science 351 (6269), 128-129.

Wittmann, F., et al. 2013. Habitat specifity, endemism and the neotropical distribution of Amazonian white-water floodplain trees. Ecography, 36(6), 690-707.

Zhang, X., et al. 2014b. Instability of the Atlantic overturning circulation during Marine Isotope Stage 3. Geophys. Res. Lett. 41, doi:10.1002/2014GL060321.

Zhang, X., Lohmann, G., Knorr, G., Purcell, C. 2014a. Abrupt glacial climate shifts controlled by ice sheet changes. Nature 512, 290-294.

Zhang, X., Prange, M., Merkel, U., Schulz, M. 2015a. Spatial fingerpring and magnitude of changes in the Atlantic meridional overturning circulation during Marine Isotope Stage 3. Geophys. Res. Lett. 42, doi:10.1002/2014GL063003.

Zhang, Y., et al. 2015b. Origin of increased terrigenous supply to the NE-South American continental margin during Heinrich Stadial 1 and the Younger Dryas, Earth Planet. Sci. Lett. 432, 493-500.

Zweng, M.M, et al. 2013. World Ocean Atlas 2013. 2, Salinity. S. Levitus, Ed., A. Mishonov Technical Ed.; NOAA Atlas NESDIS 74, 39 pp.

4.9 Supplementary Material

Fig.S4-1. Comparison between calibrated ^{14}C ages (black dots) and new age model of sediment core GeoB16224-1. Color lines mark the median age (grey) and 2σ uncertainty (dashed grey) derived from the BACON software (section 2.2). We tuned the age within the error ranges from 28-41 ka (red) to better match with the NGRIP ice core $\delta^{18}O$ record (Rasmussen et al., 2014). The ^{14}C date at 550 cm was excluded for the age model.

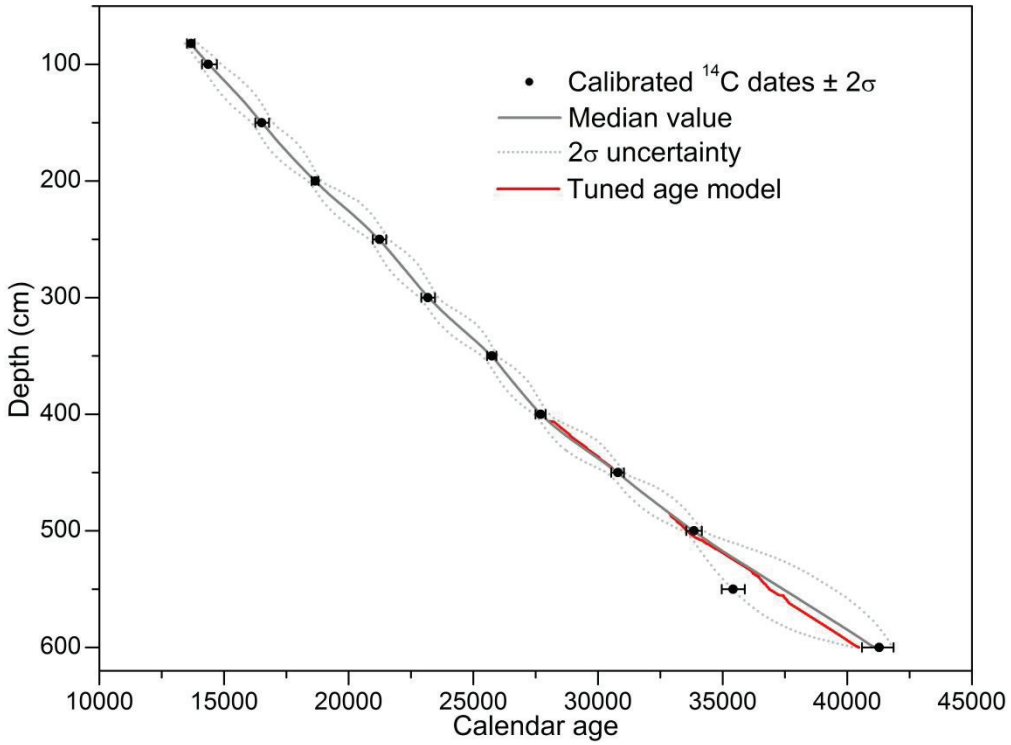

Fig.S4-2. Comparison between EDP-XRF and calibrated elemental ratios of core GeoB16224-1. Downcore ln(Fe/Ca) values are presented versus depth for the XRF-calibrated data (grey line) and the EDP-XRF measurements (crossed dots) (R^2=0.83, which is the mean R^2 of all element/Ca log-ratio regressions; Weltje and Tjallingii, 2008).

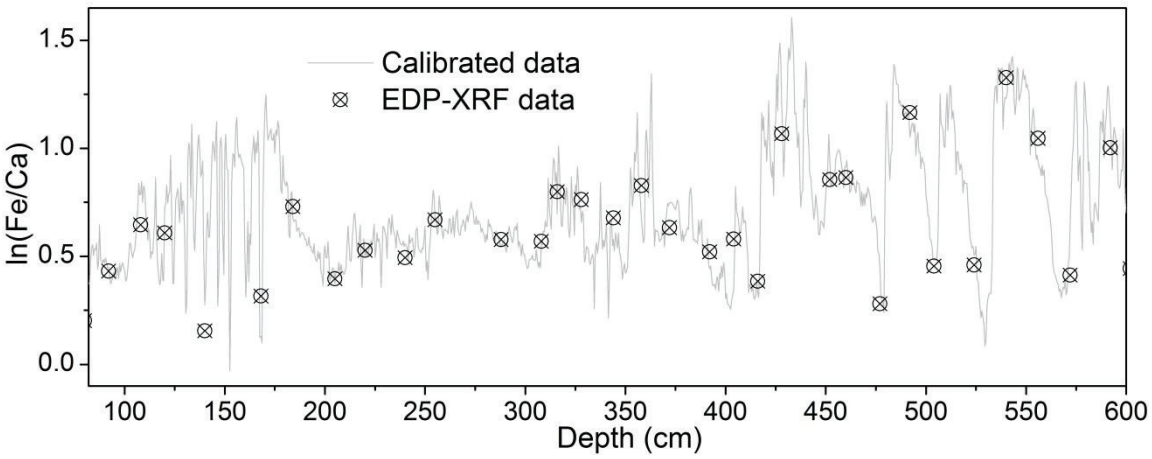

Table S4-1. Major element composition of river suspended material used in the endmember unmixing analysis (Elemental proportions are given in weight percent and were calculated such as the sum of the six elements considered in this study is 100%).

No.	River	Lat	Long	Al (%)	Si (%)*	K (%)	Ca (%)	Fe (%)	Ti (%)	Reference
1	Madeira MAO 22b	-3.64	-59.02	22.09	60.00	5.12	0.77	11.22	0.81	This study
2	Madeira MAO 25c	-3.53	-58.91	22.04	60.00	5.17	0.75	11.20	0.83	This study
3	Madeira MAO 28c	-3.44	-58.80	21.99	60.00	5.22	0.78	11.21	0.80	This study
4	Madeira MAO 38	-3.66	-59.07	20.95	60.00	5.61	0.79	11.55	1.11	This study
5	Madeira MAO 42	-3.52	-58.90	21.39	60.00	5.27	0.69	11.72	0.92	This study
6	Madeira MAO 45	-3.42	-58.79	21.10	60.00	5.24	0.67	12.12	0.87	This study
7	Madeira AM-06-35	-3.41	-58.79	22.75	57.66	5.94	0.66	11.79	1.19	Bouchez et al., 2011
8	Madeira AM-06-38	-3.41	-58.79	19.36	63.45	5.18	0.65	10.20	1.16	Bouchez et al., 2011
9	Madeira AM-06-43	-3.41	-58.78	21.47	60.13	5.63	0.65	10.95	1.17	Bouchez et al., 2011
10	Madeira AM-05-15	-3.45	-58.81	22.41	58.66	5.86	0.69	11.22	1.17	Bouchez et al., 2011
11	Beni AM-07-09	-11.00	-66.09	18.11	65.71	5.29	0.48	9.34	1.07	Bouchez et al., 2012
12	Madre de Dios AM-07-14	-10.96	-66.10	20.76	60.45	4.81	1.20	11.46	1.32	Bouchez et al., 2012
13	Beni AM-07-04	-14.47	-67.53	20.43	62.01	5.81	0.57	10.13	1.05	Bouchez et al., 2012
14	Solimões MAO 05d	-3.29	-60.02	28.5	60.00	1.21	0.26	8.82	1.21	This study
15	Solimões MAO 10d	-3.27	-60.29	22.2	60.00	4.15	1.86	10.69	1.10	This study
16	Solimões MAO 13d	-3.20	-59.89	22.32	60.00	4.05	1.78	10.81	1.04	This study
17	Solimões MAO 72	-3.29	-60.40	19.77	60.00	3.29	1.94	14.05	0.96	This study
18	Solimões MAO 77	-3.31	-60.04	19.46	60.00	3.35	1.85	14.37	0.98	This study
19	Solimões MAO 80	-3.22	-59.88	19.92	60.00	3.27	1.91	13.89	1.02	This study
20	Solimões AM-06-09	-3.31	-60.55	21.98	59.20	4.61	1.94	11.14	1.13	Bouchez et al., 2011
21	Marañón AM-08-24	-4.52	-73.91	19.99	61.24	4.37	3.44	9.91	1.07	Bouchez et al., 2012
22	Marañón AM-08-33	-4.48	-73.55	19.92	56.52	4.40	8.78	9.31	1.06	Bouchez et al., 2012

23	Amazonas AM-08-05	-4.00	-73.16	19.14	62.34	4.74	2.77	9.89	1.13	Bouchez et al., 2012
24	Rio Negro	-2.00	-61.20	34.60	45.00	1.80	0.90	17.00	0.80	Sholkovitz et al., 1978
25	Rio Negro MAO 01	-3.06	-60.30	38.20	45.00	1.30	0.50	13.50	1.50	Govin et al., 2014
26	Rio Negro MAO 02f	-3.05	-60.35	30.60	45.00	5.70	2.50	14.80	1.40	Govin et al., 2014
27	Rio Negro MAO 03c	-3.08	-60.21	38.30	45.00	1.70	0.50	13.20	1.40	Govin et al., 2014
28	Rio Negro MAO 81	-3.02	-60.44	32.40	45.00	2.50	1.30	17.30	1.50	Govin et al., 2014
29	Rio Negro MAO 83	-3.06	-60.29	33.40	45.00	0.70	1.00	18.40	1.40	Govin et al., 2014
30	Rio Negro MAO 93	-3.18	-60.00	33.50	45.00	0.00	0.80	19.20	1.40	Govin et al., 2014
31	Tapajós STM 24	-2.81	-55.07	37.42	45.00	1.56	2.98	12.05	0.99	This study
32	Tapajós STM 33	-3.59	-55.33	40.44	45.00	1.30	1.10	11.18	0.98	This study
33	Tapajós STM 37	-2.47	-54.99	36.95	45.00	0.84	2.10	14.06	1.05	This study
34	Tapajós STM 39	-2.43	-54.94	35.25	45.00	1.37	3.42	14.03	0.92	This study
35	Tapajós STM 11	-2.43	-54.92	33.93	45.00	0.34	1.34	18.48	0.91	This study
36	Tapajós STM 13	-2.80	-55.08	34.27	45.00	0.37	0.75	18.73	0.88	This study
37	Tapajós STM 19	-2.47	-55.00	31.28	45.00	1.00	1.71	20.28	0.73	This study
38	Xingu XA 01	-3.22	-52.15	34.02	45.00	4.12	2.22	13.59	1.04	This study
39	Xingu XA 19	-3.88	-52.59	35.37	45.00	3.00	2.07	13.44	1.12	This study
40	Xingu XA 23	-3.49	-51.69	36.74	45.00	2.95	1.66	12.56	1.08	This study
41	Xingu XA 26	-2.65	-51.98	34.97	45.00	3.82	1.68	13.40	1.13	This study
42	Xingu XA 28	-3.01	-51.85	35.20	45.00	3.05	1.83	13.84	1.08	This study
43	Xingu XA 39	-3.22	-52.14	33.05	45.00	1.29	1.76	17.76	1.13	This study
44	Xingu XA 49	-3.40	-51.97	33.87	45.00	0.97	1.35	17.80	1.01	This study
45	Xingu XA 53	-2.63	-51.97	30.67	45.00	0.92	2.08	20.52	0.81	This study
46	Xingu XA 73	-2.22	-52.16	29.38	45.00	0.82	1.44	22.60	0.76	This study

* Because of Si loss during total digestion procedure, the Si proportion of new river samples is fixed, i.e., 60% for samples in Andean tributaries Solimões and Madeira based on previously published data (Bouchez et al., 2011, 2012), 45% for samples in lowland tributaries Negro (Govin et al., 2014) and Tapajós and Xingu Sholkovitz et al. (1978). An error of ± 2.5 % on Si proportion is included in the endmember unmixing analysis. We run three sets of 1000 Monte-Carlo iterations with different Si proportions of river samples.

Because the 45% Si hypothesis for lowland tributaries was based only on samples from Negro River (see No. 24-30 in Table S4-1), we also used the different Si concentrations (e.g., 30%, 60% Si hypothesis) to perform the endmember unmixing analysis (Fig.S4-3). For 30% Si hypothesis, we obtain high Andean proportion (within terrigenous components) about 84% (while ca. 38% for 60% Si hypothesis, ca. 72% for 45% Si hypothesis). Previous studies (e.g., Milliman and Meade, 1983; Rimington, 1999) showed that Andean materials are likely to account for about 70-80% of Amazon sediment discharge. Thus, 30%-45% Si hypothesis is proper in our case.

Fig.S4-3. Different Si hypothesis for lowland tributaries used for the endmember analysis.

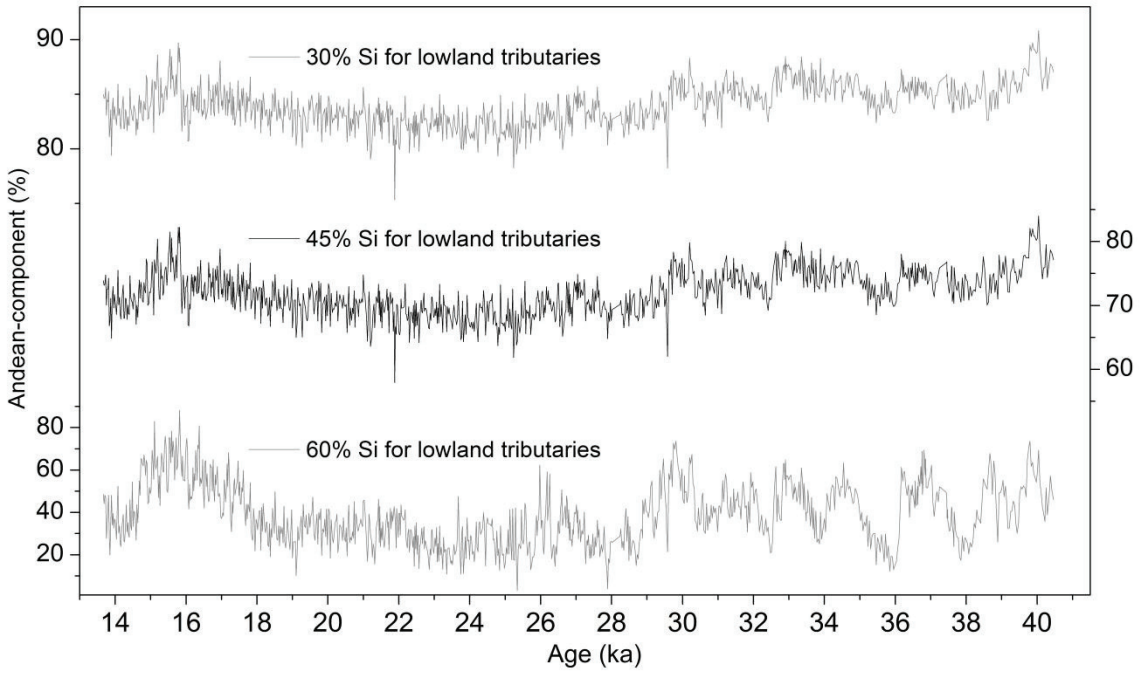

Table S4-2. Summary of the terrigenous and marine biogenic endmembers (EM) used in the unmixing analysis (section 4.3.4) for sediment core GeoB16224-1. Numbers in terrigenous EM columns refer to Table S4-1.

Core site	1st terrigenous EM	2nd terrigenous EM	Marine EM[a]
GeoB16224-1	Andean tributaries (1-23)	Lowland tributaries (24-46)	87.5 (± 1) % Ca 12.5 (± 1) % Si[b]

[a] The marine biogenic endmember includes only Ca and Si composition, which are derived from the carbonate and biogenic opal content of surface sediment in nearby sites (Lochte et al., 2000; http://doi.pangaea.de/10.1594/PANGAEA.53229). Values in brackets are the errors on the composition included in the 95% confidence intervals of endmember unmixing analysis.

[b] Nutrient-rich freshwater from the Amazon River stimulate siliceous productivity in surface waters off the Amazon mouth, as substantiated by high diatom abundance and high biogenic silica (up to 40 %) (DeMaster et al., 1983). However, the low carbonate content (ca. 7.5 %) measured in our study area indicates low biological activity which was not sufficiently large to raise the carbonates to 10% (Gibbs, 1973). Thus, the low biogenic silica content (< 1 %) of surface sediments still generates the high Si proportion in the endmember's composition. In addition, the error on respective Ca and Si proportions that we used during the Monte-Carlo analysis accounts for small variations in biogenic opal content.

4.9.1. Reference

Bouchez, J., et al. 2011. Grain size control of river suspended sediment geochemistry: Clues from Amazon River depth profiles, Geochem. Geophys. Geosyst., 12, Q03008, 10.1029/2010gc003380.

Bouchez, J., et al. 2012. Floodplains of large rivers: Weathering reactors or simple silos? Chem. Geol. 332–333, 166–184.

DeMaster, D.J., et al. 1983. Biological uptake and accumulation of silica on the Amazon continental shelf. Geochimica et Cosmochimica Acta, 47, 1713–1723.

Gibbs, R.J., 1973. The bottom sediments of the Amazon shelf and tropical Atlantic Ocean. Marine Geology 14, 39–45.

Govin, A., et al. 2014. Terrigenous input off northern South America driven by changes in Amazonian climate and the North Brazil Current retroflection during the last 250 ka, Clim. Past 10, 843–862.

Lochte, K., et al. 2000. Atlantic data base for exchange processes at the deep sea floor (ADEPD). Data collected and published through EU-project ADEPD (MAS3-CT97-0126-ADEPD) 1998/99, Institute for Baltic Sea Research, Warnemünde, Germany, hdl:10013/epic.32910.d001.

Milliman, J.D., Meade, R.H. 1983. World-wide delivery of river sediments to the oceans. Journal of Geology, 91, 1-21.

Rasmussen, S.O., et al. 2014. A stratigraphic framework for abrupt climatic changes during the Last Glacial period based on three synchronized Greenland ice-core records: refining and extending the INTIMATE event stratigraphy. Quat. Sci. Rev. 106, 14–28.

Rimington, N. 1999. Depositional history of sands on the Amazon Fan. Ph.D. thesis, University of Cardiff.

Sholkovitz, E.R., et al. 1978. The major-element composition of suspended matter in the Zaire river and estuary, Netherlands Journal of Sea Research, 12, 407–413.

Weltje, G.J., Tjallingii, R., 2008. Calibration of XRF core scanners for quantitative geochemical logging of sediment cores: Theory and application. Earth Planet. Sci. Lett. 274, 423–438.

Chapter V

Conclusion and Outlook

5.1. General overview

In this thesis, we scrutinize the physical mechanisms and regional characteristics of South American precipitation in response to Heinrich and DO Stadials. To summarize the main results, conclusions are described below together with the working hypothesis in the same order as they were listed in section 1.4.

Hypothesis 1: If the NBC was reversed during HS1, Amazon sediments delivered to the continental margin offshore NE South America would be redistributed along the NBC pathway.

Based on the compilation of stratigraphic data of 108 sediment cores collected across the western tropical Atlantic, we show an extreme rise in sedimentation rates off the Parnaíba River mouth (about 2°S, off NE Brazil), from ca. 25 cm/ka during the LGM to ca. 80 cm/ka during HS1, while no evident change off French Guiana (ca. 7°N), ca. 15 cm/ka during both the LGM and HS1. Because the NBC carries a large amount of Amazon-sourced terrigenous sediments northwestward along the NE South American continental margin, downcore $\varepsilon_{Nd(0)}$ data of two sediment cores raised off the Parnaíba River mouth (to the southeast of the Amazon River mouth) and French Guiana (to the northwest of the Amazon River mouth) are able to trace the sources of the deposited terrigenous materials, testing the hypothesis of the NBC reversal during HS1.

Together with previously published $\varepsilon_{Nd(0)}$ data of terrestrial materials from the Amazon Basin and new $\varepsilon_{Nd(0)}$ values from a set of geological units from the Parnaíba River basin, our downcore results suggest that the terrigenous sediments deposited over the last 30 ka off the Parnaíba River mouth and French Guiana are mainly from the Parnaíba Basin and the Amazon Basin, respectively. We clarify here for the first time that the NBC reversal hypothesis during HS1 should be rejected. Accordingly, the enhanced input of terrigenous sediments offshore NE Brazil is the product of past climate changes directly over NE Brazil. Combined with major element compositions from sediment core GeoB16206-1 collected off the Parnaíba River mouth, we further suggest that an increased precipitation over NE Brazil and a weakened NBC, both associated with a weakened AMOC during HS1, worked together to account for the extraordinarily high sedimentation rates.

Hypothesis 2: If South American precipitation during HS1 was only influenced by the North Atlantic climate, other oceans would have no contribution to the regional characteristics of South American precipitation.

By compiling 107 published quality-controlled paleoclimate records across tropical South America, we evaluated the regional characteristics of precipitation changes during HS1 relative to the LGM. In general, dry conditions were experienced in northernmost South America, while wet conditions characterized NE and SE Brazil as well as the western Amazon and the adjacent Andes. To explore the individual contributions of the Atlantic and other oceans (in particular the Pacific) on this response, we operated a set of climate model sensitivity experiments. The results show that the Atlantic interhemispheric SST gradient associated with freshwater perturbation at the high latitudes of the North Atlantic, although produces dry conditions in northernmost South America and wet conditions in NE Brazil, cannot explain the wet conditions prevailing over the western Amazon and the adjacent Andes.

Interestingly, the superimposition of the eastern equatorial Pacific SST variations upon the Atlantic SST changes for a HS1-like event is able to capture the overall characteristics of South American precipitation anomaly as reconstructed in the compilation. We suggest

that the SST changes over the Atlantic and the eastern equatorial Pacific associated to the AMOC slowdown are together necessary to generate the regional characteristics of South American precipitation during HS1. We hence reject this hypothesis for interpreting paleorecords over tropical South America, in particular those from the western Amazon and the adjacent Andes.

Hypothesis 3: If the AMOC strength underwent moderate reduction during the DO Stadials in comparison to the HS, then an intermediate response in tropical South American precipitation (e.g., between weak AMOC during HS1 and strong AMOC during the late Holocene) should be observed during the DO Stadials.

The marine sediment core GeoB16224-1 collected at about 7°N off French Guiana enable us to determine the possible relationship between the enhanced input of Amazon-sourced terrigenous sediments and periods of decreased strength in the AMOC (e.g., Heinrich and DO Stadials). We further compared the GeoB16224-1 record to four published terrestrial paleoprecipitation records along a transect across Central and South America. The results show that both the Heinrich and the DO Stadials lead to a decreased precipitation over northernmost South America and an increased precipitation over the western Amazon and the adjacent Andes.

However, precipitation over NE Brazil experiences significant increases only during the HS while no evident change occurred during the DO Stadials. We propose that the ITCZ southward migration during the DO Stadials was unlikely to reach NE Brazil. This was probably related to the moderate magnitude of the AMOC reduction in comparison to the substantial slowdown (or nearly shutdown) during HS. The absence of changes in rainfall over NE Brazil during the DO Stadials, is supported by model simulations (e.g., Zhang et al., 2014). The hypothesis is accordingly accepted, and we also speculate that future AMOC slowdown (ca. 20-40%, e.g., Weaver et al., 2012) would have little impact on NE Brazilian precipitation.

5.2. Future perspective

We propose the following topics to further consolidate and expand the conclusion of this thesis.

In Chapter 2 we applied the Al/Si ratio to sediment cores GeoB16206-1 and GeoB16224-1 as a grain size proxy, based on the robust relationship established by Bouchez et al. (2011). However, the direct determination grain sizes would be much welcome to exclude the effect of other competing parameters.

In Chapter 3, it became evident that the lack of high temporal-resolution hydroclimate reconstructions covering HS1 from central Amazonia hinders a more direct comparison to model results. Well-dated high temporal-resolution paleoclimate records from this region, such as stalagmite $\delta^{18}O$ records, are thus highly desirable to provide precious insights into the climate changes during HS1. Furthermore, some paleodata suggested wet conditions over SE Brazil, but such precipitation anomaly is not reproduced by both our model and previous simulations (e.g., Kageyama et al., 2013). Therefore, additional investigations on paleoclimate records and model simulations are necessary to clarify this point.

In Chapter 4, since there are only a few terrestrial paleorecords for reconstructing the DO Stadials, e.g., stalagmites from the Peruvian Andes published by Kanner et al. (2012) and from the Ecuadorian Andes published by Mosblech et al. (2012), more highly-resolved paleoclimate records from SE Brazil (e.g., stalagmite) would improve our understanding about the regional characteristics of precipitation pattern during the DO Stadials relative to the HS. Moreover, more comparisons between climate models and paleorecords will most probably continue to provide more insights into the mechanisms of South American precipitation response to Heinrich and DO Stadials.

5.3. References

Bouchez, J., et al. 2011. Grain size control of river suspended sediment geochemistry: Clues from Amazon River depth profiles. Geochem. Geophys. Geosyst. 12, Q03008, doi: 10.1029/2010gc003380.

Kageyama, M., et al. 2013. Climatic impacts of fresh water hosing under Last Glacial Maximum conditions a multi-model study. Clim. Past 9, 935-953.

Kanner, L.C., et al. 2012. High latitude forcing of the South American Summer Monsoon during the Last Glacial. Science 335, 570-573.

Mosblech, N.A.S., et al. 2012. North Atlantic forcing of Amazonian precipitation during the last ice age. Nat. Geosci. 5, 817-820.

Weaver, A.J., et al. 2012. Stability of the Atlantic meridional overturning circulation: A model intercomparison. Geophys. Res. Lett. 272 39, doi:10.1029/2012GL053763.

Zhang, X., et al. 2014. Abrupt glacial climate shifts controlled by ice sheet changes. Nature 512, 290-294.